# Boiler feed pump low load – leak off recirculation study


**Prepared by:**

Daniël van Tonder

VTNDAN007

Department of Mechanical Engineering

University of Cape Town

**Supervisor:**

A/Prof. Wim Fuls

**2019**

Submitted to the Department of Mechanical Engineering at the University of Cape Town in partial fulfilment of the academic requirements for a Masters of Science degree in Mechanical Engineering

**Key Words:** BOILER FEED PUMP, LEAK OFF, CAVITATION, PRESSURE DROP, CRITICAL VALVE

# *Abstract*

For power plants that make use of high energy boiler feed pumps, there is a risk that the boiler feed pump may experience cavitation and overheating at low load and start-up conditions. These plants make use of a leak off or recirculation system that diverts some of the flow back to the feed water tank, ensuring that a minimum flow through the pump is maintained at low load and start-up operating conditions. The recirculation valve, also known as a leak off valve, experiences a very high pressure difference and cavitation pitting is common due to the water being close to saturation.

There are various ways in which the recirculation flow is controlled in the industry such as open orifice, on/off binary type control valves, automatic recirculation valves (ARC) or modern modulating leak off systems. The valves themselves can also be simple plug type or make use of pressure staging to reduce the risk of cavitation.

This project involves modelling the flow system around the boiler feed pump and its control for the various architectures employed in Eskom. This is to assist in understanding the reasons for cavitation damage that is found in some recirculation valves as well as the low load capability of the system.

Single stage components with extremely high pressure drops are singled out as components with the highest risk of cavitation in the systems. Although extremely high pressure drops are found across the leak off valves themselves, the majority of the valves are multistage valves which are specifically designed to accommodate cavitation development and are therefore not of major concern.

Some of the findings of the study are: The rule of thumb used within Eskom to determine the amount of pressure reducing stages on leak off valves could be more conservative. The specification of new valves and components for the leak off systems requires accurate specification based on detailed process models, such as the ones developed for this study. The full range of all possible operational cases must also be considered during the design.

# *Declaration*

I, Daniël Pieter van Tonder, hereby declare the work contained in this dissertation to be my own. All information which has been gained from various journal articles, text books or other sources has been referenced accordingly. I have not allowed, and will not allow, anyone to copy my work with the intention of passing it off as their own work or part thereof.

Signed by candidate

_____ _____

Daniël Pieter van Tonder Date

# *Acknowledgements*

The author would like to express his gratitude to all those who assisted in making this study possible.

A special thank you to the following:

- Eskom for funding the research through the Eskom Power Plant Engineering Institute (EPPEI)
- My manager, Kapil Sukhnandan, for allowing me the opportunity to complete the research study
- Willem van der Westhuizen (Industrial Supervisor) for his assistance, knowledge and information sharing throughout the study
- A/Prof. Wim Fuls (Academic Supervisor) for all the discussions, suggestions, comments, guidance and support
- Sulzer Pumps and the various Eskom system engineers for the sharing of the feed pump system data
- and last but not least my wife for her motivation, patience and support.

# *Table of Contents*

# List of Figures

# List of Tables

# List of Nomenclature

## General symbols

| | |
|---|---|
| $c_F$ | Speed of sound inside the fluid |
| Cv | Valve flow coefficient (Imperial units) |
| D / d | Diameter |
| e | Surface roughness |
| f | Friction factor |
| $F_{DC}$ | Duty cycle factor |
| $F_F$ | Liquid critical pressure ratio factor |
| $F_L$ | Recovery factor |
| $F_U$ | Velocity factor |
| $F_T$ | Temperature factor |
| g | Gravitational constant |
| h | Enthalpy |
| H | Head |
| I | Intensity index |
| k | Constant |
| $K_R$ | Cavitation resistance value |
| Kv | Valve flow coefficient (Metric units) |
| M | Motor |
| $\dot{m}$ | Mass flow rate |
| N | Rotational speed |
| n | Number of |
| $n_q$ | Pump specific speed |
| p | Pressure |
| P | Power |

| | |
|---|---|
| $p_1$ | Upstream pressure |
| $p_2$ | Downstream pressure |
| $p_a$ | Ambient pressure |
| $p_B$ | Pressure inside the bubble |
| $p_c$ | Critical pressure of the nucleus |
| $p_g$ | Gas pressure inside the bubble |
| $p_L$ | Liquid pressure at bubble wall |
| $p_{min}$ | Minimum pressure |
| $p_S$ | Pressure effect caused by surface tension |
| $p_v$ | Vapour pressure |
| $p_\infty$ | Pressure at a distance far away from the bubble |
| Q | Volume flow rate |
| R | Bubble radius |
| $R_c$ | Critical radius of the bubble |
| $R_E$ | Final bubble radius |
| $R_m$ | Maximum bubble radius |
| Re | Reynolds number |
| S | Surface tension |
| s | Distance |
| T | Temperature |
| $T_B$ | Temperature inside the bubble |
| $T_{BL}$ | Boiling temperature of liquid |
| t | Time |
| $t_p$ | Bubble collapse time |
| v | Specific volume |
| V | Volume |
| U | Velocity |

| | |
|---|---|
| $X_F$ | Coefficient of cavitation |
| $X_{FZ}$ | Valve specific coefficient of cavitation |
| Z | Static height/elevation |

## Greek symbols

| | |
|---|---|
| β | Diameter ratio |
| Δ | difference |
| ε | Gas saturation level |
| ε | Strain (Section 3.5.1) |
| ϒ | Ratio of heat capacities of gas inside the bubble |
| $ϒ_c$ | Critical tension |
| σ | Cavitation number |
| $σ_c$ | Cavitation number at constant cavitation |
| $σ_{ch}$ | Cavitation number at choking |
| $σ_i$ | Cavitation number at inception |
| $σ_{id}$ | Cavitation number at incipient damage |
| $σ_{mr}$ | Cavitation number at manufacturers recommended limit |
| $σ_{mv}$ | Cavitation number at maximum intensity and vibration |
| $σ_{ss}$ | Severity of service factor |
| $Ø_{KE}$ | Kinetic energy of the liquid |
| ρ | Density |
| μ | Dynamic viscosity |

## Acronyms and Abbreviations

| | |
|---|---|
| ARC | Automatic recirculation valve |
| BEP | Best efficiency point |

| | |
|---|---|
| BFP | Boiler feed pump |
| BFPT | Boiler feed pump turbine |
| CFD | Computational fluid dynamics |
| CV | Control volume |
| DCS | Distributed control system |
| EFP | Electric feed pump |
| EPPEI | Eskom power plant engineering institute |
| EPRI | Electric power research institute |
| FME | Foreign material exclusion |
| FW | Feed water |
| FWT | Feed water tank |
| GPM | Gallons per minute |
| HP | High pressure |
| IP | Intermediate pressure |
| ISA | Instrument society of America |
| Iso | Isolation |
| LO | Leak off |
| MCR | Maximum continuous rating |
| N/A | Not applicable |
| NPSHA | Nett positive suction head available |
| NRV | Non return valve |
| OEM | Original equipment manufacturer |
| PRV | Pressure regulating valve |
| PSE | Pressure scale effect |
| P&IDs | Piping and instrument diagrams |
| SFP | Steam feed pump |
| SSE | Size scale effect |

| | |
|---|---|
| UR | Ultimate resilience |
| US | United States |
| VOL | Volume of fluid |

# 1. Introduction

## 1.1 Background

Coal and nuclear power plants make use of high energy boiler feed pumps (BFP). These critical pumps carry a risk of low flow cavitation and overheating at low unit load and start-up conditions. To prevent damage and failure of the feed pumps these plants employ a leak off or recirculation system that will divert some of the flow back to the de-aerator or feed water tank ensuring that a minimum flow through the pump is maintained. These systems consist of expensive and technologically advanced valves that are of critical importance for safe operation of the boiler feed pumps.

In the past, the boiler feed pumps operated for much of its life close to the duty point. In recent times the pumps are required to operate more in the low flow range due to frequent unit trips, two shifting of units where an increase and decrease in load is required due to morning and evening peaks, an increased number of pump starts due to unavailability as well as modernised pump operating regimes (frequent pump changeovers to proof the pump's reliability).

According to a leading leak off valve designer and manufacturer [1] cavitation is the main cause of leak off valve failures. Conditions during start-up with the valves at small opening percentages is given as the main concern.

## 1.2 Problem description

Several projects have been registered of late within Eskom to replace the existing leak off valves and components due to poor performance, unreliability, obsolescence and low life expectancy. Erosion caused by cavitation are highlighted as a concern, especially at critical areas such as the isolation areas of the system. Other failure types such as actuator reliability are also mentioned.

A recent study conducted by EPRI shows that feed water minimum flow valves (FMV) suffer the highest number of body erosion failures of all the severe duty valves found on a coal fired power plant. Table 1 below summarises the results of the study.

With the introduction of supercritical boiler designs, higher boiler feed pump discharge pressures are required which warrants a study into the damaging mechanisms of high pressure breakdown.

*Table 1: EPRI severe duty valve analysis results [2]*

| Failure Cause | Failure Case Percent of Valve Failures for Service Indicated | | | | | |
|---|---|---|---|---|---|---|
| | All | Atmospheric dump valves | Condenser dump valves | Feed water minimum flow valves | Feed water regulating valves | Pressurizer spray valves |
| Plug / cage | 19 | 15 | 4 | 0 | 0 | 17 |
| Plug / seat | 17 | 6 | 8 | 0 | 2 | 0 |
| Plug / stem | 17 | 2 | 6 | 0 | 8 | 17 |
| Pilot | 6 | 2 | 4 | 0 | 0 | 0 |
| Stem | 6 | 0 | 2 | 2 | 2 | 17 |
| Body erosion | 2 | 0 | 0 | 2 | 0 | 0 |
| Packing | 19 | 2 | 0 | 2 | 15 | 50 |
| FME | 15 | 0 | 6 | 0 | 8 | 0 |

## 1.3 Purpose of the study

The purpose of this study is to identify which leak off system types used within Eskom's coal fired fleet have the highest risk of suffering from cavitation damage and which operating conditions contribute the most to the cavitation erosion damage.

In order to achieve the goals of the study, the following activities need to be completed:

1. Identify the different leak off devices used throughout the coal fired fleet
2. Categorise the different leak off systems into 3 or 4 categories based on the type and operation
3. Select a representative plant from each of the categories
4. Identify the different leak off system components and failures
5. Gather the operating parameters and philosophies for each of the selected plants
6. Research methods of numerically predicting incipient cavitation in valves
7. Identify the different types of cavitation
8. Identify which conditions can lead to cavitation
9. Identify methods of reducing the effect of cavitation

10. Model each of the representative plants using the Flownex Simulation Environment software
11. Verify each model using actual plant data
12. Identify operating cases for each model that results in conditions likely for cavitation erosion
13. Identify possible methods of eliminating or reducing the effect of cavitation for the different operating cases.

## 1.4 Limitations and exclusions

The study has some limitations which are described below:

1. Only process related failures will be investigated with specific focus on cavitation erosion. Therefore, failure as a result of poor workmanship, any form of mechanical failure etc. will be neglected.
2. The study is conducted using one dimensional flow simulation software. Component specific internal geometries and flow paths will therefore not be taken into account as this would require a detailed computational fluid dynamics (CFD) analysis.
3. Other plant layouts and operating conditions within Eskom may vary from the representative plants that were selected for this study. The findings based on the stations that were modelled may not necessarily apply to all stations.

# 2. System description

The purpose of this section is to provide the necessary background information of the boiler feed pump system found on a typical coal fired power plant as well as the description of the minimum flow leak off bypass system that forms the foundation of this study.

## 2.1 Boiler feed pump system overview

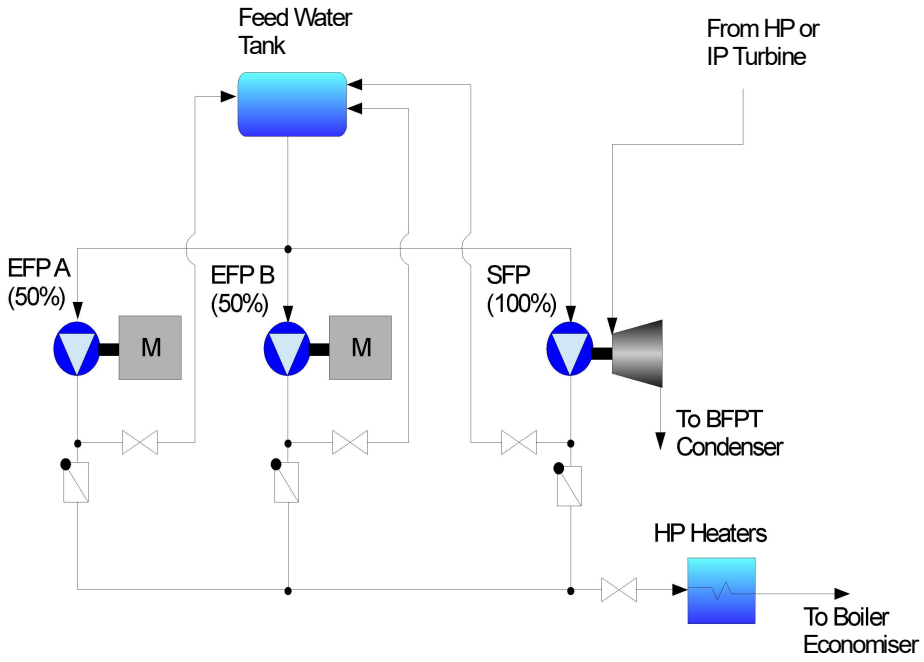


*Figure 2-1: Typical BFP plant layout*

The boiler feed pumps are the heart of every coal fired power station. The pumps form part of the main Rankine steam-water cycle process and pump the water from the feed water storage tanks (FWT) to the boiler economiser through the high pressure (HP) heaters. The majority of the Eskom coal fired fleet are equipped with two 50 % electric motor driven boiler feed pumps (EFP) and one 100 % steam turbine driven boiler feed pump (SFP) as illustrated in Figure 2-1. Collectively the EFPs and SFPs are referred to as the boiler feed pumps (BFPs). The EFPs are used for unit start-up and shut-down and when the SFP is not available. The SFP is used during normal running conditions at loads higher than ~30 % of the turbine maximum continuous rating (MCR).

Other variations of the BFP plant are also found such 2 x 100 % EFPs as well as the newer plants with 3 x 50 % EFPs.

## 2.2 Boiler feed pump and leak off system

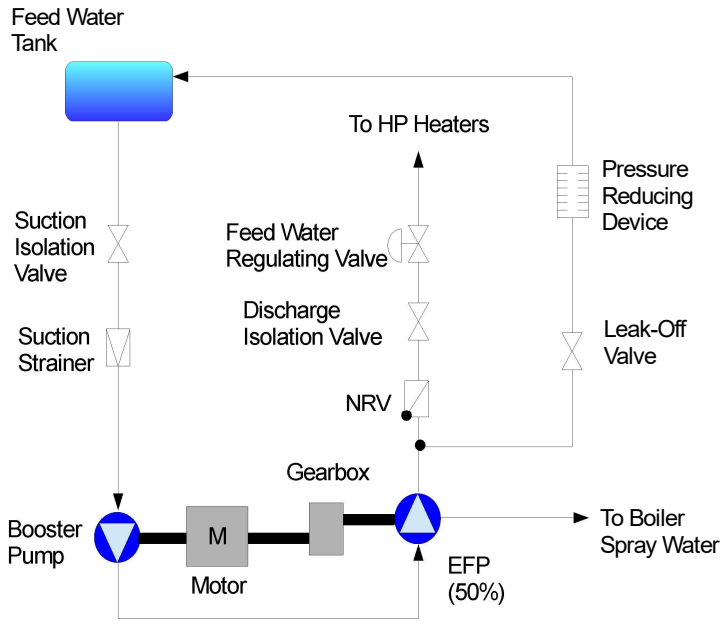


*Figure 2-2: Typical EFP system schematic*

Figure 2-2 shows the schematic layout of a typical EFP system. Feed water taken from the FWT passes through a low speed booster pump which discharges into the suction of the high speed main pump. The booster pump increases the net positive suction head available (NPSHA) to prevent the main pump from cavitating. The main pump discharge parameters are controlled by varying the main pump shaft speed through a variable speed gearbox as well as a feed water regulating valve installed downstream of the BFP system. The variable speed gearbox can not reduce the speed of the main pump to the requirements of the leak off valves due to the required discharge head to open the discharge NRVs when another BFP is already in service. The booster pumps are fixed speed pumps which also requires a minimum flow.

On the majority of stations, an intermediate take off is installed on the main pump that provides a small amount of feed water at a lower pressure to the boiler attemperator spray system.

On the discharge pipework immediately downstream of the main pump, and before the non-return valve (NRV), a minimum flow leak off line is found that circulates feed water back to the FWT during low flow conditions.

The purpose of the leak off system is to ensure that a predetermined minimum flowrate always passes through the pump to prevent it from overheating due to heat energy caused by friction inside the pump. A further result of very low flow conditions are hydraulic instability and impeller reverse

flow [3]. The leak off system is therefore in operation during low flow conditions such as BFP start-up, shut down, boiler filling and light up conditions.

The BFP leak off system is closed 90-95 % of the time. The high differential pressure acting across its seat, highest of any valve in the plant, makes it one of the most severe duty valves in a generating plant [4]. Any damage to the seat due to cavitation will result in continuous leak back to the FWT which increases energy wastage and in severe cases result in inability to supply the required minimum economiser flow rates.

## 2.3 Determining minimum flow requirement

According to SULZER [3] the minimum flowrate is the lowest possible pump delivery that can be achieved for extended periods of time without excessive wear of the pump components or damage.

GÜLICH [5] quoted the following three criteria that determine the minimum flowrate of a centrifugal pump:

1. the thermal minimum flow limits the temperature rise of the fluid
2. the hydraulic minimum flow attempts to limit the hydraulic excitation forces and vibrations
3. excessive cavitation induced by part load recirculation must be considered.

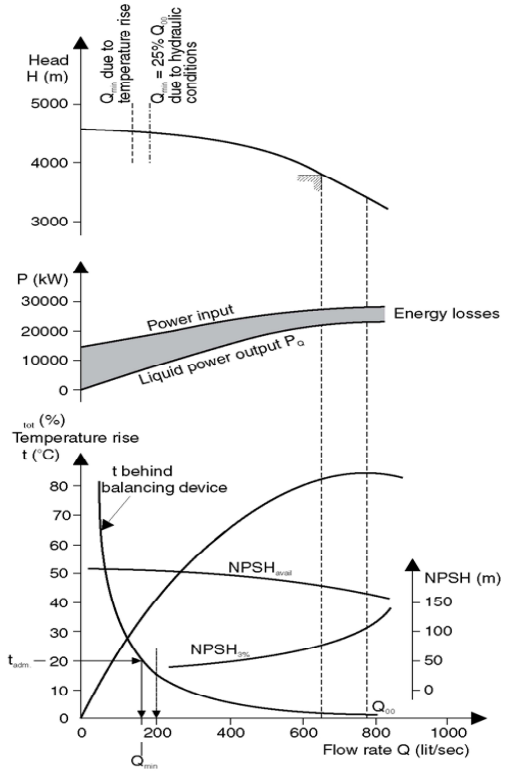


*Figure 2-3: Temperature rise of liquid through a pump and admissible minimum flowrate [3]*

The temperature rise versus flow rate graph in Figure 2-3 clearly illustrates how the fluid temperature behind the balance device increases asymptotically as the flow is reduced. Due to lower pump efficiency, a higher amount of internal energy loss is converted into heat. The head versus flowrate graph shows the minimum required flowrate to prevent temperature rise as well as the 25 % minimum flowrate to prevent hydraulic conditions such as low flow recirculation.

Various methods exist to determine the required minimum flowrate, all are based on some emperical value inputs. In a new method developed by Gopalakrishnan [6] it is recommended to make additional allowances that accommodate specific pump designs and applications. For this reason, Eskom has adopted a rule of thumb that BFP minimum flow must be at least 25 % of the pump best effieciency point (BEP). This aligns well with the recommendation made by Sulzer (Figure 2-4) [3] for pumps with low specific speeds as well as Gülich [5]. Some older power stations in the coal fired fleet that have not been through a leak off valve replacement in recent years still operate with minimum flowrates less than 25 %.

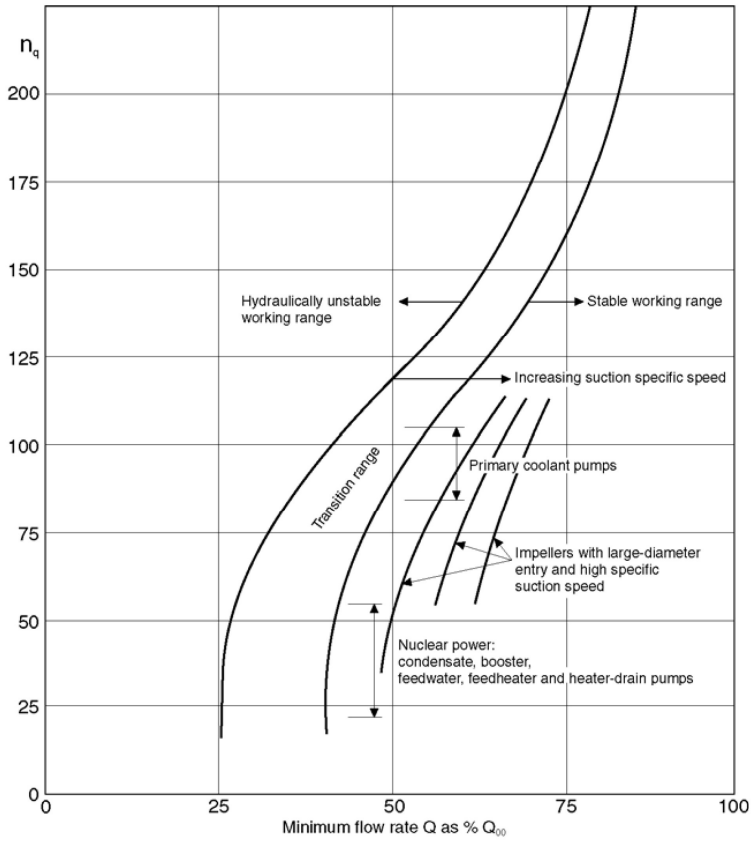


*Figure 2-4: Pump specific speed vs minimum flowrate [3]*

## 2.4 Types of leak off systems

Older leak off system designs found in the industry make use of an always open system equipped with only fixed orifice plates [7]. Inefficiency exists with the old design due to unnecessary feed water that is circulated back to the FWT during normal operation. Unnecessary high flowrates through the pump result in high additional running costs. For this reason none of these designs exists within Eskom on the BFP plants.

Modern leak off systems include a pressure reduction device that reduces the pressure from the BFP discharge pressure as well as an isolation device that is used to isolate the system during higher forward feed[1] flowrates. Some leak off system designs combine these functions into a single valve.

The leak off devices used within Eskom can be categorised into 3 different types, namely:

a) Binary type (On/Off valves)
   i) Separate isolation valve and pressure reduction device
   ii) Integrated valve
b) Modulating type
c) Automatic recirculation valve (ARC)

### 2.4.1 Binary type

The binary type leak off valves only has an On/Off function which means the valve will be fully closed if the measured feed water flowrate is above a specified value and will open fully if the measured feed water flow drops below a specified value. Along with modulating systems, these are the most common types of leak off systems found on modern power generating stations [4].

i) <u>Separate isolation valve and pressure reduction device</u>

This type of binary leak off system consist of an isolation valve, normally a venturi design parallel slide valve, with a throttle device / pressure reducer also known as a diffuser which is installed downstream of the isolation valve. Figure 2-5 shows the isolation valve installed vertically with the diffuser mounted horizontally on the concrete plinth.

[1] Forward feed is the normal forward flow process where the feed water is pumped by the boiler feed pump to the boiler economizer through the HP heaters.

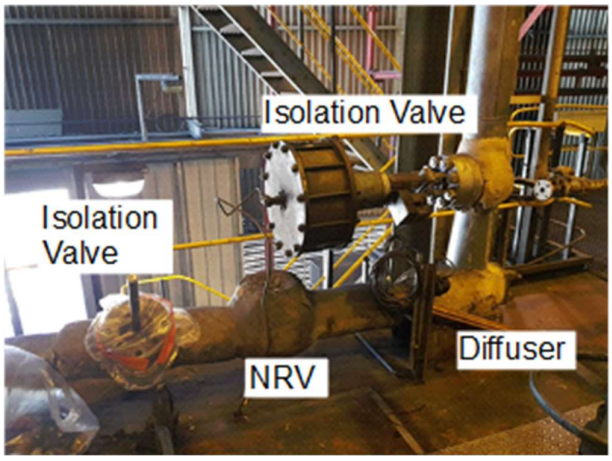


*Figure 2-5: Binary type (Separate) isolation valve and diffuser photo*

The isolation valve is used to open and close the system through an actuator (hydraulic, pneumatic or electric) that receives a signal from the distributed control system (DCS). These valves are normally smaller diameter parallel slide valves due to the high actuator torque requirement for larger valves at such high differential pressures. The diffuser reduces the pressure through a series of fixed orifice-like stages (Figure 2-6).

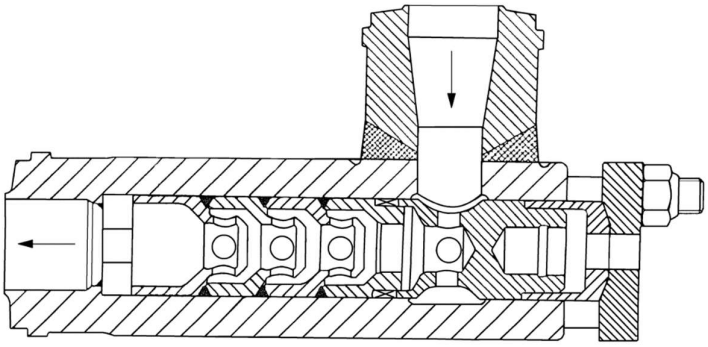

*Figure 2-6: Binary type (Separate) diffuser section drawing (Desensitised from undisclosed source)*

ii) Integrated valve

The integrated valve performs both the isolation and pressure reduction function (Figure 2-7). Similar to the isolation valve previously mentioned, the actuator receives a signal from the DCS to open or close the valve. With the valve in the open position, the flow passes through the valve in an axial direction to the spindle and the pressure is reduced through each stage. The valve is equiped with a metal to metal seat to isolate the flow in the closed position.

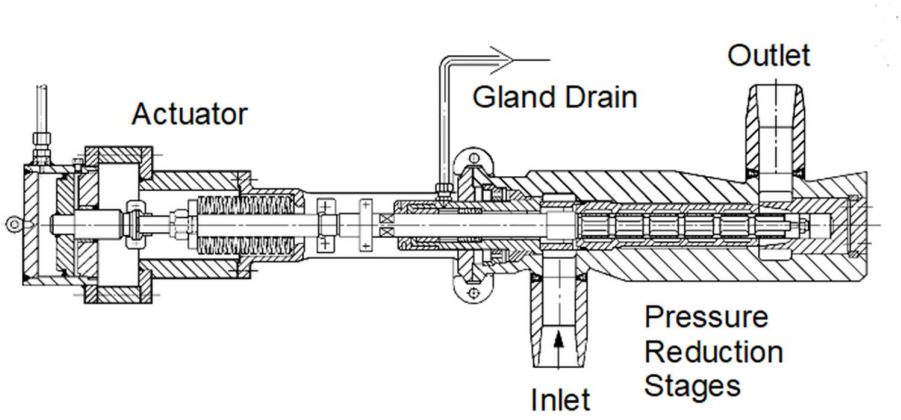


*Figure 2-7: Binary type - Integrated valve type section drawing (Desensitised from undisclosed source)*

The majority of leak off valves found on the Eskom BFP systems are binary type with the integrated valve being the most common type. Based on feedback from the various site engineers, the integrated valves are highly reliable with the actuators being the biggest contributor to unavailability. On the separate isolation valve and pressure reducer type, some sites have recorded various failures on the isolation valve downstream seats due to severe cavitation damage (Figure 2-8).


*Figure 2-8: Binary type - Separate isolation valve seat damage photo*

A drawback of the binary valve types is the effect of opening and closing the valve too quickly or too slowly. Rapid opening of these valves could cause unstable system fluctuations and water hammer, however too slow opening and closing times result in severe cavitation erosion. A further disadvantage is the near perfect plug-to-seat alignment that is required for metal seat designs to ensure zero leakage which is very difficult to achieve due to machining tolerances [4].

### 2.4.2 Modulating valves

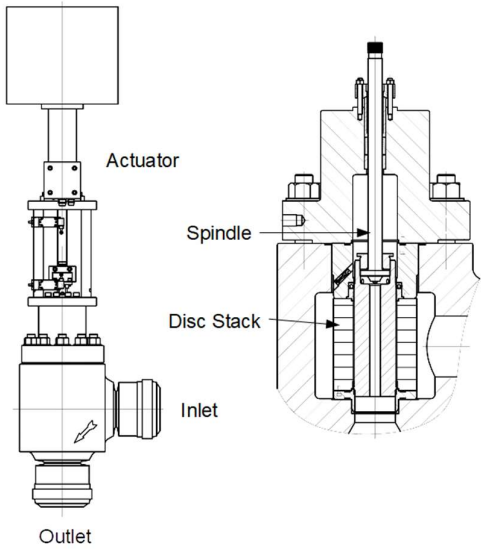


*Figure 2-9: Modulating valve type section drawing (Desensitised from undisclosed source)*

Modulating leak off valves (Figure 2-9) operate as control valves that modulate during low load conditions. The benefit of these valves over the binary type is the energy saving as illustrated on the graph in Figure 2-10. The highlighted area shows the energy loss with the binary system due to unnecessary high flow through the leak off bypass as soon as forward feeding has started. This energy saving applies to the modulating and the ARC type valves.

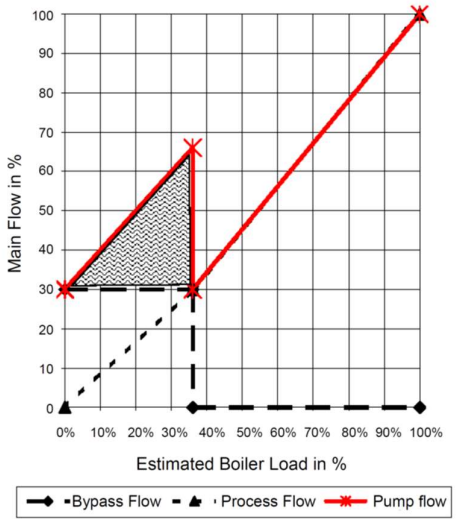


*Figure 2-10: Energy loss of an On/Off system [8]*

These valves are controlled by an actuator that receives a percentage signal from the DCS to open or close depending on the measured flowrate through the pump. By controlling the valve position

it ensures that the combined flow (forward feed flow & leak off flow) is always higher or equal to the required minimum flowrate. The valves used within Eskom consists of various slotted discs (Figure 2-11) that are stacked together to form a disruptive flow path that creates the high pressure loss. The flow enters the valve body on the outside of the valve disk stack, passes radially through the disc stack, collects on the inside of the stack and exits at the bottom of the valve.

*Figure 2-11: Modulating valve type single disk photo*

Due to the small openings created by the stacked discs the valves are susceptible to blocking by dirt in the system resulting in higher differential pressures and reduced leak off flowrates. A further downside of these types is that prolonged operation of the valve at low lifts could result in extensive damage. Operating at low lift position would see the valve continuously throttling across the valve seating surfaces resulting in wear, wire-drawing or cavitation damage on the seats [4].

## 2.4.3 Automatic recirculation valves (ARC)

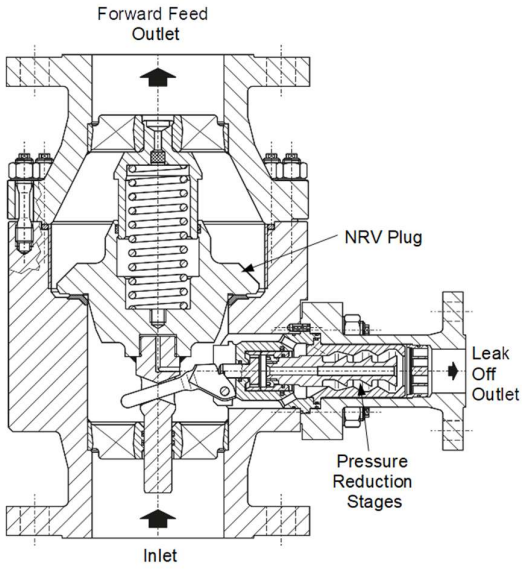


*Figure 2-12: ARC type valve section drawing (Desensitised from undisclosed source)*

The automatic recirculation valves (ARC) (Figure 2-12) performs the function of a leak off valve and a non-return valve (NRV) in the forward feed system. It does not require any external drives such as actuators. The ARC valve's leak off bypass opens and closes mechanically based on the NRV plug position which is a function of the pressure differential in the forward flow direction. The valves are specifically designed for each individual set of parameters and are therefore not interchangeable between two pumps with different characteristic curves.

With the discharge isolation valve (installed downstream of the ARC valve) in the closed position, the pressure on the inlet- and outlet side of the ARC is equalised. The spring forces the NRV closed which opens the leak off bypass through a lever and pin system. The bypass assembly consists of a multistage pressure reducer and a multi-hole or cone type diffuser.

Wear on the moving components within the valve have been reported as well as high rates of cavitation damage on the leak off bypass assembly and diffuser (Figure 2-13). Coating the bypass assembly surfaces with Stellite has seen a reduction in cavitation damage and acceptable service life.

*Figure 2-13: ARC type leak off valve diffuser damage*

## 2.5 Summary of Eskom leak off systems

Figure 2-14 shows the distribution of the Eskom leak off systems divided into the 4 categories mentioned above. The majority of the systems are of the Binary (Integrated) type with the ARC type the second most commonly found within the coal fired fleet. The number of boiler feed pumps (BFPs) with the specific type of leak off system is also indicated.

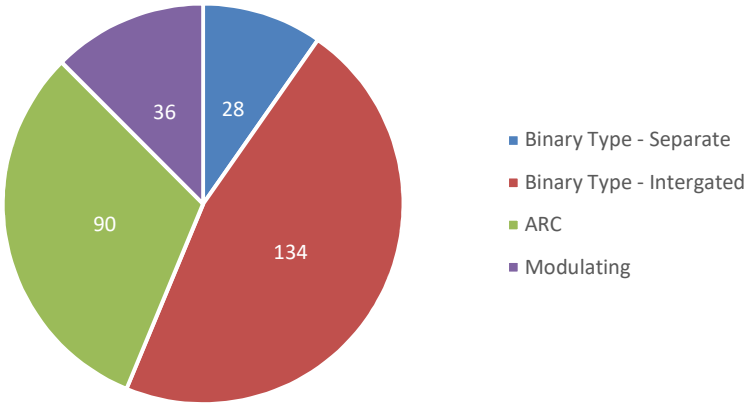


*Figure 2-14: Eskom leak off system types*

Figure 2-15 shows the design leak off flow as a percentage of the pump's BEP compared to the 25% rule of thumb as discussed in 2.3.

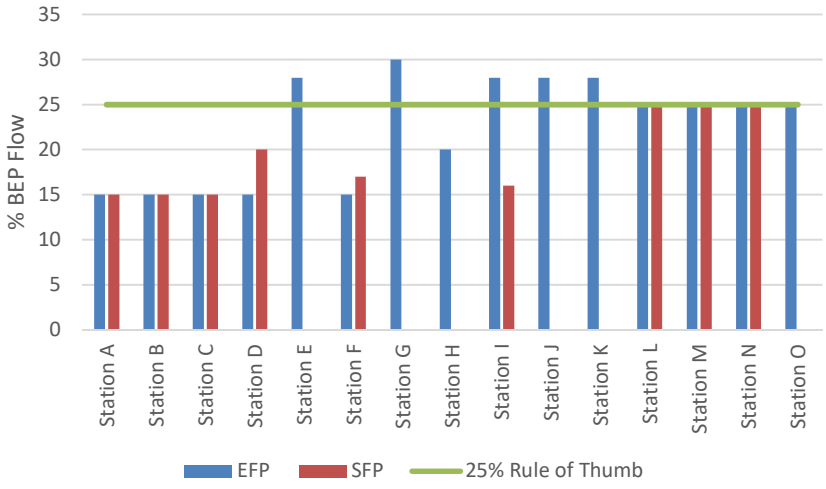


*Figure 2-15: Eskom BFP minimum flow as a percentage of BEP flow*

# 3. Literature review

## 3.1 Introduction to cavitation

### 3.1.1 History

Since the end of the 19th century cavitation has been documented as an undesirable fluid flow phenomenon resulting in effects such as erosion, vibration and noise. The cavitation of rotating machinery handling liquids was first identified by Torricelli and later by Euler and Newton [9]. In 1983 Parsons noted the effect of cavitation on the propellers of ships and constructed the first ever cavitation tunnel [10].

Two research areas followed based on theoretical and numerical approaches. The first research area focused on the dynamics of the cavitation bubble of which major contributions were made by Rayleigh (1917), Lamb (1923), Cole (1948), Blake (1949) and Plesset (1949). During this time, the bubble was considered to be spherical which simplified their studies. Developed cavities or supercavities were the second research area with Helmholtz (1868), Kirchhoff (1869), Levi-Civita (1907), Villat (1913) and Riabouchinski (1920) making contributions. This was based on the old wake theory that considered the wakes as areas of uniform pressure, limited by surfaces on which the tangential velocity is not continuous. This theory was adapted by Tulin (1953) and Wu (1956) through linearization procedures to assess slender bodies such as wings and blades [9].

In recent years, researchers have taken much interest in the cavitation phenomena and although some aspects of cavitation are not yet fully understood, sufficient progress has been made to accurately model, predict and avoid the destructive effects of cavitation.

### 3.1.2 Difference between cavitation and boiling

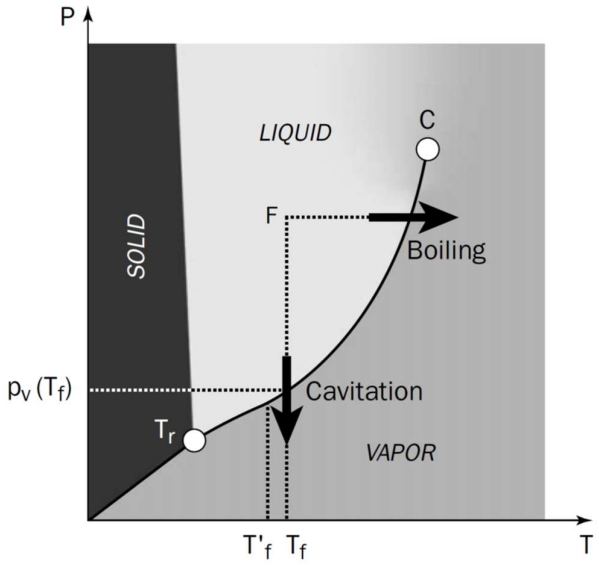


*Figure 3-1: Phase diagram [9]*

From Figure 3-1, it is clear that a phase change from a liquid to a vapour is possible by increasing the fluid temperature (boiling) or by reducing the fluid pressure (Cavitation formation).

Boiling therefore occurs when the temperature of a fluid is increased resulting in a phase change from a liquid to a vapour (vapourisation). The phase change occurs when the fluid crosses the liquid/vapour line, shown as the line connecting the critical point (C) and the triple point ($T_r$). The process is reversible in static or equilibrium conditions when the fluid changes from a vapour phase to a liquid phase (condensation).

The term cavitation refers to the vapourisation of a liquid when the local fluid hydrostatic pressure decreases below the fluid's vapour pressure ($p_v$) at nearly constant temperature ($T_f$). The vapour pressure of a fluid is a function of the temperature of the fluid. Similar to boiling, cavitation is a phase change from a liquid to a vapour with the difference that the driving mechanism is not a temperature change but a pressure change.

### 3.1.3 Contributors to cavitation development

The change in local fluid pressure can be due to a process related change, such as the opening of a pressure relief valve, due to flow dynamics or by rapid vibration of a boundary [11]. It may not be possible to avoid the development of cavitation completely, which is why it is important to know what conditions are favourable for cavitation development, the quantity and quality of damage that

can be expected for a given degree of cavitation [12]. The following paragraphs describe contributors that play a role in the development and quantity of cavitation.

Narrow restrictions

Low pressure zones in piping systems are generally created by a local increase in velocity which is illustrated in Figure 3-2 and which has been modified from [13]. As the flow passes through an opening, such as a valve or an orifice, the velocity increases due to the reduction in flow area. It reaches a maximum at the smallest flow area called the vena contracta. The vena contracta is found some distance downstream of the opening and is also where the fluid pressure is at a minimum before recovering to the outlet pressure as the velocity decreases.

These principles are proven by the use of Bernoulli's theorem formulated in equation (1) below, where Z represents the elevation component, p represents the static pressure component, U represents the velocity pressure component and $H_L$ is the head loss.

$$Z_1 + \frac{p_1}{\rho_1} + \frac{U_1^2}{2g_n} = Z_2 + \frac{p_2}{\rho_2} + \frac{U_2^2}{2g_n} + H_L \quad (1)$$

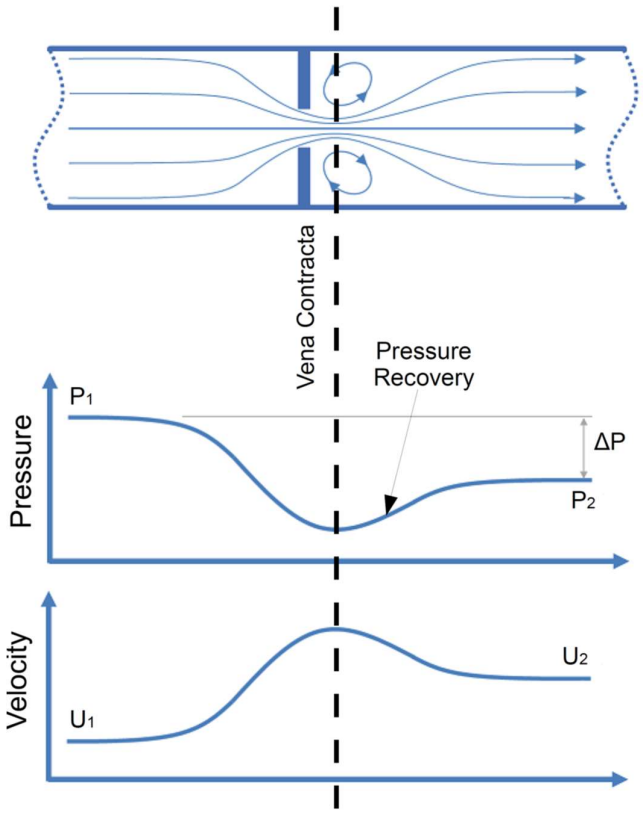


*Figure 3-2: Flow through an opening [13]*

Flow separation

Eisenberg [14] discussed the results of tests conducted at the Iowa Institute of Hydraulic Research which found that in flow separated regions, areas with low pressures can develop as a result of vortex flows even though the ambient pressures are relatively high. These areas includes sharp edges, abrupt expansion etc. Flow separation can also occur during water hammer [11] and large turbulent pressure fluctuations [9].

Surface finish

A rough surface finish with sharply varying contours produces local wakes in which small cavities may develop. As explained by Eisenberg [14], much work has been done on non-cavitating flow regimes over rough surfaces, but not enough results are available to establish surface roughness limits that are acceptable for cavitation prevention.

A secondary effect caused by surface condition is the global impact on the pressure and velocity fields which may delay the boundary layer separation [15].

Effects of water chemistry and condition

Garcia and Hammitt [12] believed that the reason for the discrepancies in their laboratory tests with water were due to the water chemistry. The water chemistry and condition plays a significant role in the water surface tension which is explained in more detail in section 3.2.5.

### 3.1.4 Different types of cavitation

Since high speed videos were taken by Knapp (1952) [16], many authors have investigated the different shapes of cavitation bubbles, including Knapp and Hollander (1948) and Parkin (1952). Many also attempted to understand, identify and categorised the different types of cavitation distinguishing between the traveling bubble and attached cavitation [15].

Franc [17] summarised the different types of cavitation into four main categories based on shape:

1. **Attached cavities** in which the cavity is attached to the hydrofoil. Attached cavities can be subdivided and photographs taken by Franc of each are shown below.
    a. Partial cavitation - Figure 3-3 (a)
    b. Unstable partial cavitation - Figure 3-3 (b)
    c. Super cavitation - Figure 3-3 (c)
2. **Traveling bubble cavitation** which sees isolated bubbles moving in the flow direction Figure 3-3 (d)
3. **Cavitation clouds** can take different forms which can become unstable due to re-entry jets developing - Figure 3-3 (e)

4. **Cavitating vortices** can be observed at the tip of three dimensional foils or in turbulent wakes of bluff bodies Figure 3-3 (f)

Other effects such as the interaction between the bubbles and walls, instabilities, re-entrant jet, coalescence etc. could also affect the basic shape and complicate the analysis of the liquid/vapour interface, which can make the categorisation particularly complex [17].

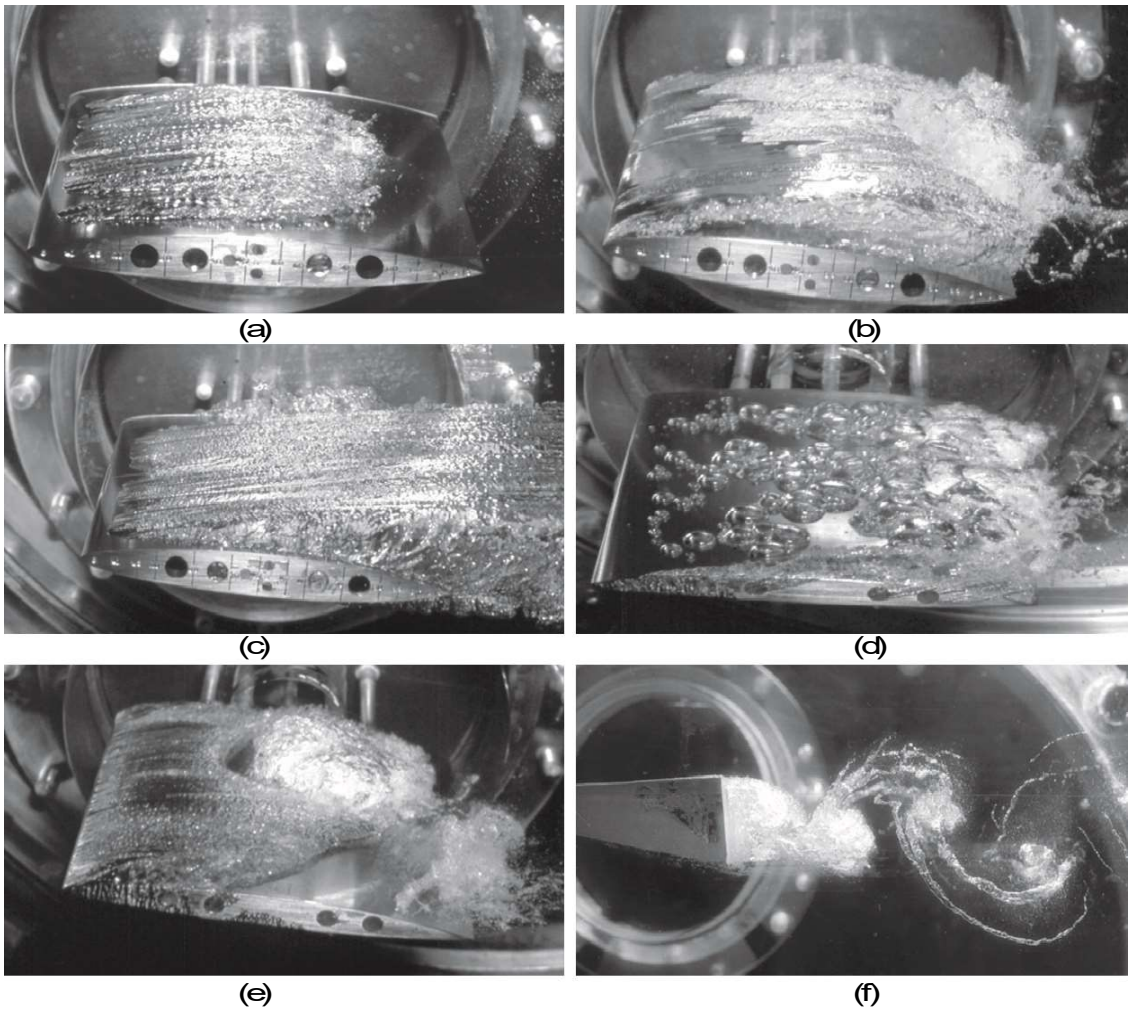


*Figure 3-3: Types of cavitation [17]*

## 3.1.5 Consequence of cavitation

The result caused by cavitation can range from little/no effect to catastrophic failure. Below is a list of consequences that can be expected in a system operating under cavitation flow:

- Changes in system performance
- Appearance of additional forces on solid structures
- Generation of noise

- Vibrations
- Pressure fluctuation
- Wall erosion.

All of these consequences are undesired in the field of generation plants, but it may not be financially feasible or practical to design components to completely avoid the development of cavitation. In areas where some degree of cavitation is acceptable, the effect thereof must be controlled and monitored.

### 3.1.6 Methods of detecting cavitation

Although no measurement device exists that can accurately measure the exact point at which cavitation is starting to develop, some tools can be used to determine if cavitation is present in a system and also for prediction of the level of cavitation. Although some methods are not practical in industry, it can be used in testing facilities under controlled conditions. As mentioned in 3.1.5 cavitation causes noise, vibration, wall erosion/material loss, pressure fluctuations and changes in system performance, therefore any device that is sensitive to these parameters can be used to detect cavitation [10]. Commonly the following methods are used:

- Visually
- Audibly
- Sound level meters/microphones, including hydrophones
- Pressure transducers
- Accelerometers.

Cavitation can be seen visually if a transparent test section is used which can be enhanced with the use of stroboscope lighting. This method is commonly used in test facilities with high speed cameras. This method is however not possible in the industry and is also not very objective. According to Brennen [15], experiments have shown that the production of noise is a simpler and more repeatable measure than visual observation.

Cavitation can be detected audibly due to the distinctive noise it makes as the vapour bubbles collapse. Incipient cavitation noise has been described as a hissing noise stemming from the downstream nozzle of the valve. As the intensity of the cavitation increases, the noise will increase until fully developed cavitation flow is present. The noise can be described as a crackling sound as if gravel is passing through the component [4].

In case more accurate measurements are required, microphones can be used to determine the noise level generated by the cavitation. Hydrophones are similar to microphones, but are used to measure noise levels under water using a transducer.

A rigidly mounted accelerometer can be used to measure the vibration of the downstream pipework to determine the presence and intensity of cavitation flow.

### 3.1.7 Pressure and pressure gradient in cavitating flows

It is always important to pay special attention to the absolute value of the pressure in cavitating flows. By simply lowering the reference pressure, cavitation can develop. It is thus important to consider the absolute value of the pressure and not just the pressure gradient / drop [9].

In order to predict the inception of cavitation theoretically or numerically, the pressure in a critical region must be calculated and compared to a threshold value which is typically the vapour pressure of the fluid at the same temperature.

According to Franc and Michel [9] the Bernoulli equation (1) is adequate to identify areas of minimum pressures and also to determine the values of these minimum pressures for one-dimensional steady state flows in pipes whilst taking into account the head losses.

### 3.1.8 Thermal effects

Two principle effects on cavitation phenomena are mentioned by Franc and Michel [9] that can be expected due to a temperature variation. These are:

1. If the ambient pressure remains constant, an increase in the fluid temperature will result in a greater ability to cavitate. It is clear from Figure 3-1 that a smaller change in pressure is required to reach the liquid-vapour phase change curve due to the increase in the vapour pressure.
2. Vapourisation requires heat transfer from the liquid to the liquid-vapour interface. The thermal delay (T – T'), as shown in Figure 3-1, tends to increase with temperature. When the temperature inside the bubble (T') is unknown, a thermal balance equation has to be developed to determine the temperature theoretically. In the case of bubbles, heat conduction is expected and for attached cavities, heat convection is predominant.

# 3.2 Cavitation inception

## 3.2.1 Stages of cavitation development

The starting point/condition where cavitation bubbles are formed is called cavitation inception. Although it is normally assumed, it is important to note that cavitation inception does not always occur when the fluid local absolute pressure equals the fluid vapour pressure ($p_v$) as simply explained in 3.1.2. This is due to the number and size of the nuclei present in the fluid which affects the fluid surface tension, which is explained in more detail in 3.2.5.

The $p_v(T)$ curve is thus not an absolute boundary between liquid and vapour phase. The difference between the vapour pressure and the actual pressure at which cavitation inception occurs is called the static delay. Furthermore a dynamic delay is the inertial phenomena associated with the time necessary for vapour cavities to be observable [9].

Small gas and vapour inclusions in the fluid are starting points for liquid breakdown and cavitation bubbles always start to form at these points, commonly referred to as cavitation nuclei. The cavitation nuclei varies in size (from a few micrometres to some hundreds of micrometres) and remain spherical at this scale due to the fluid surface tension [9].

Three stages of cavitation development are identified by Franc and Michel [9]. These different stages are theoretical and not physically measureable or differentiable. Steps 2 and 3 could also occur instantaneous.

1. Breakdown or void creation
2. Filling of the void with vapour
3. Saturation of the void with vapour.

## 3.2.2 Cavitation number

The cavitation number (σ) was first introduced by Thoma and LeRoux around the years 1923-1925 [9]. It is a dimensionless number which is used to quantify a set of process parameters in a system. The cavitation number can be used as a reference to numerically predict cavitation and cavitation type. In order to determine the cavitation numbers as reference values, initial testing is required using methods explained in paragraph 3.1.6 compared to the calculated benchmark cavitation number.

Plesset [18] conducted water tunnel investigations and defined the cavitation number as per equation (2) as well as three flow regimes for a given, suitably shaped, submerged body.

$$\sigma = \frac{p - p_v(T)}{\frac{1}{2}\rho U^2} \quad (2)$$

Where p and U are the static pressure and uniform velocity of the liquid at a distance from the body, $p_v$ is the vapour pressure of the liquid at temperature T and ρ the liquid density.

The first flow regime is where no cavitation is present (a large cavitation number) and the flow consists of a liquid only. The second regime is where the cavitation number is made smaller by decreasing the static pressure, increasing the vapour pressure or increasing the fluid velocity. Small bubbles start to appear, also known as cavitation inception ($\sigma_i$). The final flow regime occurs when the cavitation number is further reduced, which results in an increase amount of bubbles forming until they merge into one large cavity.

Knapp [16] explained the cavitation parameter very well:

"*The cavitation parameter is simply the ratio of the pressure available for collapsing the cavity to the pressure available for inducing the formation and growth of the cavity.*"

Franc and Michel [9] as well as Libera [10] defined the cavitation number for a gate as:

$$\sigma = \frac{p_2 - p_v(T)}{p_1 - p_2} \quad (3)$$

Where $p_1$ is the static pressure measured upstream of the gate, $p_2$ is the static pressure measured downstream of the gate and $p_v(T)$ is the vapour pressure of the fluid.

### 3.2.3 Cavitation number benchmarks

The Instrument Society of America (ISA) [19] recommends the use of the following benchmarks with regards to the control valve industry:

Manufacturer's recommended limit ($\sigma_{mr}$)

The manufacturer's recommended limit for cavitation is specified by the valve manufacturer for a specific valve and may differ from the incipient and constant cavitation limits of the valve.

Incipient cavitation ($\sigma_i$)

Incipient cavitation is the limit at which cavitation starts to form. Staying above the incipient cavitation limit will ensure the valve is operated free from cavitation. High recovery valves typically have incipient cavitation values around 15 and for low recovery valves around 8.

Constant cavitation ($\sigma_c$)

Constant cavitation is a condition where cavitation is forming, but at an acceptable level. It does not cause damage to the valve equipment and low levels of vibration and noise are produced.

Incipient damage cavitation ($\sigma_{id}$)

Operating at this level produces intolerable noise and vibration levels in a control valve. Minor pitting will be produced on the softer valve materials.

Choking cavitation ($\sigma_{ch}$)

The choking cavitation coefficient is calculated using equation (4) to correspond to the liquid pressure recovery factor ($F_L$).

$$\sigma_{ch} = \frac{\left(p_1 - p_v\right)}{F_L^2\left(p_1 - F_F p_v\right)} \tag{4}$$

Where $F_F$ denotes the liquid critical pressure ratio factor and are read from an empirical curve found in [20], similar to the pressure recovery factor. When the liquid flow becomes choked, a large volume of vapour forms. The cavitation has become severe enough to cause significant damage where the vapour cavities collapse within the pressure recovery zone. When fully choked, any decrease in the downstream pressure of the valve will not result in an increase in the flow rate through the valve. The pressure differential resulting in choked flow condition can be calculated using equation (5) and is illustrated in Figure 3-4.

$$\Delta p_{choked} = \left(F_L\right)^2\left(p_1 - F_F p_v\right) \tag{5}$$

Choking cavitation is considered the most severe level of cavitation in valves as maximum levels of noise, vibration and material damage is observed at this condition.

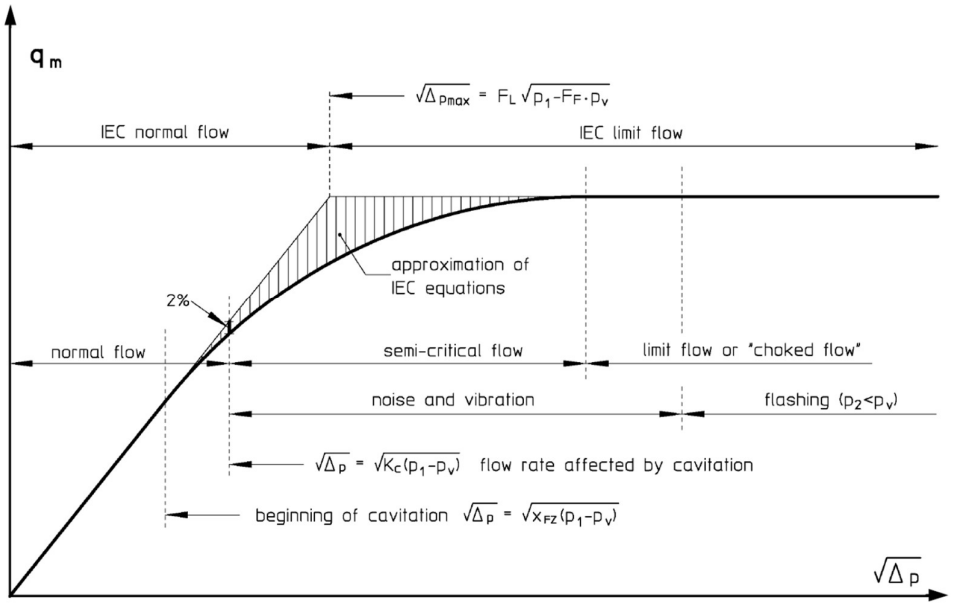


*Figure 3-4: Flowrate diagram of incompressible flow through a valve [21]*

Maximum intensity of vibration ($\sigma_{mv}$)

Similar to choking cavitation, the maximum intensity of vibration subjects valves and piping to severe levels of cavitation damage, noise and vibration. Valves in this service are generally designed for small duration service with sacrificial components.

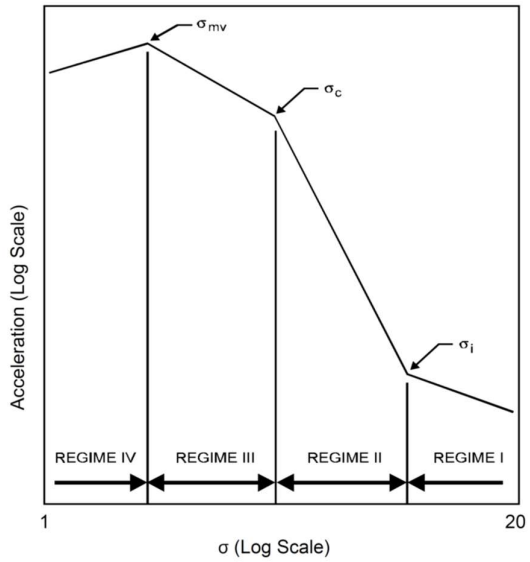


*Figure 3-5: Cavitation parameter plot [19]*

Figure 3-5 shows some of the cavitation number benchmarks on a cavitation parameter plot with the severity of the cavitation increasing as the cavitation parameter (σ) decreases.

### 3.2.4 Desinent and inception cavitation

It is important to note that an incipient cavitation number is specific to a piece of equipment. Various authors conducted flow tunnel tests to establish cavitation inception numbers for specific equipment to try and draw some sort of conclusions from the test results. Holl and Wislicenus conducted tests using various head forms of cylinders, disks and hydrofoils. Arndt and Ippen, Ball and Holl tested various surface irregularities [11].

Tullis and Govindarajan carried out cavitation flow tests through various combinations of orifice and pipe sizes [11]. The results are shown in Figure 3-6 and it is clear that a higher incipient cavitation number was measured for the larger diameter pipework, which becomes more noticeable at high diameter ratios (β). Tullis [22] continued his work and developed graphs for incipient cavitation for specific valve types, sizes and openings.

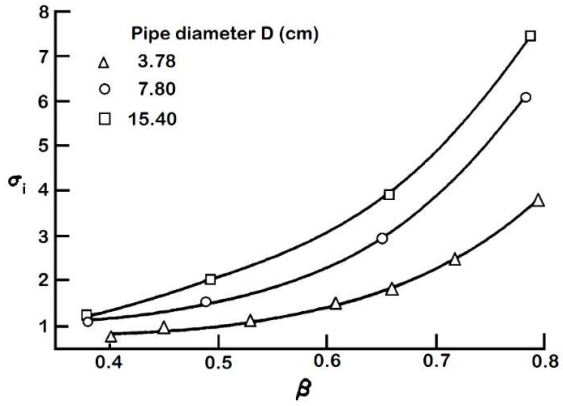


*Figure 3-6: Cavitation inception testing [11]*

Kermeen [23] conducted tests with hemispherical bodies to establish the incipient cavitation number as a function of the Reynolds number. During testing he used two methods to determine the incipient cavitation number. The first method was to allow the cavitation to become fully developed and then steadily increasing the system pressure until the cavitation disappeared, also termed desinent cavitation. The second method was to start with a non-cavitating system and allowing cavitation to start forming by lowering the ambient pressure. The results obtained through the second method were scattered and difficult to reach an accurate correlation. Kermeen identified a so called “hysteresis” when conducting the test using the two different methods [14]. His results can be seen on the plot redrawn from Eisenberg [14] in Figure 3-7.

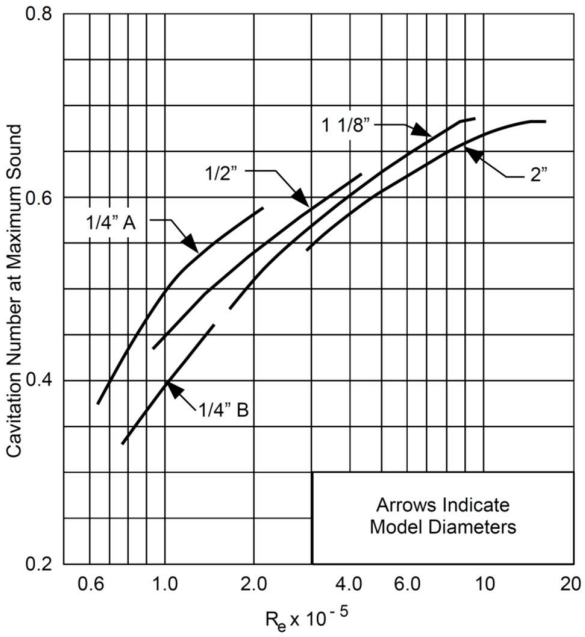


*Figure 3-7: Cavitation number as a function of Reynolds number (Reproduced from [14])*

Following the findings of Kermeen, in 1964 Lehman and Young [24] published results of water tunnel tests specifically aimed at identifying the different pressures for incipient and desinent cavitation in smooth and abrupt contour test pieces.

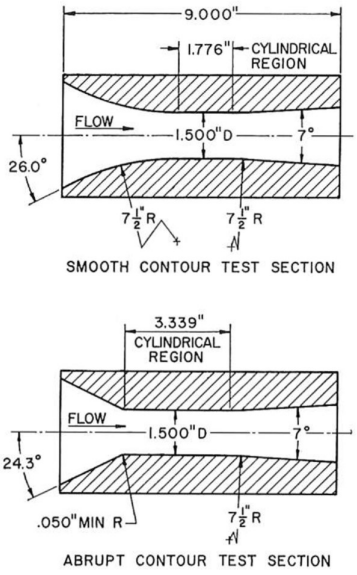


*Figure 3-8: Smooth and abrupt test pieces by Lehman and Young [24]*

Figure 3-8 shows a section view of the test pieces used in the water tunnel tests with the flow from left to right as indicated. The results of their tests show that the cavitation pressure and cavitation number (Figure 3-9) for desinent cavitation is larger than that of incipient cavitation. From the

plotted results it can also be seen that there is a greater difference between the desinent and incipient cavitation number for the abrupt contour test piece than the smooth contour test piece.

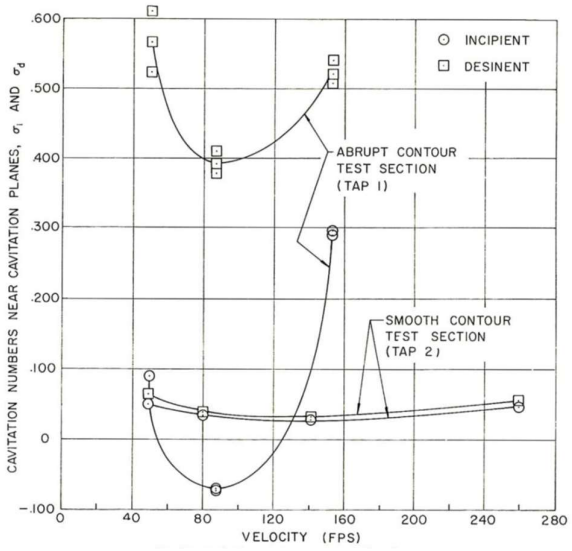


*Figure 3-9: Cavitation numbers for incipient and desinent tests by Lehman and Young [24]*

A further finding by Lehman and Young [24] was that desinent cavitation can be more easily reproduced than incipient cavitation, which agrees with the findings of Kermeen [23].

The difference between the desinent and inception of cavitation was termed “cavitation hysteresis” by Holl and Treaster in 1966 [15]. The hysteresis was explained by Brennen [15] to be twofold; the first was the effect the cavitational bubbly flow itself had on the surrounding fluid as well as the subjective nature of judgement of identifying the exact point of cavitation inception using visual inspection.

## 3.2.5 Effects of water chemistry

<u>Testing the surface tension of water</u>

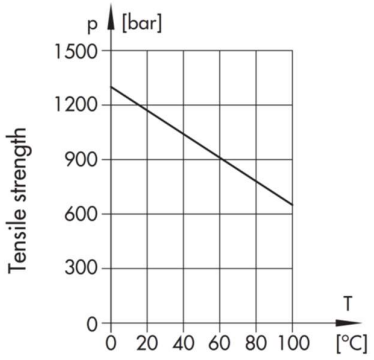


*Figure 3-10: Theoretical tensile strength of pure water [25]*

Becker and Döring [26] theoretically determined the tensile strength values for pure water as a function of its temperature in 1939 (Figure 3-10). In 1950, Briggs [27] reported test results of the actual tensile strength of highly purified water at various temperatures. He found that the maximum achievable value was 280 bar at a temperature just below 10˚C (Figure 3-11). The results show that a much lower tensile strength (approximately 4 times less) is actually achievable. A further noteworthy result was the reduction in tensile strength as the water temperature approaches freezing point due to the formation of water crystals [25].

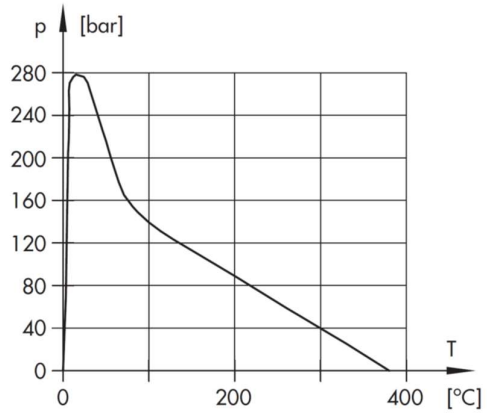


*Figure 3-11: Actual tensile strength of water [25]*

The large discrepancies between the theoretical and actual tensile strength values are as a result of the cavitation nuclei still present in the water [25]. This conclusion was proved by the tests carried out by Keller [28] in 1980. The tensile strength of tap water was measured at various levels of gas saturation levels (ε) and temperatures (Figure 3-12). From the test results it is clear that lower saturation levels result in higher tensile stresses. In his article, Mørch [29] compared the findings made by Keller and Briggs at low temperatures which further highlights the effects of water condition on the surface tension. He found that the critical tensile stress measurements by Briggs were much higher than measured by Keller as a result of the water purity. He also records a similarity between the results at temperatures approaching zero and that the temperature at which the highest tensile stress is found are not related to the different water qualities.

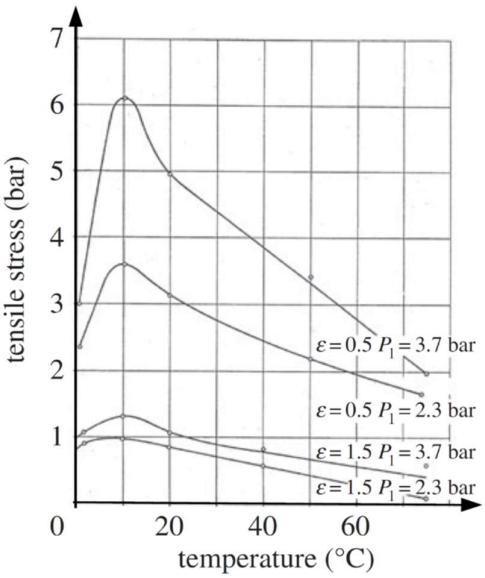


*Figure 3-12: Tensile strength of water at various temperatures and gas saturation [29]*

As proven in these test results, the disturbances in the quasi-crystalline structure of water reduce the possible tensile strength and results in great discrepancies between the theoretical and experimental values. Sub-microscopic build-ups of steam or gas molecules are created at these disturbances with the molecules being in an unstable equilibrium with the fluid. In cases of external tensile strengths (a lower external pressure), the nuclei can exceed a critical diameter ($R_c$) and then grow spontaneously. A model created by Harvey can be used to explain the existence of these nuclei in water which are a decisive factor in the occurrence of cavitation [25].

The effect of surface tension

Most liquids contain some dissolved gas and it is virtually impossible to remove all the gas from a substantial volume of liquid [15]. For a nucleation bubble containing some dissolved gas, an equilibrium pressure formula can be drawn about the pressures internal and external to the bubble.

$$p_\infty + \frac{2S}{R} = p_v + p_g \tag{6}$$

Where the fluid ambient pressure ($p_\infty$) and the surface tension factor (S) as a function of the bubble radius (R) are acting to reduce the cavity size and is equal to the sum of the partial pressure of the gas ($p_g$) and the vapour pressure ($p_v$). In equation (6), the left hand side is the sum of the external pressures acting on the bubble and the right hand side is the sum of the internal pressures acting on the bubble. The critical tension can thus be calculated as [15]:

$$\gamma_c = \frac{2S}{R} - p_g \tag{7}$$

From equation (7) it is clear that dissolved gasses will further decrease the potential tensile strength of the water.

As mentioned in 3.2.1, the threshold pressure for cavitation is not exactly the vapour pressure of the fluid. The difference between the vapour pressure ($p_v$) and the critical pressure ($p_c$) is known as the static delay. The critical pressure of the nucleus ($p_c$), also referred to as the critical pressure in this report, is not the critical pressure of the fluid (Critical point as indicated in Figure 3-1) where the liquid and vapour boundary terminates, but the pressure at which the nucleus becomes unstable as shown in Figure B-1.

There are generally an abundance of nuclei with a wide range of diameters found in water. The biggest nuclei are the weakest points because their critical pressure is the largest [17]. A larger critical radius ($R_c$) will result in a higher critical pressure ($p_c$) as can be seen from equation (8) below where S is the fluid surface tension, $p_{g0}$ is the partial pressure of the gas inside the bubble and $R_0$ is the original radius of the nuclei:

$$R_c = \sqrt{\frac{3 p_{g0} R_0^3}{2S}} \tag{8}$$

$$p_c = p_v - \frac{4S}{3R_c} \tag{9}$$

From equations (8) and (9) the critical radius and pressure depend on surface tension S and on the parameter $p_{g0}R_0^3$. The term $R_0^3$ is proportional to the volume of the bubble making $p_{g0}R_0^3$ proportional to the mass of non-condensable gas in the bubble. A nucleus is completely defined by the quantity of non-condensable gas it contains (which is assumed constant). It can also be characterized by either its critical radius or more commonly by its critical pressure [17].

These large nuclei will cavitate first and their critical pressure is known as the susceptibility pressure and also the critical pressure for cavitation. If special treatment is not applied to the liquid to remove the big nuclei, the susceptibility pressure is expected to remain close to the vapour pressure. In these cases, it is acceptable to assume that the threshold for cavitation is equal to the vapour pressure of the liquid.

The static delay observed in cavitation is much smaller than the discrepancies found between the experimental results and theoretical estimates mentioned above (usually does not exceed a few bar at most for tap water). It is expected that these points of weakness will exist in liquids that are currently used in industry [9].

In particular cases where extremely accurate results are required, it is necessary to take the state of the liquid into account; especially the temperature, spectrum of nuclei, the content of dissolved

gases, the surface tension and at which static pressure cavitation begins (generally just below the vapour pressure). In practice, it is impossible to determine a liquid's spectrum of nuclei in advance for most applications. It is therefore common practice in control valve sizing to describe the critical state of the cavitation nuclei at incipient cavitation by means of the vapour pressure of the liquid [25].

Eisenberg [14] summarises this section very well. It can be accepted that cavitation in a fluid under reduced pressure or boiling in a heated liquid begins with the growth of microscopic nuclei that contains a gas or vapour. A reduced number of such nuclei require larger forces for rupture since the surface tension forces increase. Thus, the rupture forces in well degassed liquids are in the order of what is predicted by kinetic theoretical formulations.

Experimental evidence shows that water saturated with air, but de-nucleated by the application of very high pressures, displays higher tensile strength.

The presence of nuclei is unmistakably necessary for the inception of cavitation at pressures of the order of vapour pressure. In most engineering applications within the industry, it is sufficient to assume that cavitation will occur at the vapour pressure corresponding to the temperature of the liquid. By making this assumption, it is assumed that there are sufficient nuclei of large enough initial size to grow to observable size during the time of application of reduced pressure. Lastly, for nuclei of a given size, the longer the time of exposure, at this lower pressure, the higher inception pressures is expected.

### 3.2.6 Incipient cavitation testing in valves

The test results of Libera [10] in Figure 3-13 below helps to gain some insight into the typical expected cavitation values in valves. Supplier values obtained from UseCAD 7.0, which is a specific CFD modelling software owned by VAG-Armaturen GmbH and numerical calculation were compared to the actual lab test results. Three valve types were simulated at various valve opening degrees using the software and the incipient cavitation and full cavitation numbers were plotted against the valve opening.

- Plunger type
- Globe type
- Butterfly type.

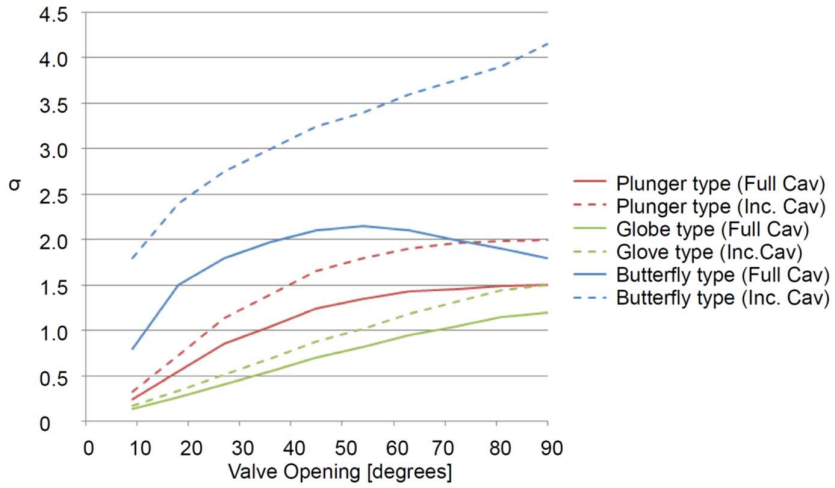


*Figure 3-13: Tested cavitation limits of valves [10]*

As can be seen from the graph, the Globe type and Plunger type have significantly lower cavitation inception and full cavitation numbers through the complete range of travel compared to the Butterfly type valve, which has a higher probability of cavitation. The conclusion drawn was the importance of selecting the right valve for the application. It was further found that for the Plunger type valve the cavitation numbers can be significantly reduced (<0.6) if slotted and orifice type cages are used on the outlet. The modulating valve used in this study is a type of plunger valve.

Valve manufacturers make use of different techniques to determine the valve specific cavitation reference data. The values are obtained either through testing, mostly at scaled conditions as discussed in section 3.4.1 or through CFD modelling to determine conditions where the local static pressure reaches values lower than vapour pressure.

## 3.3 Cavitation bubble evolution and collapse

Franc and Michel [9] describes the evolution of a nucleus through a low pressure region of limited extent using Blake's model. A one dimensional system is used to observe the bubble growth through a venturi where a critical pressure of the nucleus ($p_c$) is identified and compared to the minimum system pressure ($p_{min}$) to determine if the nucleus will return to its original state or become unstable and grows to a maximum size.

The Releigh-Plesset equation can be used to determine the time evolution of the bubble radius R(t) through the second order differential equation below.

$$\rho\left[R\ddot{R}+\frac{3}{2}\dot{R}^2\right]=\left[p_v-p_\infty(t)\right]+p_{g0}\left(\frac{R_0}{R}\right)^{3k}-\frac{2S}{R}-4\mu\frac{\dot{R}}{R} \tag{10}$$

It is possible to determine the pressure of the liquid adjacent to the collapsing bubble as well as the collapse velocity and time using equations (41) to (43).

Experimental studies have shown that the temperature of the fluid in the vicinity of the growing bubble decreases. This effect becomes more significant at higher fluid temperatures [17]. The effect of liquid temperature on the erosion rate is of importance. Dular [30] found that the cavitation aggressiveness reaches a maximum at temperatures between 50 °C and 70 °C, which is slightly higher than reported by Heathcock and shown in Figure B-4. The conclusion is consequently drawn that cavitation aggressiveness reaches a maximum at a temperature halfway between the freezing and boiling temperature of the fluid at the reference pressure.

The process of bubble evolution and collapse is discussed in more detail in Appendix B.

## 3.4 Damage mechanisms

Damage at the solid boundaries occurs due to two suggested mechanisms, namely high pressure shocks and microjets.

The high pressure shock wave is produced by the collapse of the bubble, also known as the shock wave theory. The pressure shock wave caused by the collapse of a single spherical bubble, neglecting the surface tension and the viscosity, can be calculated as:

$$p_i = c_f \rho_f U_R = \sqrt{\frac{2}{3} p_\infty \rho_f \left( \frac{R_0^{\,3}}{R_E^{\,3}} - 1 \right)} \tag{11}$$

Where $c_f$ and $\rho_f$ are the sound velocity and fluid density, $U_R$ is the centripetal velocity, $p_\infty$ the pressure at an infinite desistance from the bubble, $R_0$ the initial bubble radius and $R_E$ the final bubble radius [25]. The compressive loading caused by the shock wave impingement on the solid material surface can result in failure by fatigue (multiple loadings) or plastic deformation (single loading). This appears to be characteristic of a more symmetrical collapse [19].

Hickling and Plesset (1964) showed by means of numerical analysis that the pressure wave, caused by a cavity, is attenuated as a function of 1/R. The collapse centre must therefore be within one cavity diameter of a solid boundary to have any effect on this surface [31].

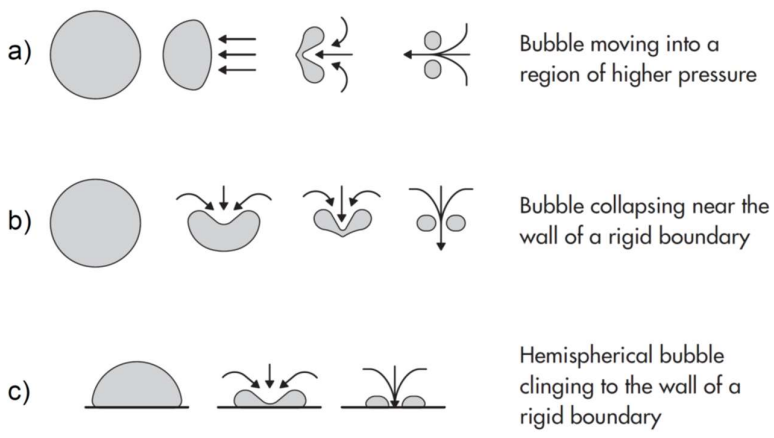


*Figure 3-14: Bubble collapse [25]*

The second is the damage caused by a microjet that forms as the bubble implodes near the solid boundary. These microjects form due to an asymmetrical pressure distribution that forms around the bubble caused by the solid boundary as shown as (c) in Figure 3-14. As it collapses, the side of the bubble away from the solid boundary reaches a higher velocity collapsing the bubble inwards. A high velocity jet forms that shoots through the centre of the bubble and impinges against the solid boundary [10]. According to Knapp, et al. (1970) the effect of microjet is more predominant for rigid surfaces, while compliant surfaces appear to repel the microjet [19].

The velocity of the microjet can be numerically estimated using the equation below [25]:

$$U_{jet} \approx \sqrt{\frac{p_{\infty} - p_v}{\rho_f}} \tag{12}$$

Tests carried out by Dular [30] analysed the cavitation erosion of water at various temperatures. Detailed results are discussed in Appendix B. As part of his work, he theorised which one of the two damage mechanisms are influenced the most by a change in fluid temperature. Although he found no conclusive results, he did find that the fluid temperature above 70 ˚C did play a larger role in the shock wave theory than on the microjet theory.

Knapp [32] reported that for a stationary cavitation zone only one out of 30,000 bubbles implode close enough to the solid boundary which causes a damaging effect.

### 3.4.1 Cavitation intensity

The intensity of cavitation is influenced by various factors and can be numerically predicted as explained by the ISA [19]. The intensity index can be considered as an approximation of how much

faster erosion will occur over the threshold damage rate. The intensity index can be calculated if the following intensity modifiers are known:

Velocity factor ($F_U$)

The velocity factor is the difference between the pitting threshold velocity ($U_o$) and the actual free-flow velocity (U).

$$F_U = \begin{cases} 1.0 \ \ if \ \ U - U_0 < 0 \\ 0.18 + 0.82e^{N_4(U-U_0)} \ \ otherwise \end{cases} \tag{13}$$

$N_4$ is a constant based on the units used for the velocity (0.256 for m/s).

Fluid temperature factor ($F_T$)

Research of water at low pressures has shown that cavitation erosion is more severe at temperatures halfway between its freezing and boiling point, as per Appendix B. The equation below can be used to take this into account.

$$F_T = 3 - 2\left(\frac{|T - T_{ave}|}{T_{BL} - T_{ave}}\right) \tag{14}$$

Where T is the fluid service temperature, $T_{BL}$ is the fluid boiling temperature at reference pressure and $T_{ave}$ is the average temperature between the boiling and freezing temperature.

Duty cycle factor ($F_{DC}$)

The duty cycle factor considers the duty cycle of the valve operating under cavitation conditions. It ranges from a rare upset value of 0.1 to a continuous or critical duty value of 3.0.

Severity of the service ($\sigma_{ss}$)

The severity of service can be calculated if the pressure scale effects (PSE) and size scale effects (SSE) values are known (see section 3.6.3):

$$\sigma_{ss} = \left(\frac{\frac{\sigma}{SSE} - 1}{PSE}\right) + 1 \tag{15}$$

The intensity index (I) can then be calculated using the equation below:

$$I = F_U F_T F_{DC}\left(\frac{\sigma_{id} - 1}{\sigma_{ss} - 1}\right) \tag{16}$$

With $\sigma_{id}$ the cavitation coefficient of incipient damage.

### 3.4.2 Cavitation erosion stages

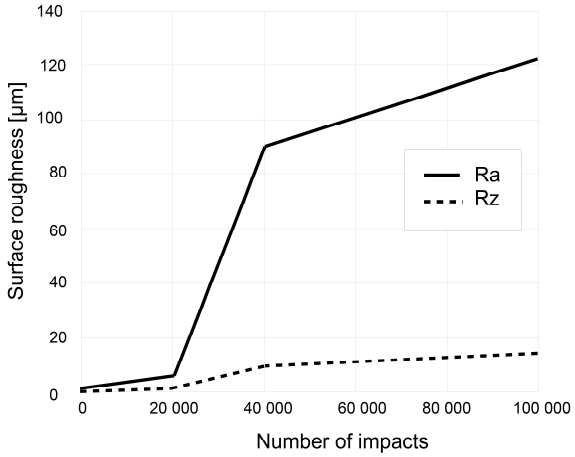


*Figure 3-15: Stages of cavitation erosion [33]*

Surfaces damaged by cavitation erosion have a typical pitted look with micro and macro pits [21]. Foldyna et. al [33] concluded that cavitation erosion occurs in three distinguishable stages. The tests were conducted by impinging the surface of a stainless steel sample with a pulsating water jet which resembles the repeated impacts caused by the collapse of a cavitation bubbles. The results are graphically illustrated Figure 3-15 (reproduced from [33]) where Ra is the average surface roughness and Rz is the difference between the highest and lowest points in the surface.

The first stage of cavitation erosion, also known as the incubation period, shows plastic or brittle deformation on the impacted surface only. At first, ductile metals only undergo elastic deformation before plastic deformation. At the end of the incubation period, fractures occur and individual particles start to break off. For brittle materials, the deformation phase is not as noticeable due to the high density of dislocation obstacles which results in internal tensions that form. When these tensions exceed that of the material strength, fractures occur which constitute a material weight loss [25]. During the incubation stage no loss of weight is measureable. The second stage is characterised by the formation of erosion pits which increases at a constant rate. The third stage sees these pits merging to form erosion craters with their depth increasing. The material starts to erode at a slower rate.

### 3.4.3 Effect of flow velocity on pitting rate

Investigations show that the pitting rate in the solid boundary increases with an increase in bulk flow velocity. The amplitude of the impulsive loads increases with flow velocity [10]. From equation (2) it is clear that the downstream pressure must increase with the increase of the velocity to keep a constant cavitation number. An increased downstream pressure will therefore increase the

impulse loads according to equation (11) and the microjet velocity in equation (12). With an increase in flow velocity, the rate at which bubbles form is also increased. The increased pitting rate due to velocity increase tests for three different materials were originally carried out by Kim, et al. (2014) and their results are graphically illustrated in Figure 3-16.

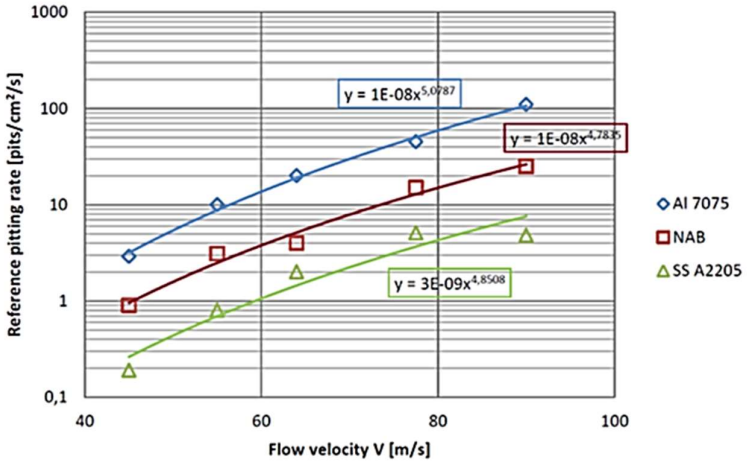


*Figure 3-16: Pitting rate at various fluid velocities [10]*

# 3.5 Limiting the effects of cavitation

## 3.5.1 Cavitation resistance of materials

The first method to reduce the effect of cavitation is by using materials that are more resistant to cavitation erosion. Laboratory test carried out by Garcia and Hammitt [12] found that the ultimate resilience (UR) of a material was the single most successful material property for preventing cavitation damage. The following properties were also tested (listed in decreasing order of success):

- tensile strength
- diamond pyramid hardness
- "true" strain energy
- "engineering" strain energy.

A cavitation resistance value $K_R$ is proportional to the deformation energy up to the point of fracture [25].

$$K_R = \sqrt{UR} \tag{17}$$

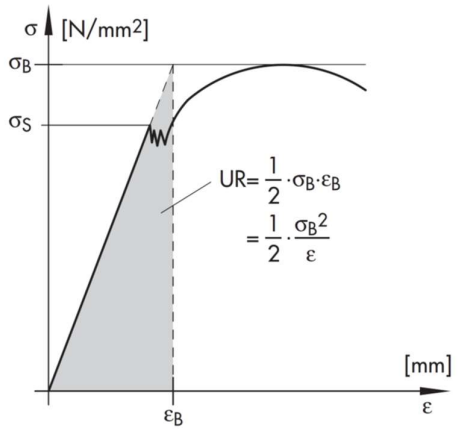


*Figure 3-17: Ultimate resilience [25]*

Figure 3-17 shows how to calculate the ultimate resilience (UR) also known as the Hobbs energy.

Heathcock [31] reported that the limitation of the concept of ultimate resilience is the assumption that all materials fail in a brittle manner. He found through his investigation that most materials failed in a ductile manner. In his report he recommended the following material properties for components used in an erosive cavitation environment:

- Alloys
- A high flow stress
- A high work hardening rate
- High strain to fracture
- A low stacking fault energy
- Ductile erosion mechanism
- A low notch and/or strain rate sensitivity
- No second phase particles.

Parcol [21] published a table showing the cavitation resistance of some common valve materials compared to that of stainless steel AISI 304/316. Table 2 below is reproduced and the values listed in brackets are for qualitative comparison only. For example the resistance to cavitation erosion of Stellite gr.6 is 20 times that of stainless steel AISI 304/316.

*Table 2: Cavitation resistance of some metallic materials [21]*

| **Index of resistance to cavitation** | |
|---|---|
| Stellite gr.6 | 20 |
| Chrome plating | (5) |
| 17-4 PH H900 | 2 |
| AISI 316/304 | 1 |
| Monel 400 | (0.8) |
| Gray cast iron | 0.75 |
| Chrome-molybdenum alloyed steels (5% chrome) | 0.67 |
| Carbon steels (WCB) | 0.38 |
| Bronze (B16) | 0.08 |
| Nickel plating | (0.07) |
| Pure aluminium | 0.006 |

From the table it can be seen that Stellite grade 6 offers the best resistance to cavitation of the materials listed which is why it is commonly used on severe duty valve components.

### 3.5.2 Valve design

In the past, valves and systems were designed to avoid the inception of cavitation. This has become an expensive method and is not always financially or technically feasible. More recently valves are designed to allow for cavitation inception, but the effect of cavitation erosion is reduced by moving the collapse of the cavities away from locations where damage can occur. The two methods in valve design are explained by EPRI [2]:

<u>No damage approach</u>

The no damage approach is referred to as the simplest approach, and consists of directing the outlet of the valve port so that the flashing and cavitation takes place away from any of the valve's surfaces. The general configuration of this design is the cage-style globe valve (Figure 3-18). The flow enters from the outside of the cage through small orifice like holes and collects in the centre of the cage.

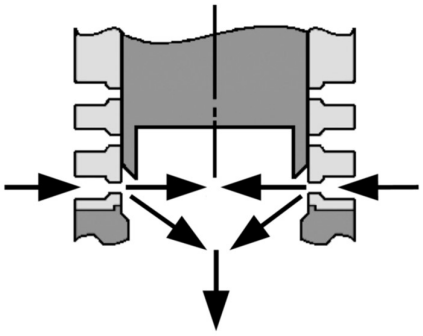

*Figure 3-18: Cage style globe valve [2]*

An assumption made for this design approach is that the velocity at the outlet of the orifice holes will be high enough to sufficiently recover the pressure to allow the cavitation bubbles to collapse in the centreline of the cage, away from the valve cage boundary.

Flashing/Cavitation prevention

Preventing cavitation erosion damage by avoiding flashing or cavitation inception is still the most commonly found method throughout the industry. The likelihood of the minimum pressure being lower than the vapour pressure is greater for high differential pressures. If the pressure drop can be achieved without the minimum pressure being lower than the vapour pressure, no flashing will occur. This can be achieved using multiple pressure drop stages each having a smaller differential pressure.

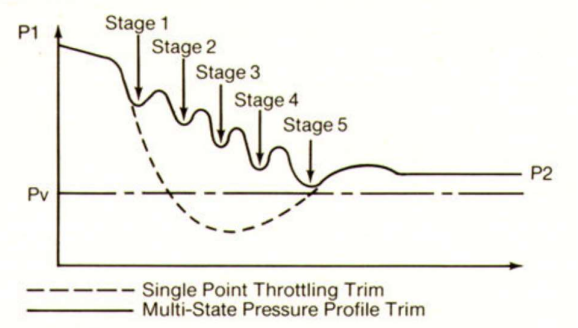


*Figure 3-19: Single vs multi-stage pressure drop [4]*

The pressure drop for a single stage valve is compared to a multi stage valve in Figure 3-19. The multi-stage valve is able to produce the same differential pressure as the single stage valve without the minimum pressure dropping below the fluid vapour pressure. To determine the number of stages is described in section 3.6.

### 3.5.3 Back pressure device

By installing a back pressure device (also known as a pressure sustaining valve) downstream of the leak off control valve, the outlet pressure of the leak off control valve can be controlled more accurately for a larger range of conditions. The back pressure device essentially acts as an additional pressure reduction stage with a controlled inlet pressure [10].

### 3.5.4 Cutting grooves into the flow boundary

Danlos et al. [34] found that by cutting longitudinal grooves (Figure 3-20) with chosen depth (h) and wavelength (λ) into the solid boundary surface can suppress cavitation, especially cloud cavitation which is the most aggressive type.

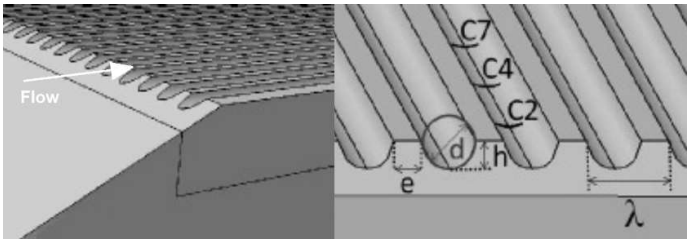


*Figure 3-20: Longitudinal grooves to suppress cavitation [34]*

### 3.5.5 Aeration

Injecting air into a system can also suppress cavitation, but only injecting small amounts of air into the system will increase cavitation due to an increase in the number of nuclei. Studies show that by increasing the amount of air injected into the system, the air content disrupts the explosive force of the imploding bubble which reduces the overall effect of cavitation erosion [10].

Some of these studies include the work completed by Tomov et al. [35] which found that injecting an air mixture into a cavitating flow of water causes radical effects on the cavitation dynamics. The investigation was based on the work completed by Davis (2008) and Dunn et al. (2010) which found that the point of cavitation inception can be spatially shifted if jet fuel fluid is aerated.

### 3.5.6 Controlling the pressure recovery

Lastly, a method to control the damaging effects of cavitation is to prevent or control the pressure recovery after the valve (Figure 3-21). This method is applicable to choked cavitation for certain valve designs, for orifices and venturies. At choked flow, the pressure at the vena contracta is at vapour pressure. If the pressure is maintained at vapour pressure, the area of cavity collapse can be

moved further downstream. The damaging effects caused by the bubble collapse can then be moved to a more suitable area downstream of the valve [22].

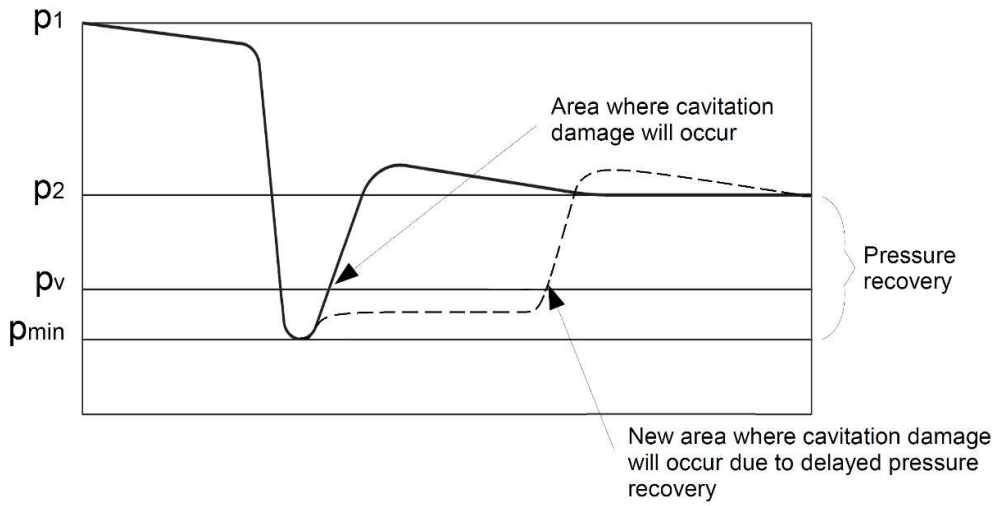


*Figure 3-21: Controlling the pressure recovery schematic*

### 3.5.7 Requirements to be met by manufacturers

SPX [4] recommends 4 requirements to be met by manufacturers to ensure cavitation free operation for valves with differential pressures higher than 124 bar:

1. The valve must be designed such that the trim is protected from cavitation damage between initial valve opening and full valve opening;
2. Foreign matter and pipe scale should not block the clearances causing galling or wire-drawing/cavitation;
3. The valve must provide zero seat leakage in the closed position;
4. The valve must maintain the zero seat leakage throughout a normal service life.

## 3.6 Relating theory to practice

Eisenberg [14] recommends that care must be taken when relating the different experimental results to practical systems. It is important to know at which cavitation number the onset of cavitation can be expected, but more importantly at which cavitation number the damaging effects of cavitation can be expected as these are not necessarily the same.

### 3.6.1 Coefficient of cavitation

The IEC [36] defines a coefficient of cavitation ($X_F$) which is used in the valve industry instead of a cavitation number. The coefficient of cavitation is also a ratio of pressure differences, similar to that of the cavitation number calculated in equation (3) and is formulated in equation (18) below.

$$X_F = \frac{p_1 - p_2}{p_1 - p_v} \tag{18}$$

The cavitation number calculation (3) has a wider range of possible values where negative values can be reached if the downstream pressure is lower than the vapour pressure. The coefficient of cavitation calculation (18) has a much smaller range (generally between zero and one), is always a positive value and reaches a value of one when the outlet pressure is equal to the vapour pressure. $X_F$ values of zero can be achieved only when the inlet and outlet pressures are the same and can never be negative as this will mean the outlet pressure is higher than the inlet pressure. Lower $X_F$ values indicate a lower risk of cavitation and the risk increases as the value of $X_F$ increases.

A valve specific cavitation coefficient is defined as $X_{FZ}$. When the operating conditions are such that the coefficient of cavitation ($X_F$) reaches the predefined $X_{FZ}$ value, the valve will suffer from cavitation. The value for $X_{FZ}$ is experimentally determined by measuring the sound levels or vibrations with accelerometers that are connected to the pipe. Figure 3-22 shows an example of such a test through the use of sound level measurement given by the standard IEC 60534-8-2 “Laboratory measurement of the noise generated by a liquid flow through a control valve” [21]. The point of incipient cavitation is indicated as the point where there is a sharp increase in the noise level.

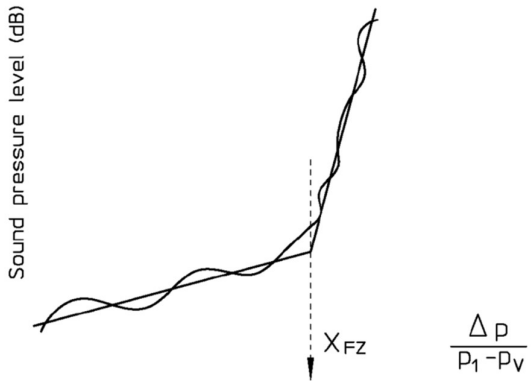


*Figure 3-22: Testing of the valve specific coefficient of cavitation [21]*

Process conditions where the measured coefficient of cavitation ($X_F$) is lower than the predefined value ($X_{FZ}$) the valve will not suffer from cavitation erosion. It is based on the conservative

assumption that the minimum pressure ($p_{min}$) of the fluid as it passes through the valve at all valve openings remains higher than the vapour pressure of the fluid ($p_v$), Figure 3-23.

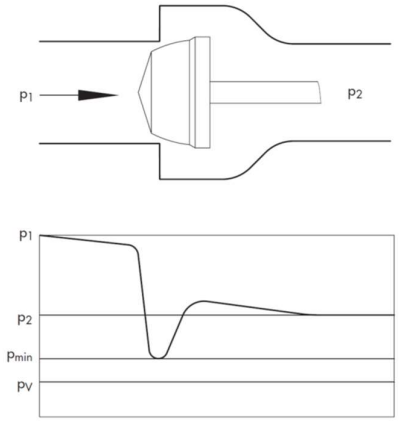


*Figure 3-23: Pressure distribution through a single stage control valve [25]*

## 3.6.2 Determining the number of pressure reduction stages

If a large pressure reduction is required, such as the case with leak off valves, it is most often recommended to use multi stage pressure reduction valves as explained in section 3.5.2.

In Eskom, the general rule of thumb is that a maximum pressure drop of 50 bar per stage is allowed. Samson [25] lists the recommended critical pressure drop per valve as a function of the valve type and amount of stages. The recommended maximum pressure drops are shown in Table 3 below for each of the valve designs.

*Table 3: Pressure differential limit values for preventing cavitation erosion [25]*

| **Valve design** | **$X_{Fcrit,cav}$ [-]** | **$\Delta P_{max,cav}$ [bar]** |
|---|---|---|
| Single-stage linear valve | 0.7 | 15 |
| Single-stage linear valve with stellited or hardened trim | 0.7 | 25 |
| 3-stage linear valves | 1.0 | 100 |
| 5-stage linear valves | 1.0 | 200 |
| Rotary plug valves | 0.4 | 10 |
| Butterfly and ball valves | 0.4 | 5 |

As the number of pressure reduction stages are increased, the allowable pressure differential per stage also increases. It can be seen that a single-stage linear valve will have an allowable pressure reduction of 25 bar if the trim is hardened or stellited. The 3-stage linear valve results in an allowable

limit of 33.3 bar per stage with the 5-stage linear valve a limit of 40 bar per stage, which is more conservative than the Eskom rule of thumb.

Parcol [21] simulated the flow through a single-stage and a multi-stage valve using computational fluid dynamics (CFD) software. The results are shown in Figure 3-24 below and it is clear that the pressure differential is not the same for all the stages. The first stage has the largest pressure reduction and the pressure drop per stage reduces with each stage. This is observed during transient state until a steady state is reached, assuming all stages are geometrically similar. It is also noted that the minimum pressure in the single-stage valve drops to below the exit pressure, which would of course then increase the risk of cavitation.

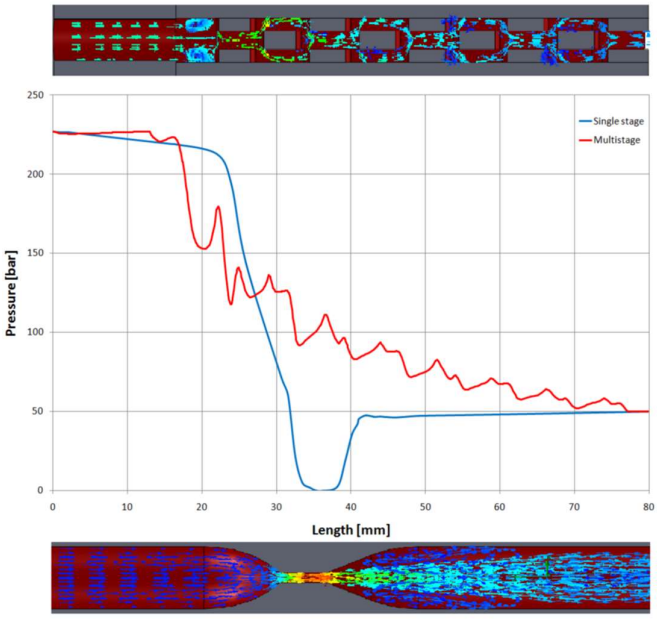


*Figure 3-24: CFD results of a single-stage and multi-stage valve [21]*

To determine the amount of stages required, it is assumed that the coefficient of cavitation value for each individual stage ($X_{FZi}$) is the same. The coefficient of cavitation value for the complete valve ($X_{FZ}$) is then given by:

$$X_{FZ} = 1 - (1 - X_{FZi})^n \tag{19}$$

Where n is the number of pressure reduction stages.

The valve flow coefficient ($K_v$) is the flow $m^3$/hr that passes through the valve, at a given valve position, that results in a 1 bar pressure drop. The $K_v$ value ratio of each stage is:

$$\frac{K_{vi}}{K_{vi+1}} = \sqrt{1 - X_{FZi}} \tag{20}$$

The $K_v$ value of an n-stage control valve is based on the $K_{vi}$ values for each individual stage and calculated as:

$$K_v = \frac{1}{\sqrt{\frac{1}{K_{v1}^2} + \frac{1}{K_{v2}^2} + \ldots + \frac{1}{K_{vn}^2}}} \tag{21}$$

To maintain a cavitation free operating pressure ratio ($X_F$), the number of pressure reduction stages (n) required can be calculated if the value of $X_{FZi}$ is known:

$$n = \frac{\lg(1 - X_F)}{\lg(1 - X_{FZi})} \tag{22}$$

The relationships between the number of stages, the coefficient of cavitation for the valve and per stage are shown in Figure 3-25 below. It is indicated that a 5-stage valve with the individual stages each having a coefficient of cavitation ($X_{ZFi}$) of 0.3 will have a valve coefficient of cavitation number of 0.84. It also shows that the valve's flow coefficient ($K_v$) value is 30% of the $K_{vn}$ value of the last stage [25].

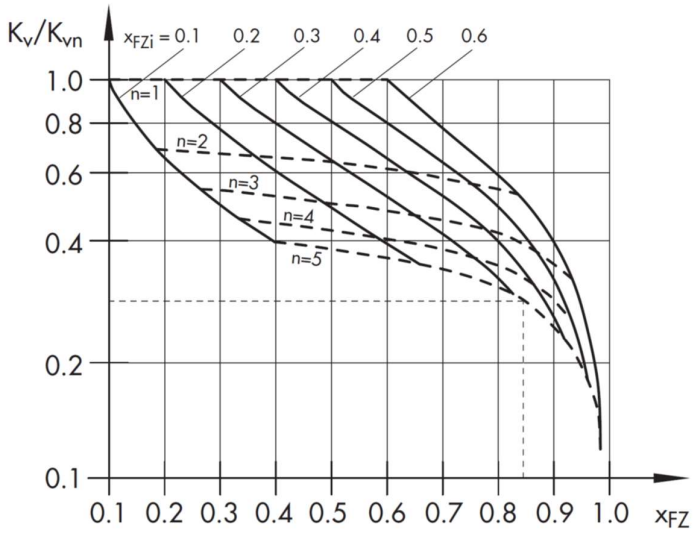


*Figure 3-25: Coefficients of cavitation for multi stage valves [25]*

From Figure 3-25 it can also be seen that for larger values of $X_{FZ}$, smaller values of the flow coefficient ratio exists. This means that for a low pressure recovery valve (high $X_{FZ}$ value) the valve requires a large opening ratio and relatively small $K_v$ values.

## 3.6.3 Scaling tests

Full scale cavitation tests are expensive and in most cases impractical due to the differences in valve geometry, high pressure and high flow requirement. In some cases, the tests can be scaled by

changing the test pressure or valve size to more practical conditions. The effects caused by scaling need to be applied in order to reach accurate full scale conditions.

In scaling experiments where the pressure is determined by the geometrical boundary conditions, the time of exposure to the low pressure will vary as well as the pressure gradients. With a decrease in model size, the pressure gradients will increase if the geometric boundaries are similar and the velocity remains the same. The dynamic response of the nuclei will initially be lagging and the initial appearance of observable cavitation inception will be delayed in an experiment of a smaller size if the properties of the liquid are independent of scale (unchanged nuclei size).

The view is consequently that the nucleus size must be inversely scaled at reduced scale model testing. In order for the nuclei to grow to an observable size, larger initial size of the nuclei must be present in the small scale experiments when the surface tension effects are considered for cavitation inception.

The number of nuclei must also be considered, as only some will grow to an observable size. For a reduced scale test, the number of nuclei must be greater than for a large scale test because the region of low pressure is reduced. Kermeen (1952) has conducted many experiments regarding the effects of scaling. His results show a definite dependence of the cavitation number for inception on the model size and absolute velocity. It can also be seen from Figure 3-7 that scaling tests cannot be correlated to Reynolds number only [14].

Scaling equations have been derived to adjust cavitation coefficients from one system pressure and size to another. Equation (23) below shows the correlation between the cavitation coefficients of a valve ($\sigma_V$) to that of the reference model ($\sigma_R$). Subscript R indicates the reference model. Data published by Tullis [37] was used to determine the correlation by the ISA [19].

$$\sigma_v = (\sigma_R SSE - 1)PSE + 1 \tag{23}$$

The size scale effect (SSE) is associated with the valve geometry whereas the pressure scale effect (PSE) is associated with the service environment [19].

The PSE is calculated as a power relationship between the difference of the actual expected valve inlet pressure and vapour pressure ($p_1 - p_v$) to the difference of the test values. The exponent, a, is based on empirical information from tests carried out on different valve types.

$$PSE = \left[ \frac{(p_1 - p_v)}{(p_1 - p_v)_R} \right]^a \tag{24}$$

The SSE can be calculated from the relationship of the valve diameter to the test valve diameter where the exponent, b, is a function of the valve characteristics such as $C_v$ and inlet diameter.

$$SSE = \left( \frac{d}{d_R} \right)^b \tag{25}$$

The ISA [19] does not recommend the application of size scale effect calculations to specialty, multi-stage, anti-cavitation valve designs which are the in fact the valve types used as leak off valves within Eskom.

For valves installed on a larger diameter pipe, reducers are used to join the smaller diameter valve to the larger diameter pipework. These reducers also have an effect on the cavitation level as they cause additional head losses and additional expansion at the valve outlet. For smaller diameter valves with larger $K_v$, the accuracy of the calculation method proposed by the ISA [19] becomes less certain.

Since a valve's geometry changes with the dimensions, scaled models are difficult to use, even considering the pressures scale effect (PSE) and the size scale effect (SSE). Using these two scaling parameters can still lead to results that are affected by other factors as explained above. For these reasons, predicting cavitation by using a numerical simulation analysis is very helpful [10].

## 3.7 Summary of literature review

Cavitation is a highly complex phenomena that is extensively studied, yet some aspects of it are still not clearly understood. For this reason numerical studies on cavitation often go hand in hand with experimental data. These studies are commonly completed with the focus on individual components such as a pump, valve, submerged body or aerofoil (of which the exact component geometries are known) and not on a system process level.

Discrepancies exists between process parameters for incipient and desinent cavitation. Water chemistry influence the surface tension of the water and causes a static delay between the vapour pressure and the actual static fluid pressure at which cavitation begins. The use of vapour pressure as the incipient pressure for cavitation is acceptable for general engineering studies.

Geometric flow paths with abrupt expansions and narrow restrictions which cause high local velocities create ideal conditions for cavitation development and are also preferable methods of pressure break down used in leak off system components. Components designed for high pressure breakdown are generally designed to avoid flashing by means of multiple pressure drop stages or by following the no damage approach. Maximum recommended pressure drops, dependent on the valve type and number of stages, as well as cavitation resistant materials are documented in international industrial standards through years of testing.

One dimensional steady state calculation is sufficient to determine areas and values of minimum pressure in process systems and is useful to determine the risk of cavitation. Most studies make use of a dimensionless cavitation number (σ), or coefficient of cavitation ($X_F$) as used in industry, to quantify process parameters as a reference at which the onset of cavitation can be referred to. Without actual test data as reference, the calculated cavitation number cannot be used to predict cavitation inception. It can however be used as a tool for understanding the risk of cavitation formation as the numerical value gives an indication of the proximity of the static pressure to that of the vapour pressure for each individual operating case.

Various factors such as fluid velocity, fluid temperature and duty cycle affects the intensity of cavitation erosion. Fluid temperature values around the midway between boiling and freezing temperatures of the fluid could increase the intensity of cavitation by a factor of 3.

Recommendations from industrial standards combined with process related simulation can be used to evaluate a system or set of components without having the detailed component geometries which is the intellectual property of the designer. A leak off system that contains a set of components can be simulated and the results can be used to categorize the components based on their risk of cavitation at various process conditions.

# 4. System simulation model development

The following sections describe the process that was followed to construct Flownex SE [38] models to simulate the different types of leak off systems found within Eskom. Flownex is a one-dimensional thermo-fluid network solver widely used throughout Eskom and other companies for modelling and simulation purposes such as process design, system analysis and process related investigations.

## 4.1 Data collection

At the start of the project as much relevant data as possible on the feed pumps and leak off systems were collected from all 15 of Eskom's coal fired power stations. The data included:

- Isometric drawings of the piping layout
- General arrangement drawings
- Heat balance diagrams of the turbine steam/water cycle
- Operating philosophies
- Pump characteristic curves
- Piping and instrument diagrams (P&IDs)
- Plant design information and system descriptions.

Line diagrams were developed from the collected plant data for each of the four leak off types. All the information needed to build and verify the model in Flownex was captured on the line diagrams. This included information such as piping dimensions, elevations, type and number of components and fittings as well as the positions and types of transmitters available for gathering process data. The development of the line diagrams made building of the Flownex models significantly easier as all the information was already captured and available from a single source. Figure 4-1 below shows the line diagram of Station O with the ARC type valve as an example.

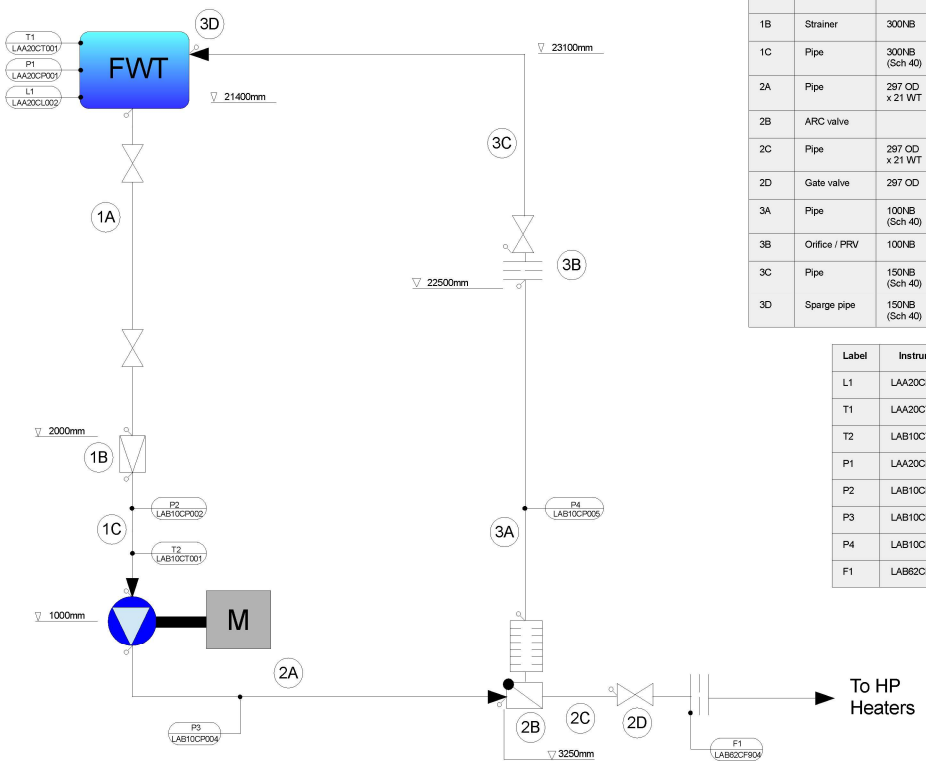


| Item | Description | Size | Length | Comment |
|---|---|---|---|---|
| 1A | Pipe | 300NB (Sch 40) | 38 665mm | 90 deg = 8<br>T branch = 1<br>Gate valves = 2 |
| 1B | Strainer | 300NB | 1 440mm | |
| 1C | Pipe | 300NB (Sch 40) | 4 100mm | 45 deg = 1 |
| 2A | Pipe | 297 OD x 21 WT | 4 100mm | 45 deg = 1 |
| 2B | ARC valve | | | |
| 2C | Pipe | 297 OD x 21 WT | 1 400mm | |
| 2D | Gate valve | 297 OD | | |
| 3A | Pipe | 100NB (Sch 40) | 47 755mm | 90 deg = 15<br>T straight = 1 |
| 3B | Orifice / PRV | 100NB | | Set at 12 bar / Dia 40mm |
| 3C | Pipe | 150NB (Sch 40) | 2 845mm | 90 deg = 2<br>Ball valve |
| 3D | Sparge pipe | 150NB (Sch 40) | 1 200mm | 3 holes (80 x 200 each) |

| Label | Instrument Tag | Description |
|---|---|---|
| L1 | LAA20CL002 | Storage tank liquid level |
| T1 | LAA20CT001 | Storage tank temperature |
| T2 | LAB10CT001 | Pump suction temperature |
| P1 | LAA20CP002 | Storage tank pressure |
| P2 | LAB10CP002 | Pump suction pressure |
| P3 | LAB10CP004 | Pump discharge pressure |
| P4 | LAB10CP005 | Leak off pressure |
| F1 | LAB62CF904 | Feed water flow |

*Figure 4-1: Line diagram for the ARC type leak off system*

## 4.2 Site selection

The site data was sorted and the 15 stations were divided into the four categories (Refer to Appendix A):

1. Binary type system with separate isolation and pressure reduction device
2. Binary type system where the isolation and pressure reduction is integrated in a single valve
3. Modulating valve type
4. ARC valve type.

Three representative sites were selected for modelling the different leak off types. The three selected stations contained the four different types of leak off systems and were selected based on their location, ease of access to information and the availability of operational data. Each station with its leak off system type is displayed in Table 4.

*Table 4: Selected stations and leak off system types*

| Station | Leak off type |
|---|---|
| Station A (Unit 1-5) | Binary type with separate isolation valve and pressure reduction device |
| Station A (Unit 6) | Binary type with integrated valve with pressure reduction device |
| Station K | Modulating valve type |
| Station O | ARC valve type |

## 4.3 Flownex components selection

Flownex offers a large range of process modelling components which the analyst can use to create any level of process complexity. Some components describe a specific industrial component, while others are generic types which can be used to emulate actual components. The choice of which component to use depends upon a proper understanding of the fundamental physics built into each component and it's applicability to the process to be modelled. The availability of information also plays a major role in component selection.

The following sections presents the chosen component that were used to represent the various actual system elements, motivated by presenting the fundamentals captured by the components.

### 4.3.1 Feed water tank (FWT)

Flownex offers a range of standard container components available to the user. The two most relevant components are a Two-phase tank and an Open container component. For both components, the user specifies the tank geometry and elevation as inputs with the difference in the process parameter inputs being the tank pressure or temperature and quality which can be set as boundary conditions on the tank.

A two-phase tank is essentially a fixed volume containing a fluid in mixture state at thermal equilibrium (i.e. vapour and liquid is at the same pressure and temperature). The quality of the fluid in the tank is used to calculate the physical level inside. For the majority of the operation the two-phase tank would be the ideal component to use as the FWT contains both steam and water during normal running plant conditions. For specific cases, such as cold start conditions where the fluid in the tank is subcooled, the two-phase tank cannot be used as the minimum achievable temperature is saturation temperature at the specified atmospheric pressure. These cases are of particular

interest in this project and therefore the open container was selected due to a wider range of conditions that could be simulated.

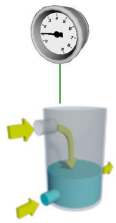

*Figure 4-2: Flownex open container component (FWT) with boundary condition*

For the open container the free surface pressure and fluid level is specified by the user as process input parameter and the temperature is specified as a boundary condition on the component.

On all sites the FWT fluid level, pressure and temperature are measured and could be used as direct input to the open container with only changing the gauge pressure readings from the plant into absolute pressure inputs for the model. This was done by adding the ambient air pressure for the specific site to the gauge pressure reading.

The software uses mass and energy conservation equations to solve the finite control volume of the open container component [39]. A control volume for the open container is depicted in Figure 4-3 below for reference.

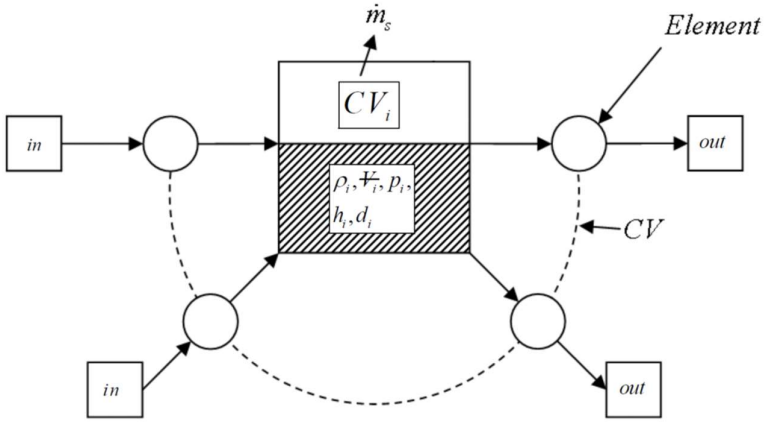


*Figure 4-3: Open container control volume [39]*

All the models only required the use of a single inlet (leak off system pipework) and a single outlet (pump suction pipework) from the open container. The mass flow of steam to the atmosphere from the control volume ( $\dot{m}_s$ ) was set to zero. The fluid properties within the control volume are denoted with subscript *i*.

Where

$\rho_i$ = control volume fluid density [kg/m$^3$]

$V_i$ = Total control volume [m$^3$]

$h_i$ = control volume fluid enthalpy [kJ/kg]

$p_i$ = control volume pressure [kPa]

$d_i$ = control volume mass source [kg/s]

The software assumes one dimensional flow at the inlet and outlets with the fluid conditions to be static when the container volume is specified.

The relative height of the outflow can be specified, which either will result in liquid or saturated vapour at the exit. For this case, the outlet was set at the bottom.

### 4.3.2 Piping

*Figure 4-4: Flownex pipe component*

The standard Flownex pipe component was used which includes arrows that show the chosen positive direction of flow. The geometry of the pipe was selected from the built in table in the software to correspond to the geometry found on site. For the majority of pipework this included the nominal pipe size and schedule. By specifying these values, the software automatically calculates the pipe inside diameter. In some instances where the pipe sizes on site are custom, the pipe inside diameter was directly specified as an input.

The overall pipe length (L) was also added as an input as it is used to determine the pressure drop across the piping section as can be seen in the Darcy Weisbach equation below. For pipes that contain a non-return valve (NRV) the pipe component was set to prevent reverse flow. By activating this parameter the calculated direction of flow is compared to the assigned flow direction of the component. If reverse flow is found, the piping section acts as if isolated and the flow is set to 0.

The majority of the plant's BFP pipework are still in good condition based on inspection reports hence the roughness of all the pipe sections was set at 67.5 µm which is the built in roughness value for commercial steel in the software. The pipe inside wall roughness is used to determine the

dimensionless friction factor (f) also known as the Fanning friction factor which is used in the Darcy Weisbach formula.

For single phase, incompressible flow, the pressure drop is calculated as follows:

For laminar flow (Re<2300), the friction factor is independent on the surface roughness and is calculated as:

$$f = \frac{64}{\mathrm{Re}} \tag{26}$$

For turbulent flow ($5000 \leq \mathrm{Re} \leq 10^8$ and $10^{-6} \leq \left(\frac{e}{D}\right) \leq 10^{-2}$) the friction factor is calculated using:

$$f = \frac{0.25}{\left[\log\left\{\left(e/3.7D\right) + 5.74/\mathrm{Re}^{0.9}\right\}\right]^2} \tag{27}$$

Where

$f$ = friction factor

$e$ = pipe inside wall surface roughness [µm]

$\mathrm{Re}$ = Reynolds number

$D$ = pipe diameter [m]

In the transition region between laminar and turbulent flow (2300<Re<5000) a linear interpolation is done between equation (26) and (27).

The total loss coefficient value (K), which is the sum of the secondary losses ($K_s$) and the built-in sharp edged orifice ($K_R$), is automatically calculated by the software by simply selecting the type and amount of fittings for the section of pipe. The given secondary loss coefficient values for the standard fittings are based on literature or manufacturer's data and the effect thereof on the pressure drop is defined as:

$$K_s = \frac{\Delta p_{0s}}{1/2\rho U^2} \tag{28}$$

$K_s$ = sum of all secondary loss coefficients

$\Delta p_{0s}$ = total pressure drop across the component [Pa]

$\rho$ = density of the fluid [kg/m$^3$]

$U$ = mean velocity based on the pipe inside diameter [m/s]

Each piping component in the software has a build-in orifice that can be used to simulate a sharp edged orifice or in case of more detailed orifice designs the user can use a separate orifice element. For this section the loss coefficient of sharp edged built-in orifices ($K_R$) were left to be zero because all the orifices were handled separately (see the paragraph on restrictors with discharge coefficients below).

The total pressure drop over each piping section using the incompressible steady state is then:

$$\Delta p_0 = \left( \frac{fL}{D} + \sum K_s + K_R \right) \frac{\rho |U| U}{2} + \rho g \Delta z + \frac{1}{2} K \rho |U| U \tag{29}$$

Where

$f$ = friction factor

$L$ = length of the pipe [m]

$D$ = inside diameter of the pipe [m]

$\rho$ = fluid density [kg/m$^3$]

$U$ = mean velocity based on pipe diameter [m/s]

$K$ = forward or reverse loss coefficient

$\Delta z = z_e - z_i$ = static height difference between inlet and outlet [m]

$\sum K_s$ = some of secondary loss coefficients such as bends and valves

$K_R$ = loss coefficient of sharp edged orifices

Two phase flow:

It is expected that two phase flow will develop in the leak off valve and pipework as the pressure is reduced. Flownex uses empirical multipliers which are applied to the frictional component losses and the secondary pressure losses. These multipliers are added to the single phase pressure drop calculations for all fittings selected as part of the piping component to include the effects caused by the two phase mixture.

The frictional multiplier is calculated using the Lockhart-Martinelli method which can be manipulated to give a single two-phase friction factor ( $f$ ) in terms of the individual gas and liquid component friction factors and densities by considering the quality of the two phase fluid.

### 4.3.3 Strainers

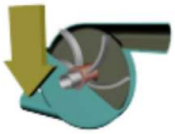

*Figure 4-5: Flownex user specified pressure drop component*

Strainers do not always behave like pipes or orifices, hence it is better to make use of an empirical pressure drop relationship. A user specified pressure drop component was therefore used to represent the strainers. Pressure drop versus flow rate correlations were created based on process data collected from site. When the trainers start to block, an alarm in the control room initiates. The strainers are cleaned before any significant effect can be seen on the pump discharge.

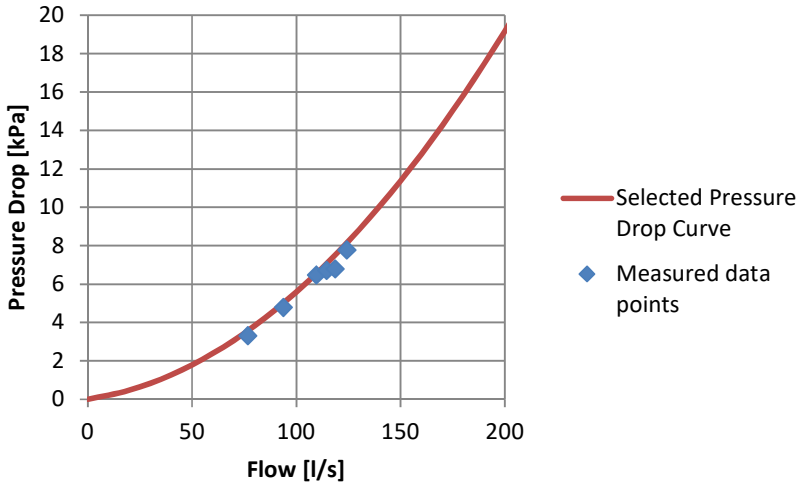


*Figure 4-6: Suction Strainer pressure drop correlation*

Figure 4-6 shows the correlation developed between the suction strainer deferential pressure and the measured flowrate passing through the strainer. The reference density used was averaged with only cold water conditions (cold start of the units) used to plot the data points. A quadratic curve was used to correlate the flow to the expected pressure drop over the strainer. Good agreement was achieved due to the common quadratic nature of pressure drop vs flow velocity, see equation (29).

This correlation was then used as input for the user specified pressure drop component seen in Figure 4-7. The software automatically scales the pressure drop vs volume flow rate curve depending on the determined density when calculating the pressure drop.

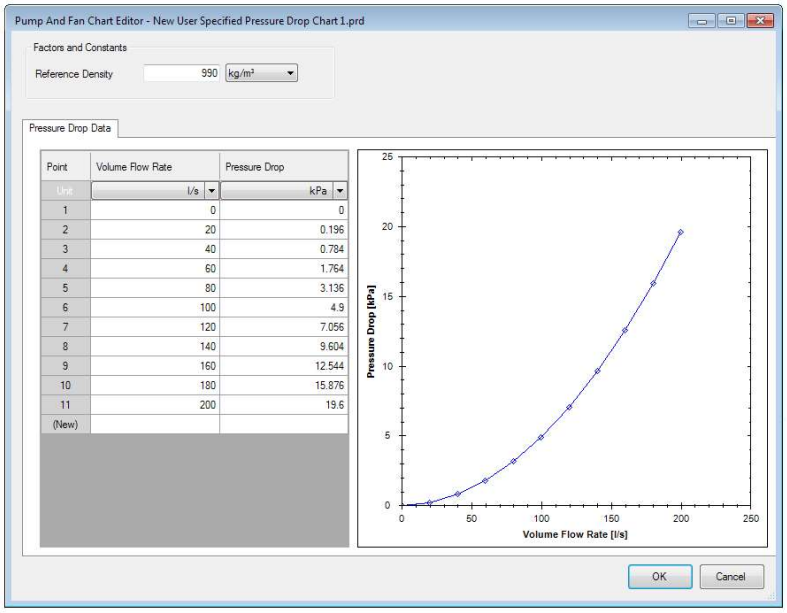


*Figure 4-7: Suction strainer user specified pressure drop input*

## 4.3.4 Orifice and sparge pipes

*Figure 4-8: Flownex restrictor with discharge coefficient component*

Restrictors with discharge coefficients were used to represent all narrow openings used as throttling devices such as orifices and sparge pipes. The sparge pipe design shown in Figure 4-9 below is the most complex of all the designs and is installed at Station K. It consists of two orifice like plates in series (each with 3 holes) and a 3rd stage orifice-like endcap with a single hole.

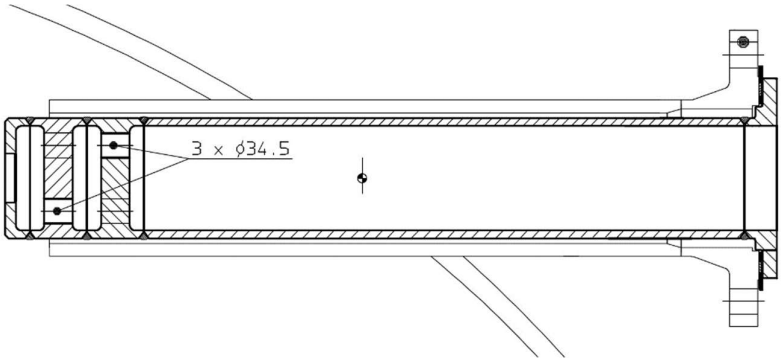


*Figure 4-9: Sparge pipe (Desensitised from undisclosed source)*

This sparge pipe was modelled using a single orifice (with 34,5mm diameter hole) component representing each stage, 3 orifice components in series. The software allows the user to specify if more than one orifice is installed in parallel. The number of orifices in parallel for this case was set to 3, which is the amount of holes for stage 1 and 2. Stage 3 was modelled using a third orifice in series with a single hole.

The discharge coefficient ($C_d$) is a function of the ratio of the pipe diameter and the orifice diameter.

$$C_d = 0.5959 + 0.0312\beta^{2.1} - 0.184\beta^8 + 0.0029\beta^{2.5}\left[\frac{10^6}{\mathrm{Re}}\right]^{0.75} + \kappa L_1\beta^4\left(1-\beta^4\right)^{-1} - 0.0337L_2\beta^3 \quad (30)$$

Where

$\beta$ = diameter ratio d/D

$L_1$ = $l_1$/D the quotient of the distance of the upstream pressure tapping point from the upstream face of the orifice plate divided by the pipe diameter

$L_2$ = $l_2$/D the quotient of the distance of the downstream pressure tapping point from the downstream face of the orifice plate divided by the pipe diameter

$\kappa$ = 0.09 if $L_1$ < 0.4333 or 0.39 if $L_1$ > 0.4333

The pressure drop across the orifice is a function of the effective cross sectional throat area and for incompressible flow the pressure drop is calculated by

$$\Delta p_0 = \frac{\rho Q^2}{2\left(C_d A\right)^2} \quad (31)$$

where

$\rho$ = mean density based on pressure and temperature in kg/m$^3$ and

Q = volume flow rate based on the density in m$^3$/s.

A is the actual throat area of the restrictor [m$^2$] and $C_d$ is the discharge coefficient.

For two phase flow, Flownex makes use the following equation to calculate the pressure drop:

$$\Delta p_0 = p_{01}\left(1-\frac{p_s}{p_{01}}\right) \quad (32)$$

where

$p_{01}$ = upstream total pressure [Pa]

$p_s$ = static pressure in the throat of the restrictor [Pa].

The mass flow rate is given by

$$\dot{m} = \rho_2 \sqrt{2\left(h_{01} - h_2\right)} C_d A \tag{33}$$

where the density $\rho_2$ is determined from the two-phase property table.

### 4.3.5 Pressure regulating valve

*Figure 4-10: Flownex pressure regulating valve component*

The pressure regulating valve (PRV) element in Flownex was used to represent the back pressure valve installed at Station O. These valves are installed on two units and it was proposed by the contractor to replace the remaining units' orifices with back pressure valves.

The flow characteristics of the PRV element in Flownex are not dependant on the valve geometry and are governed by reference data the user specifies as input. The valve fully open reference characteristics are used to determine the valve flow characteristics when fully open and subsequently the valve's pressure regulating range.

For this model the element was set to control the upstream pressure at the specified set point from the contractor's manual, which is 1200 kPa. The fully open mass flow rate reference, fully open pressure differential reference and fully open reference density was based on the design information given to the contractor at the time of the initial design change.

The valve fully open reference characteristic constant $k_{ref}$ is determined using the formula:

$$k_{ref} = \frac{2\Delta p_{0ref}}{\rho_{ref} \dot{m}_{ref}^2} \tag{34}$$

The pressure regulating range of the PRV is represented in Figure 4-11 below.

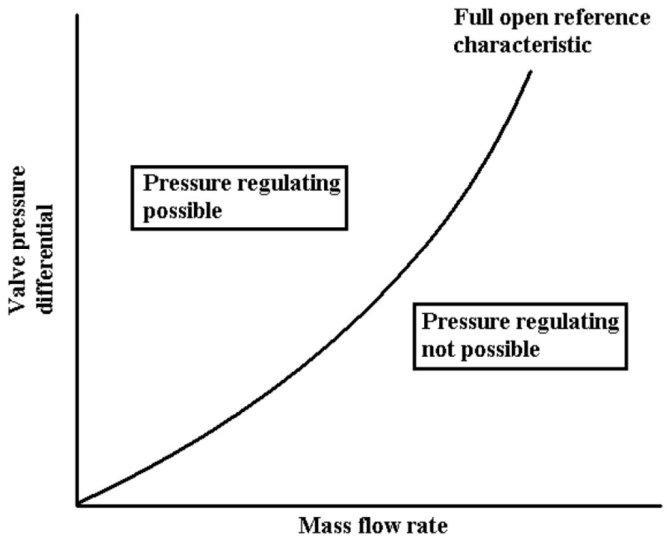


*Figure 4-11: Pressure regulating range schematic for the PRV in Flownex [39]*

The PRV therefore regulates the upstream pressure at the specified set point and determines the pressure differential based on the mass flow rate.

### 4.3.6 Pumps

*Figure 4-12: Flownex variable speed pump component*

The applicable pump OEM performance test curve was used as input for the variable speed pump element for each model. Figure 4-13 below shows the input to the variable speed BFP element. A single characteristic curve was used as input with a reference speed and reference fluid density. For a variation in shaft speed, the curve is automatically adjusted by the software using pump scaling laws.

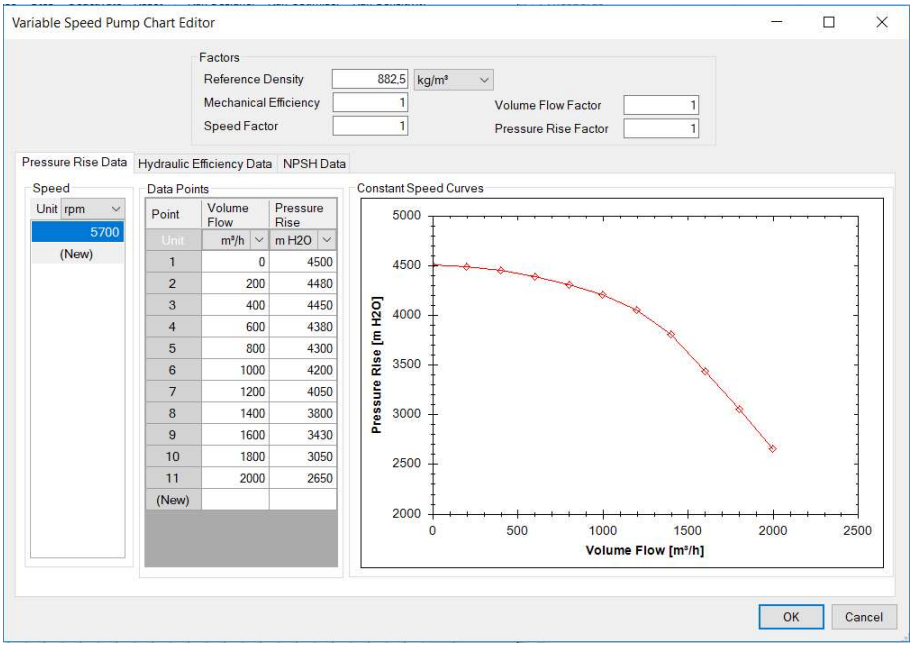


*Figure 4-13: Input table for the boiler feed pump*

With only one curve given as input, the software uses the following formula to determine the new volumetric flow rate ($Q_2$) and head ($H_2$) at the new rotational speed ($N_2$):

$$\frac{Q_2}{Q_1} = \frac{N_2}{N_1}$$
$$\frac{H_2}{H_1} = \left(\frac{N_2}{N_1}\right)^2 \quad (35)$$

A more accurate method is also available which uses a linearly interpolated result between multiple curves for different speeds, but the majority of the simulated pumps for this study are single speed pumps (all boosters as well as main pump for Station O) and the single curve input method proved to be sufficiently accurate within the expected boiler feed pump operating range when compared to the actual measured pump performance.

The software has a built in unit selector that allows the user to select the units of measure for the volumetric flowrate and pressure rise through the pump. This function simplified the process as the values from the actual pump characteristic curves could be taken directly from the different suppliers' data sheets and was automatically converted by the software to the units measured on site.

### 4.3.7 Nodes and elevation

*Figure 4-14: Flownex node component*

Large elevation differences exist between the FWT and the BFP. There is also a specific interest in the static pressure at various points throughout the system to determine if/where flashing is taking place. The effect on pressure due to elevation is thus an important concept for this study.

For this reason, the elevation of each component and node in the models was specified to correspond to the elevation found on site.

The difference in elevation is also factored into the Darcy Weisbach equation (29), the ΔZ component, as well as the pressure head of the level in the tank which is used within the software.

### 4.3.8 Leak off valves

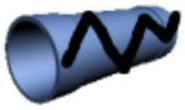

*Figure 4-15: Flownex flow resistance component*

Flow resistance components and ANSI control valves were used to represent the leak off valve and pressure reduction components.

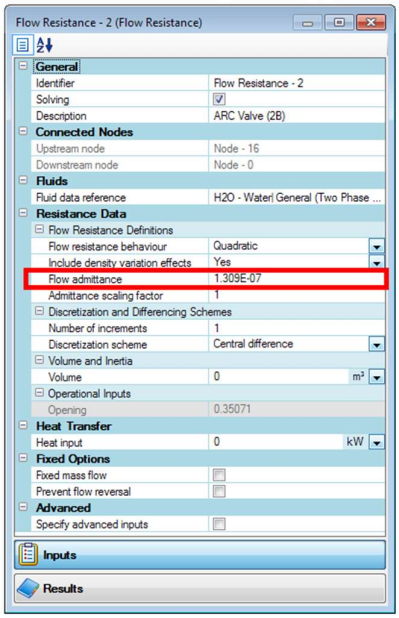


*Figure 4-16: Flow resistance input for ARC type valve*

Flow resistance components with quadratic and linear resistance behaviour were used, depending on the valve or pressure reduction device characteristic. The flow admittance ($A_f$), shown as an input parameter in Figure 4-16, was selected by using the designer function in the software such that it correlates with process data captured from site when the leak off valve was in the 100% open position. The designer tool allows the user to specify constraints with a target value and an independent variable. It then uses a gradient-based optimization routine to find the values for the independent variables to ensure the constraint target values are met.

A quadratic or linear resistance behaviour can be specified dependant on the device characteristics. A quadratic resistance behaviour is selected for pressure drop versus typical flow through typical pressure drop components such as the ones used in this study. Some valve geometries result in a linear change for which the linear resistance behaviour model must be used.

The total pressure drop over such a quadratic device is defined as:

$$\Delta p_0 = \frac{|\dot{m}|\dot{m}}{A_f \cdot A_{sf} \cdot A_O} + \rho g \Delta Z \tag{36}$$

where

$\dot{m}$ = mass flow through the component [kg/s]

$\Delta Z$ = difference in elevation of the outlet to the inlet [m]

$A_f$ = flow admittance

$A_{sf}$ =admittance scaling factor

$A_O$ = opening of the component.

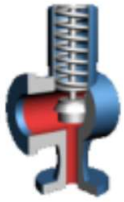

*Figure 4-17: Flownex ANSI control valve component*

For the modulating type system (Station K) an ANSI control valve component was used to represent the leak off valve. Station K has no pressure or flow transmitters on the leak off system. Without the process data no correlation could be drawn between the flow passing through the system and the pressure drop across the valve. The only information available was the valve flow coefficient ($C_v$) which was specified in the valve manual.

The mass flow rate through the ANSI control valve is given as a function of the pressure drop over the valve:

$$\dot{m} = N_1 F_P F_R C_v \sqrt{\frac{\rho_w \left( p_1 - p_2 \right)}{\rho}} \tag{37}$$

where

$N_1$ = numerical constant dependent on the measurement units used (value can be calculated from data found in ANSI/ISA standard 75.01– 1985 (R1995))

$F_P$ = piping geometry factor

$F_R$ = Reynolds number factor (value can be calculated from data found in ANSI/ISA standard 75.01–1985 (R1995))

$C_v$ = valve flow coefficient defined as the volume flow rate (US GPM) of 60°F water that flows through a valve with a 1psi pressure drop

$\rho$ = fluid density [Unit dependent on the numerical constant found in ANSI/ISA standard 75.01–1985 (R1995)]

$\rho_w$ = fluid density of water at 15.6˚C [Unit dependent on the numerical constant found in ANSI/ISA standard 75.01–1985 (R1995)]

$p_1$ = absolute pressure measured upstream of the valve [Unit dependent on the numerical constant found in ANSI/ISA standard 75.01–1985 (R1995)]

$p_2$ = absolute pressure measured downstream of the valve [Unit dependent on the numerical constant found in ANSI/ISA standard 75.01–1985 (R1995)].

### 4.3.9 Valve control

*Figure 4-18: Flownex quick script component*

A script component was used to model the control of the leak off valve opening. In cases where the leak off valve opening is not measured / controlled by an actuator, the opening was varied through trial and error or by using the designer tool within the software. This was done until the expected downstream conditions (pressure or flow) were reached for various operational and valve opening cases.

The flow passing through the pump is calculated by the software as a steady state condition. The flow value is then used as input to the script. The script is worded as a series of "IF" functions which then returns the leak off valve opening as an output. The input and output components are joined to the script using data transfer links, see Figure 4-19 below.

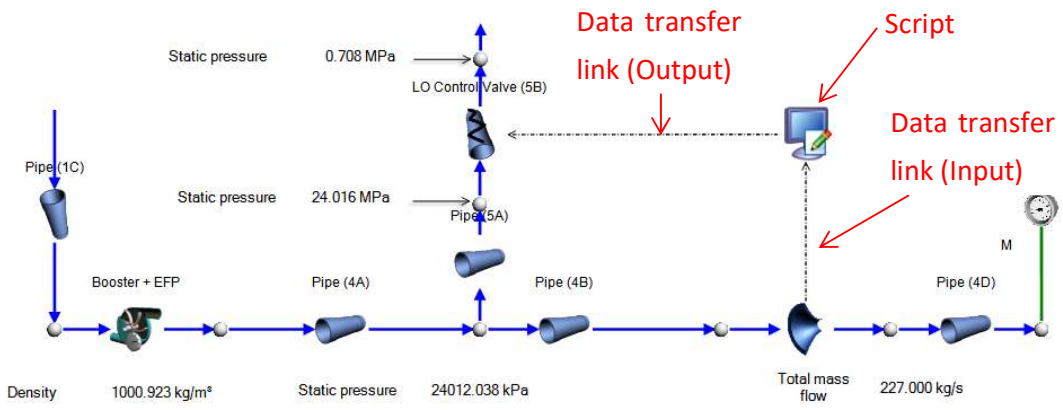


*Figure 4-19: Scripting and transfer link icons*

**Binary valve scripting**

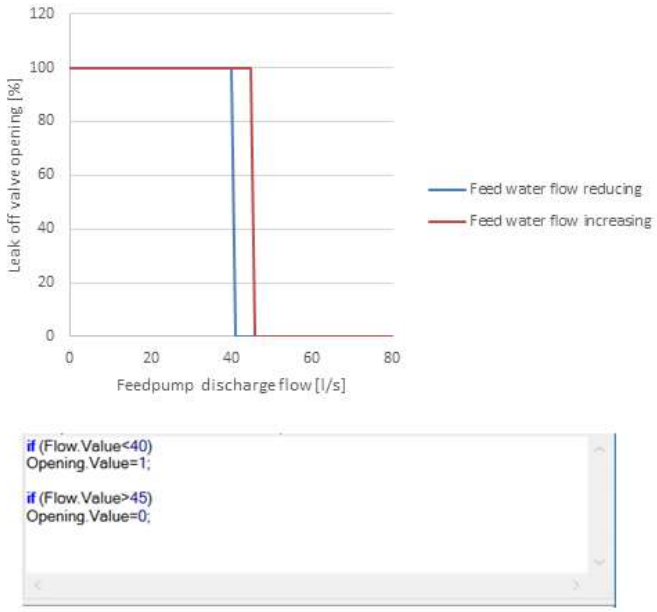


*Figure 4-20: Binary valve script*

Figure 4-20 shows the script for the binary valve type. The scripting for the binary valve was developed based on the operating and control philosophy of Station A. It allows the valve to be fully closed at a volume flow rate higher than 45 l/s and fully open at volume flow rates less than 40 l/s. The flow for each pump is measured downstream of the main boiler feed pump outlet.

**Modulating valve scripting**

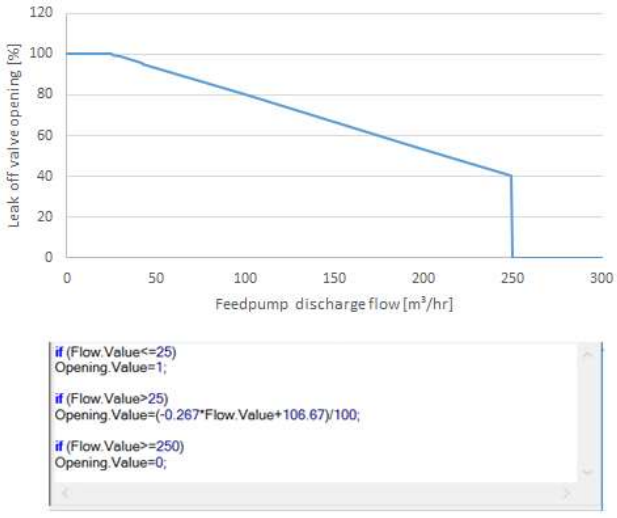


*Figure 4-21: Modulating valve script*

Figure 4-21 shows the scripting used for the modulating leak off valve of Station K. The equation was extracted from the control system logic documentation. The volume flowrate [$m^3$/hr] is measured at the intermediate pipework between the booster and main BFP.

The script opens the valve fully at volume flow rates less than 25 $m^3$/hr and closes the valve at volume flow rates higher than 250 $m^3$/hr. At volume flow rates between 25 and 250 the script uses a linear sliding scale that opens the valve more as the volume flow rate decreases.

**ARC valve scripting**

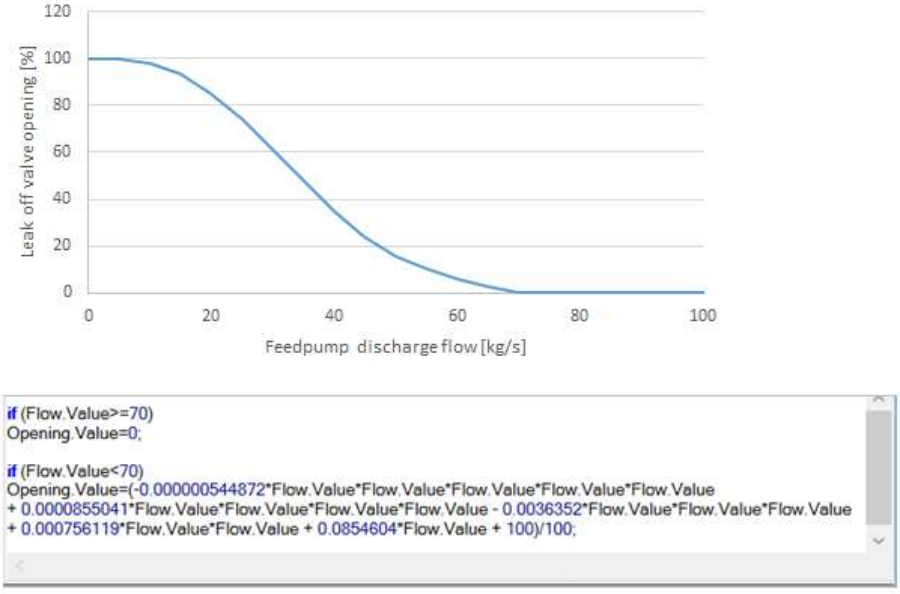


*Figure 4-22: ARC valve script*

The scripting that controls the ARC valve opening was completed through a trial and error process. The valve is not controlled by an actuator and does not have any form of position switch or percentage open indication. It was first assumed that the leak off bypass opens linearly as the forward feed flow is reduced. The actual leak off line pressure, measured at the outlet of the leak off valve, was compared to the pressure determined by the model at various load cases. It was then found that the valve follows a non-linear opening trend, see Figure 4-23. The non-linear trend can be due to two reasons: 1) a non-linear motion by the lever that connects the leak off bypass section of the valve to the NRV plug spindle or 2) due to variation in the flow area of the bypass pressure reduction section of the valve.

It was also found that the leak off bypass section of the valve is fully closed when the forward flow reaches 70 kg/s. This was done by monitoring the decreasing leak off line pressure of the running pump as the feed water flow increases and noting the mass flow rate at which the leak off line pressure reaches the same leak off line pressure as the standby pump.

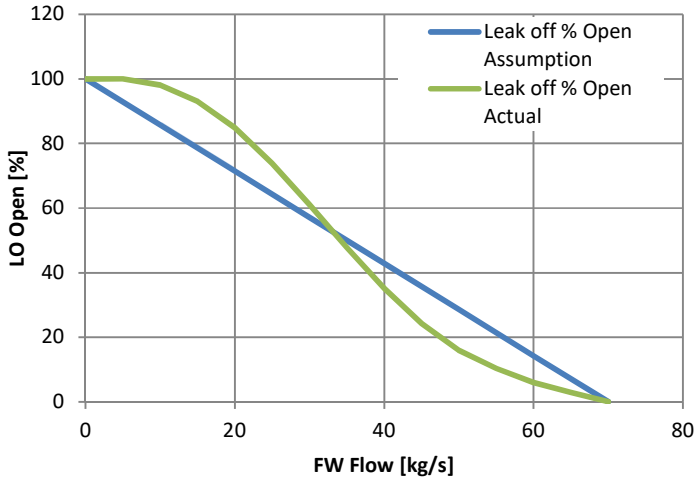


*Figure 4-23: ARC valve percentage open trend*

The flow measured at Station O is a common measurement for both 100% pumps. All tests were therefore done with only one pump in operation. The flow rate is measured in mass flow [kg/s] which is done downstream of the HP heaters just before the economiser inlet. The script was completed by using the data from Figure 4-23. For mass flow rates higher than 70 kg/s the valve is fully closed and for mass flow rates lower than 70 kg/s, the valve opening follows the fifth order polynomial trend above.

## 4.4 Model setup methodology

A model was created for each of the four different leak off system types as per the selection given in section 4.2. The line diagrams were used as the major source of information. The models represent the plant in a simplistic manner with the individual components named and numbered similar to the line diagrams for ease of reference.

Each model was built using the same methodology with only some changes to the input parameters and component types used, depending on the availability of information or the design of the plant. Water with a two-phase characteristic was selected as the fluid medium.

First the forward feed section of the plant was built and simulated (see Figure 4-24). This section includes the feed water tank (FWT), the suction pipework including strainers, booster pump and intermediate pipework (where applicable), the main feed pump and the discharge pipework up to a predetermined boundary point before the high pressure (HP) heater inlet.

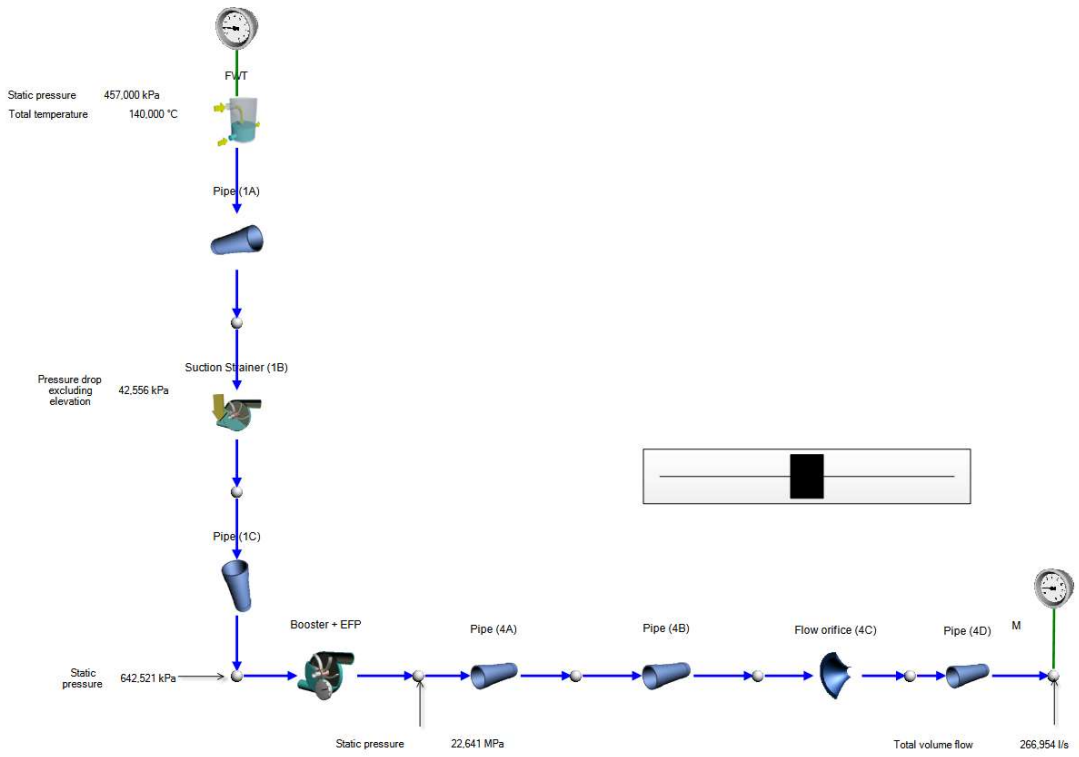


*Figure 4-24: Forward feed model (Station A)*

When the layout was completed, the geometries and characteristics of each component was added based on the design and construction information available, or through correlations that were drawn based on transmitter measurements from actual plant instrumentation.

The simulation was then run at various forward feed load cases and compared to the actual plant instrumentation measurements (site conditions where the leak off valves are closed) to determine the accuracy of the forward feed case. A slider bar, as depicted in Figure 4-24, was used for quick adjustment of the feed water flow rate to re-run the simulation and removed when the parameter table (Figure 4-26) was populated with the various load case parameters.

Following this, the model was optimised for these cases to replicate the plant within an acceptable error margin of 3%. This mostly involved varying the feed pump characteristic curve. These changes could be due to a difference in pump performance from the available pump curve as a result of improvements to the pumps over the years, lower pump efficiencies due to wear, variation in characteristic curves for similar design pumps due to manufacturing tolerances or inaccurate pump speed measurement (as was found on Station A for example).

With the forward feed section within acceptable tolerance, the leak off section was added to the model. The geometries and component characteristics were then added to the leak off line components.

In cases were design or construction information for the high pressure drop components were not available, a flow resistance component was used. Correlations drawn from plant transmitter readings were used to adjust the flow admittance of the component using the designer function in the software to mimic the results from the correlations. This was done for the operating case where the leak off valve was at 100% open. The leak off valve was then set open at various percentages and the results from the model were compared to site process data. If required, the correlations were reviewed, updated and the process was repeated.

Lastly, a script component was added to control the opening of the leak off valve based on the type of system.

## 4.5 Simulation boundary conditions

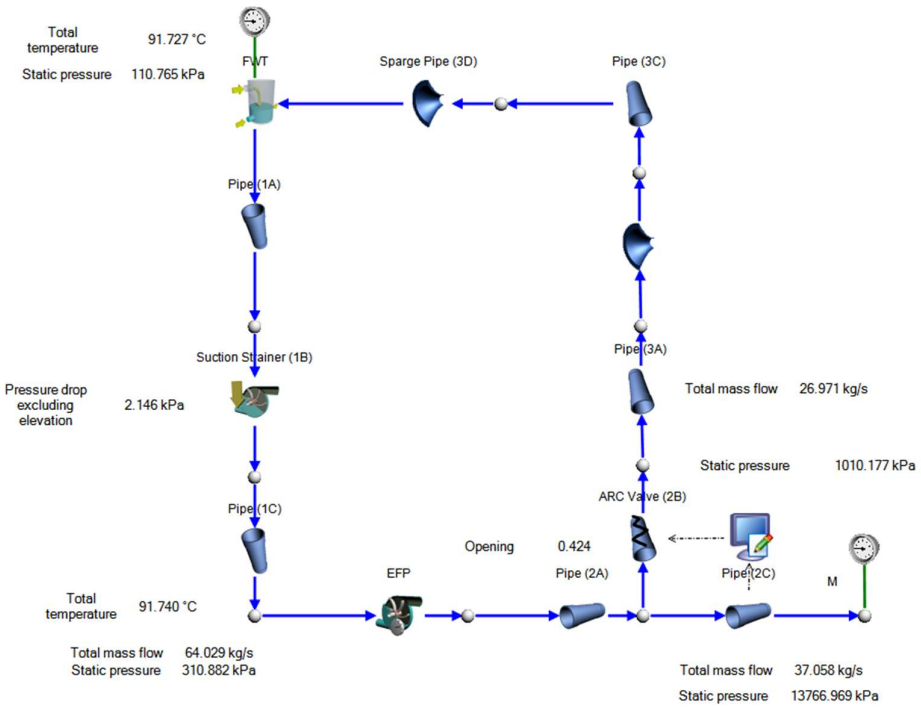


*Figure 4-25: Flownex model of the ARC type leak off system (Station O)*

Figure 4-25 shows a solved steady state model for Station O (ARC type valve) with the leak off bypass in the 100% open position as an example.

The models are set up such that some boundary conditions are specified as input parameters. These boundary conditions are typically the conditions in the feed water tank and feed water system upstream of the HP heater inlet. The input parameters specified will determine the load case to be simulated. The inputs required for each model are set out in Table 5 below.

*Table 5: Input parameters for Flownex models*

| Parameter | Station A | Station K | Station O |
|---|---|---|---|
| Feed Water Tank (FWT) Pressure (absolute) | X | X | X |
| Feed Water Tank (FWT) Temperature | X | X | X |
| Boiler Feed Pump (BFP) Speed | X | X | |
| Feed water Flow | X | | X |
| Feed water pressure (absolute) | | X | |

To fully define the models, a pressure or mass source needs to be specified at a boundary point downstream of the leak off connection to the feed water pipework. The models for Station A and O use a mass source as the boundary condition downstream of the BFP on the feed water section because the pressure tapping points for the main BFP discharge are located upstream of the leak off connection. A pressure boundary can only be used if the pressure measurement is at the network outlet. The flow rate is measured at a location downstream of the leak off line tap off point.

For Station O the mass flow rate at the pump outlet is assumed to be equal to the mass flow rate at the economiser inlet with the attemperator spray water closed, therefore assuming no vent or drain valves are open and that there are no tube leaks in the heaters.

It was not possible to specify the feed water flow rate for Station K downstream of the leak off tapping point as the flow rate is measured between the booster and main BFP. For this reason the pressure on the common discharge pipework was used which requires the model to include all the pipework and fittings up to this point.

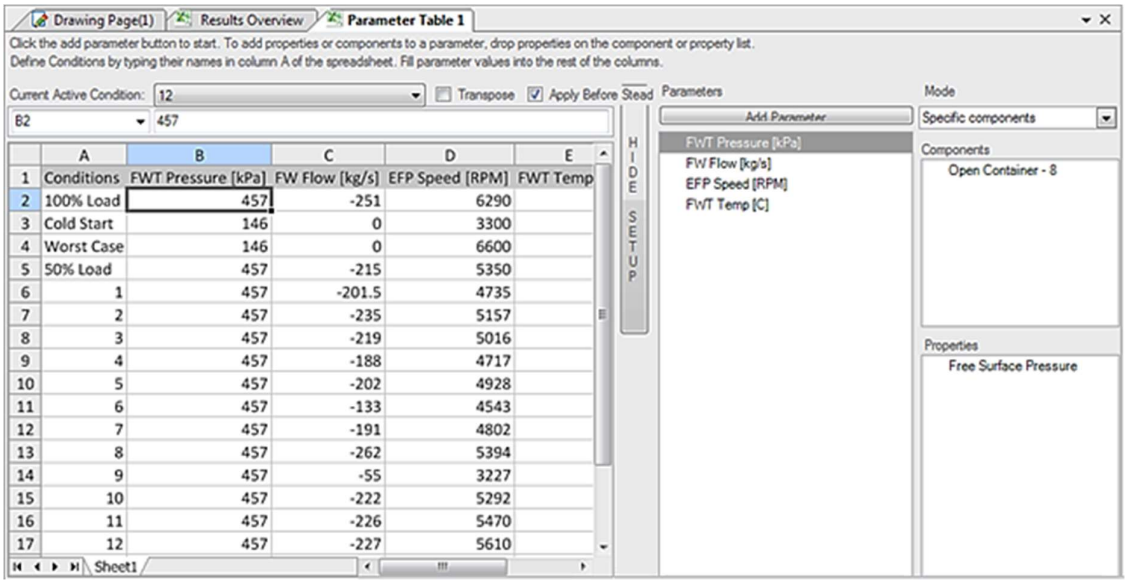


| | A | B | C | D | E |
|---|---|---|---|---|---|
| 1 | Conditions | FWT Pressure [kPa] | FW Flow [kg/s] | EFP Speed [RPM] | FWT Temp |
| 2 | 100% Load | 457 | -251 | 6290 | |
| 3 | Cold Start | 146 | 0 | 3300 | |
| 4 | Worst Case | 146 | 0 | 6600 | |
| 5 | 50% Load | 457 | -215 | 5350 | |
| 6 | 1 | 457 | -201.5 | 4735 | |
| 7 | 2 | 457 | -235 | 5157 | |
| 8 | 3 | 457 | -219 | 5016 | |
| 9 | 4 | 457 | -188 | 4717 | |
| 10 | 5 | 457 | -202 | 4928 | |
| 11 | 6 | 457 | -133 | 4543 | |
| 12 | 7 | 457 | -191 | 4802 | |
| 13 | 8 | 457 | -262 | 5394 | |
| 14 | 9 | 457 | -55 | 3227 | |
| 15 | 10 | 457 | -222 | 5292 | |
| 16 | 11 | 457 | -226 | 5470 | |
| 17 | 12 | 457 | -227 | 5610 | |

*Figure 4-26: Input parameter table*

To simplify the process of running specific operating cases, preselected input parameters were added to a parameter table that replicates various load cases. From the parameter table, a load case can be selected and the model can be solved for steady state. Figure 4-26 shows a screenshot of the parameter table for Station A with preselected cases which were used to verify the model. The variable parameters are the FWT pressure, FWT temperature, FW flow and the rotational speed of the main BFP.

## 4.6 Validation

The Flownex models were validated by comparing actual plant data to the models at various load cases. The operational data for a specific load case was extracted using the eDNA software tool which can remotely access available plant transmitter data from the DCS. The eDNA software updates and trends the data every second. The sample time of the transmitters that are used on site ranges between 45 and 200 milliseconds (Station O and A respectively). Figure 4-27 below shows a trend of the process parameters of the EFPs during a typical unit start up using eDNA software. Attention is immediately drawn to the large scale fluctuation of the feed water flow delivered by the EFPs (grey and blue lines). Data at a fixed point was used and averaged for the short space of time where the different process parameters did not show significant fluctuation in values.

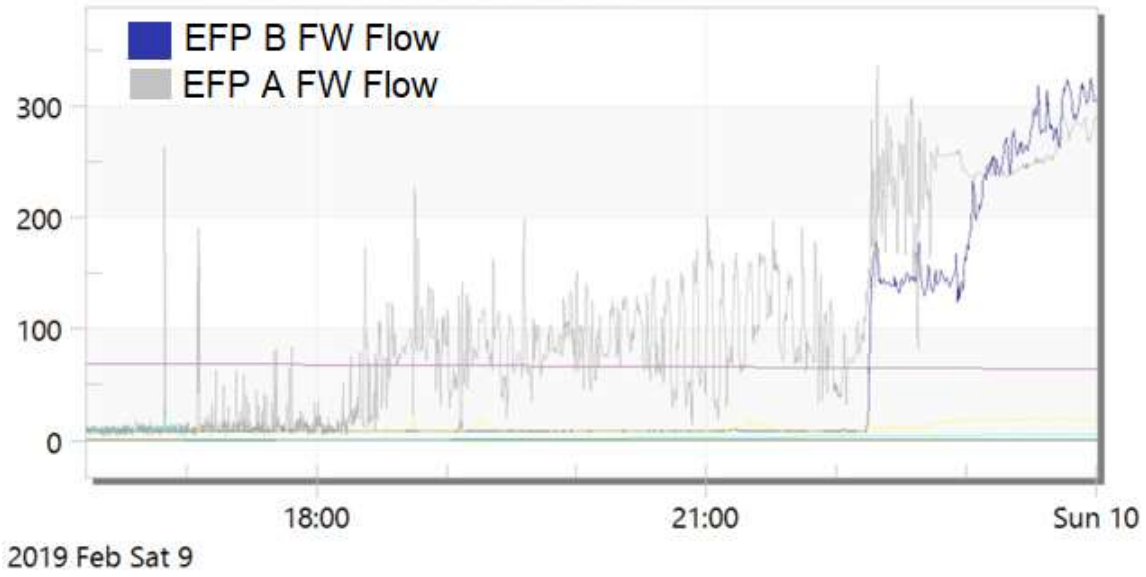


*Figure 4-27: EFP plant parameters during unit start up*

For Station O, with the modulating valve type, the plant leak off conditions were obtained from the operator training simulator that is used for the station because there are no physical leak off transmitters on the plant. The simulator values are based on heat and mass balance calculations

developed by the OEM and compared to available station transmitter readings during the commissioning phase of the plant.

Table 6 below highlights the critical parameter values for three different load cases, as an example, which were used in the validation process of the model. The table also include an average error value over the three cases for each of the parameters. The error value is the average value of the three cases, with the average error of the model calculated as the average of all the errors.

For cases where pressures where used as a given, the calculated flow rates were compared to actual measured flow rates. For cases where the flow rates where used as a given, the calculated pressure was compared to actual measured pressures.

*Table 6: ARC type leak off system (Station O) - model validation*

| **Input** | | | | | | | | |
|---|---|---|---|---|---|---|---|---|
| **Parameter** | **Unit** | **Case 1** | | **Case 2** | | **Case 3** | | |
| Pump Speed | RPM | 1490 | | 1490 | | 1490 | | |
| FWT Temp | °C | 73.8 | | 74.4 | | 91.7 | | |
| FW Flow | kg/s | 0.30 | | 16.77 | | 37.06 | | |
| FWT Pressure | kPa(a) | 105.62 | | 106.24 | | 110.77 | | |
| **Output** | | | | | | | | |
| **Parameter** | **Unit** | **Case 1** | | **Case 2** | | **Case 3** | | |
| | | **Model** | **Actual** | **Model** | **Actual** | **Model** | **Actual** | **Error** |
| FW Pressure | MPa(a) | 14.07 | 13.98 | 14.04 | 14.10 | 13.68 | 13.91 | 0,9% |
| Leak Off Pressure | kPa(a) | 1790.31 | 1856.42 | 1751.08 | 1815.40 | 926.18 | 899.61 | 3.4% |
| ARC Simulation Model Average Error | | | | | | | | **2.1%** |

In a similar way, the other models were validated with average errors of 3% or less.

## 4.7 Consideration for attemperator spray water

The model for Station A was modified to study the effect the attemperator spray water extraction has on the BFP discharge and leak off system. The spray water is used to control the boiler outlet steam temperature (main and reheat steam) and is tapped off from an intermediate stage on the main BFP (Station A and K).

To model the spray water system, a tap off with the spray water flowrate was added to the system. The tap off had no noticeable effect on the model due to the small quantities of spray water used compared (12-20 kg/s) to the high flowrate delivered by the BFP (480 kg/s).

During the event that the spray water system is used, the pump speeds up to meet the boiler flow and pressure demand. This means that only the BFP speed would be slightly higher compared to the model and the conditions around the leak off system would remain the same. The attemperator spray water for Station O is tapped off downstream of the HP heaters and therefor has no effect on the model.

The spray water is also not used during unit start-ups when the pumps are running at conditions where the leak off systems are in operation. It was therefore decided not to include the attemperator spray water as part of the study.

## 4.8 Operating cases considered

The following cases were originally considered as part of this study:

1. The different load cases as per the station heat balance diagrams. These generally include 40%, 60%, 80% and 100% turbine MCR (Maximum continuous rating) load cases.
2. Hot and cold operational cases at various valve openings. The hot and cold cases referred to are the conditions inside the feed water storage tank. For the hot case the turbine is at 100% load with the fluid at maximum operating temperature (125 to 142 degrees Celsius – differs from station to station). The cold condition is with the feed water storage tank at ambient conditions (around 20 degrees Celsius and atmospheric pressure). The conditions were taken from the heat balance diagram and actual plant transmitter data.
3. Initially three valve opening percentages were modelled:
    a. 1% open so represent the switch point when the valve starts to open (See point 5 below)
    b. 50% midway point between fully open and fully closed
    c. 100% valve opening at full flow leak off conditions
4. It was then decided to model various valve opening percentages throughout the travel range of the leak off valve to determine the change in leak off parameters as the valve is opening or closing. A better visualisation could be achieved by adding additional points especially at the smaller valve openings. This was done to determine at which valve openings the process values start to plateau.
5. Special attention is given to the switch point of the leak off valves. These cases include start up conditions as well as putting the second pump into service. During this time the flow between the two running pumps is shared equally, assuming the two pumps perform identically. This could result in both pumps operating at the switch point of their respective leak off valves. The leak off valve switch points in terms of feed water flow rates are:
    a. Binary type: 40 l/s and 45 l/s

   b. Modulating type: 250 $m^3$/hr
   c. ARC type: 70 kg/s

6. During data collection it was noticed that all the leak off system nozzles on the FWTs are situated at a level above the tank water level. It was subsequently decided to also consider the effect on the leak off components if the nozzle was located at the bottom of the tank.
7. The effects of specific design changes that were proposed to Station A and O were also considered. These are detailed in each individual section of chapter 5 below. The proposals include changing the flow measuring orifice size on Station A from 40 mm to 60 mm and replacing the back pressure orifice on Station O with a pressure sustaining valve.

# 5. Results

## 5.1 Data processing

The process conditions that are important for this study such as the static pressure, temperature, quality and flowrate can be extracted at any node or piping section increment for any of the various load cases from the Flownex model.

To determine the vapour pressure of the fluid at the various locations the 1996 update [40] of the Buck formula was used:

$$P_S(T) = 0.61121e^{\left(\left(18.678-\frac{T}{234.5}\right)\left(\frac{T}{257.14+T}\right)\right)} \tag{38}$$

where

T = Temperature [˚C]

$P_S(T)$ = Saturated vapour pressure of water [kPa].

After running the models in Flownex, the relevant results were extracted into Microsoft Excel where the data was tabled and graphed.

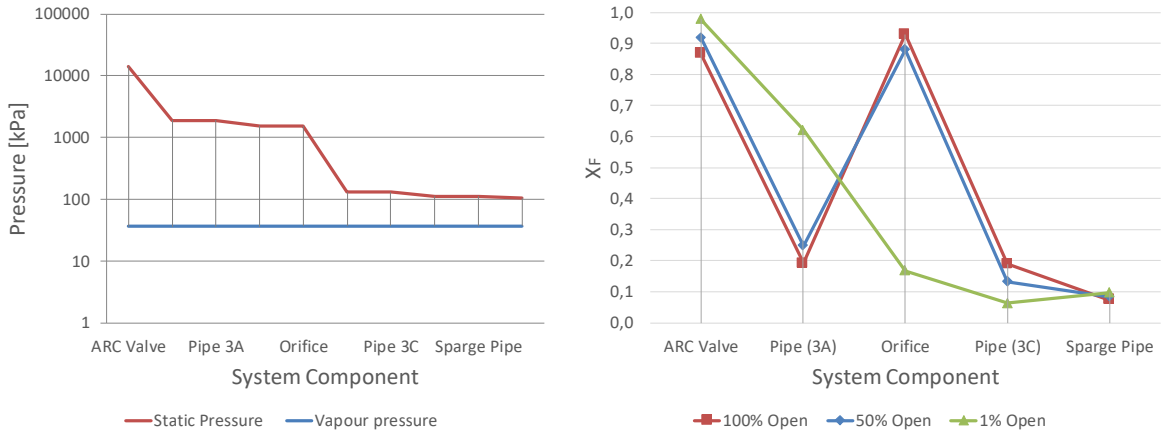


*Figure 5-1: ARC system static pressures vs vapour pressure for the 100% open case (left) compared to the $X_F$ values for each component in the system at three valve opening cases (right)*

Figure 5-1 (left) compares the each component's inlet- and outlet static pressure to the vapour pressure throughout the ARC type leak off system of Station O for a cold condition where the leak off valve is 100 % open. The pressure values are plotted on a logarithmic scale on the vertical axis due to the large difference between the pressure at the inlet of the valve and the vapour pressure of the fluid. The components are plotted in sequential order on the horizontal axis starting with the leak off valve and ending at the FWT nozzle. Locations where the static system pressure are close to

the vapour pressure would highlight problematic areas where cavitation formation will occur. Attention can then be given to these areas.

By comparing the static pressures throughout the system to the vapour pressure, the amount of data that can be presented on one graph is limited due to the change in vapour pressure as the temperature of the fluid changes with each operating case. Also, looking and static pressure or pressure drop per components alone is not an adequate measure of cavitation risk. By calculating the coefficient of cavitation ($X_F$) for each component, the vapour pressure is automatically taken into account and different load cases can be plotted on one graph and easily compared. High $X_F$ values point to high risk components that could suffer from cavitation damage. Figure 5-1 (right) shows the $X_F$ values of the different components for the cold case at three different valve openings. Results are therefore presented in terms of $X_F$ values rather than absolute pressures.

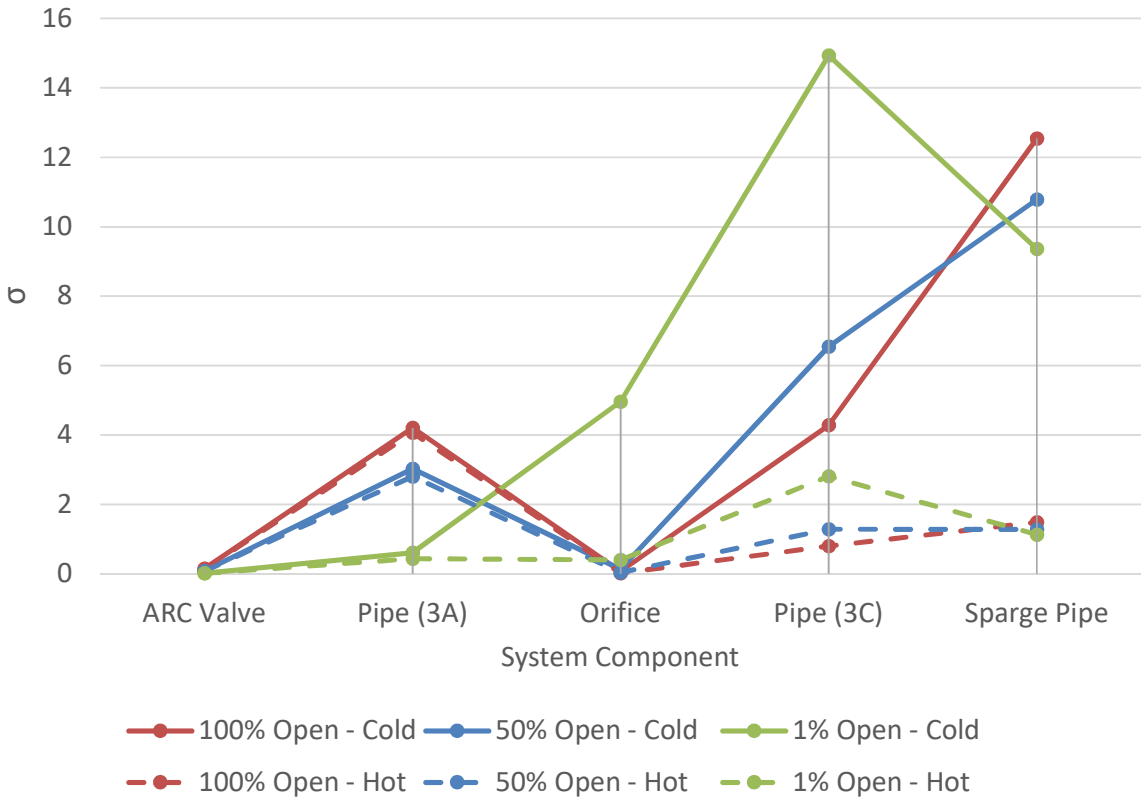


*Figure 5-2: Cavitation numbers of each component in the ARC leak off system at various valve openings for the cold and hot condition*

Figure 5-2 compares the cavitation number as per equation (3) of the cold condition at various valve openings to the hot condition at various valve openings for the ARC type leak off system. Scaling of the vertical axis is challenging when using the cavitation number (σ) due to the much smaller values

during the hot conditions compared to the larger cold condition values. Whereas the coefficient of cavitation ($X_F$) generally remains within the range 0 to 1.

## 5.2 General observations

When solving the models at the various load cases related to the station heat balance diagrams, it was found that the leak off systems are mostly isolated at turbine load cases of 40 % and higher. Station O is the exception, with the leak off valve open at load cases below 55 % of the turbine MCR. The load cases based on the heat balance diagrams were then disregarded and attention was given to hot and cold cases at various valve openings.

As the leak off valves close, the $X_F$ values of all the valves themselves increase and the $X_F$ values of the downstream components in the system decrease. It was found that the $X_F$ values of all the components in the system increase with the temperature of the fluid. This points to a higher risk of cavitation. This is expected due to the increase in the vapour pressure and decreases the density of the fluid (See section 3.1.8).

Paragraphs 5.3 to 5.6 below discuss the results of the different systems types individually and paragraph 5.7 discuss the results of other studies that were performed.

## 5.3 Binary type (Separate) leak off valve (Station A)

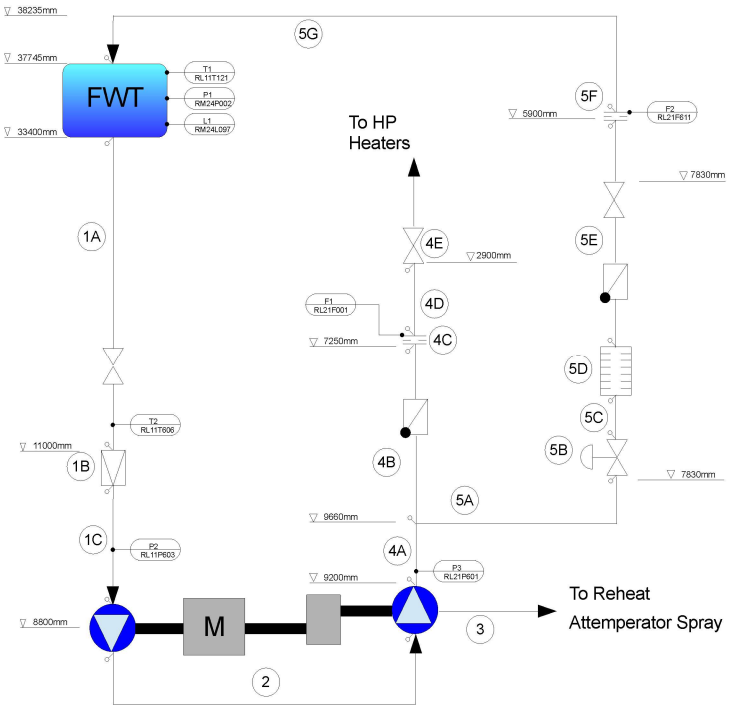


| Item | Description | Size | Length | Comment |
|---|---|---|---|---|
| 1A | Pipe | 400NB (Std Sch) | 42 934mm | 90 deg = 1<br>45 deg = 3<br>Gate valve |
| 1B | Strainer | | | |
| 1C | Pipe | 400NB (Std Sch) | 500mm | |
| 2 | Pipe | 300NB (Std Sch) | 28 928mm | 90 deg = 6<br>45 deg = 2 |
| 3 | Pipe | | | |
| 4A | Pipe | ID 300 x WT 27.5 | 460mm | |
| 4B | Pipe | ID 300 x WT 27.5 | 13 866mm | Swing check NRV<br>90 deg = 2<br>45 deg = 1 |
| 4C | Orifice | | | Hole dia 160.79mm |
| 4D | Pipe | ID 300 x WT 27.5 | 13 148mm | T Piece (Branch)<br>90 deg = 1<br>Gate valve |
| 4E | Control valve | 300NB | | |
| 5A | Pipe | ID 100 x WT 25 | 2 920mm | 90 deg = 1 (long) |
| 5B | Control valve | 100NB | | |
| 5C | Pipe | ID 100 x WT 25 | 250mm | |
| 5D | Diffuser | | | |
| 5E | Pipe | 100NB | 12 975mm | 90 deg = 4<br>45 deg = 2<br>Swing check NRV<br>Gate valve |
| 5F | Orifice | | | Hole dia 40mm |
| 5G | Pipe | 100NB | 79 037mm | 90 deg = 8<br>45 deg = 5 |

| Label | Instrument Tag | Description |
|---|---|---|
| L1 | RM24L097 | Storage tank liquid level |
| T1 | RL11T121 | Storage tank temperature |
| T2 | RL11T606 | Pump suction temperature |
| P1 | RM24P002 | Storage tank pressure |
| P2 | RL11P603 | Pump suction pressure |
| P3 | RL21P601 | Pump discharge pressure |
| F1 | RL21F001 | Feed water flow |
| F2 | RL21F611 | Leak off flow |

*Figure 5-3: Binary (Separate) system type line diagram*

The system was modelled at various valve openings even though the system is the binary type (open or closed). This was done to determine the cavitation risk of the components at the quasi-steady conditions for a slow opening and closing valve. Figure 5-3 is the line diagram that shows the system configuration.

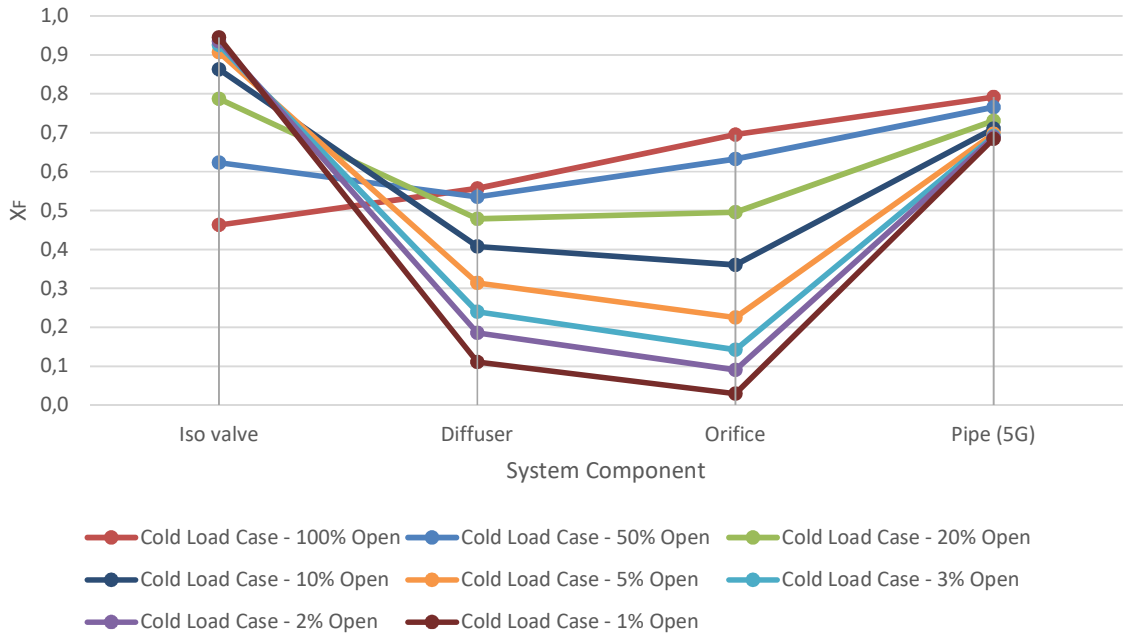


*Figure 5-4: Binary type (Separate) – Cold case with various openings*

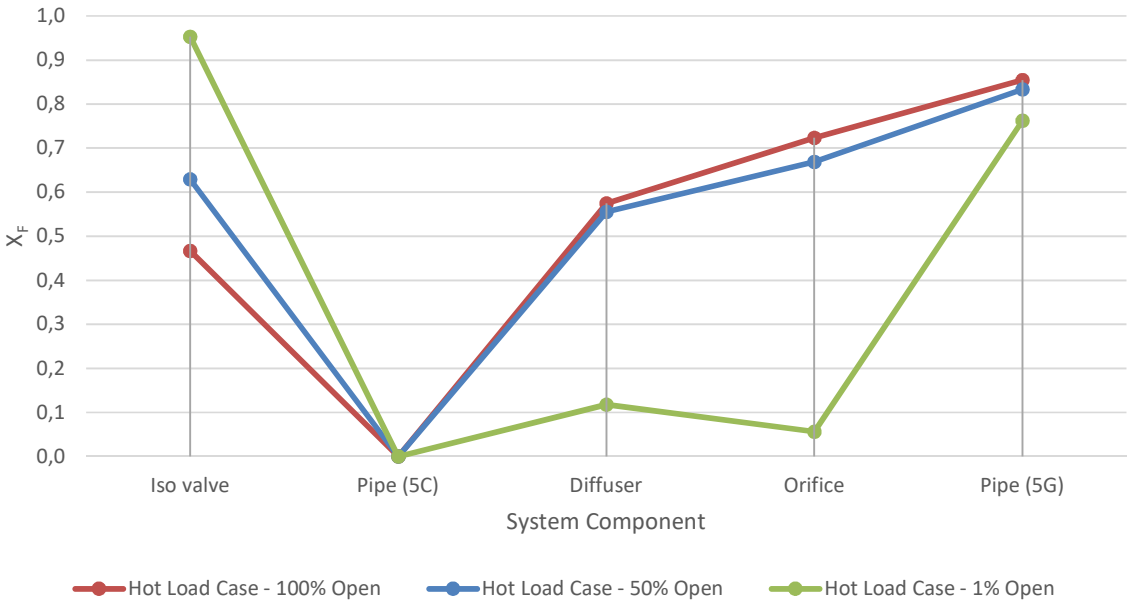


*Figure 5-5: Binary type (Separate) – Hot case with various openings*

From Figure 5-4 and Figure 5-5 it can be seen that extremely high $X_F$ values are found for the isolation valve at openings smaller than 20 %. This highlights a large risk of cavitation due to the valve being a single stage parallel slide valve. During these low flow conditions the diffuser is not the largest pressure reducing component and therefore does not provide sufficient back pressure on the isolation valve to prevent cavitation formation on the isolation valve outlet.

Smaller sections of pipework in between the more critical components have been left out due the small impact they have on the overall system.

The flow measuring orifice has very high $X_F$ values at higher flow rates for a single stage component especially considering that is only intended for the purpose of flow measurement. The high pressure drop over the orifice has been identified as a problematic area on site due to deformation of the orifice plate. A design change was proposed to increase the orifice inside diameter from 40mm to 60mm and the results of the proposed change is discussed in section 5.7.1.

Pipe (5G) is the longest section of pipework for this plant and runs from the BFP floor level (5.9m) to the FWT level (33.4m). A high $X_F$ value is found across this section, which increases with flowrate, due to the pipe exhausting directly into the FWT with no sparge pipe to provide any form of back pressure. Relatively high $X_F$ values across piping sections are not of a major concern as no pressure recovery takes place over a pipe. This means that the outlet pressure is the lowest pressure point on this component. As long as the outlet pressure remains higher than the vapour pressure at that point, $X_F$ value is not equal to 1, no cavitation inception is expected.

Very small changes in $X_F$ values are noted for a change in temperature on this type of system at the various flowrates.

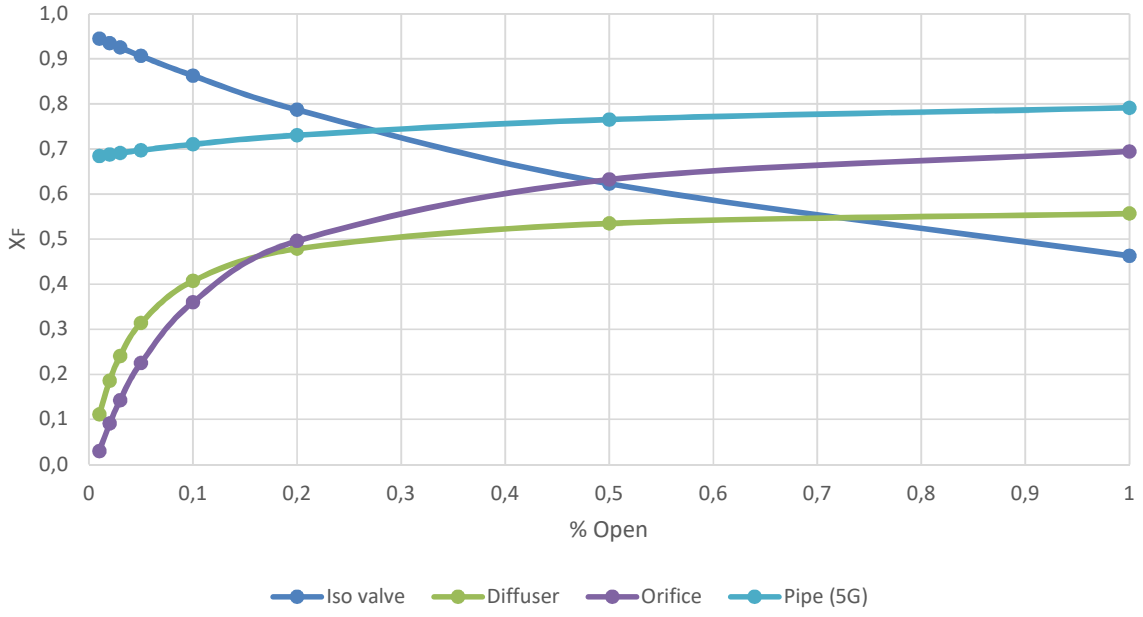


*Figure 5-6: Binary type (Separate) – $X_F$ vs percentage open (Cold case)*

Figure 5-6 shows the change in $X_F$ values of each component as the valve is opened and the flow increases through the system. The $X_F$ value of the isolation valve decreases significantly as it opens

with the $X_F$ values of the diffuser and the flow measuring orifice increasing to 0.56 and 0.72 respectively.

## 5.4 Binary type (Integrated) leak off valve (Station A)

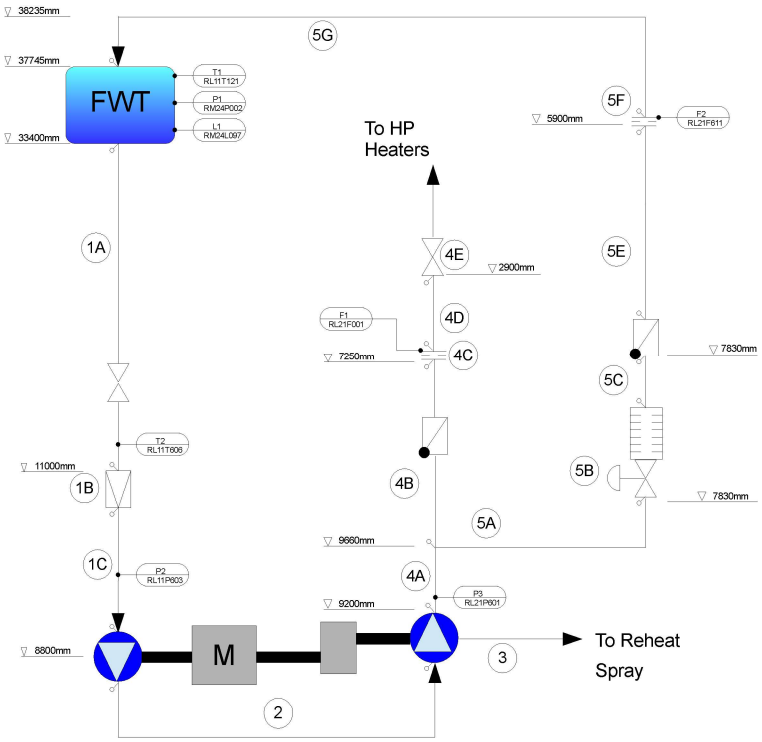


| Item | Description | Size | Length | Comment |
|---|---|---|---|---|
| 1A | Pipe | 400NB (Std Sch) | 42 934mm | 90 deg = 1<br>45 deg = 3<br>Gate valve |
| 1B | Strainer | | | |
| 1C | Pipe | 400NB (Std Sch) | 500mm | |
| 2 | Pipe | 300NB (Std Sch) | 28 928mm | 90 deg = 6<br>45 deg = 2 |
| 3 | Pipe | | | |
| 4A | Pipe | ID 300 x WT 27.5 | 460mm | |
| 4B | Pipe | ID 300 x WT 27.5 | 13 866mm | Swing check NRV<br>90 deg = 2<br>45 deg = 1 |
| 4C | Orifice | | | Hole dia 160.79mm |
| 4D | Pipe | ID 300 x WT 27.5 | 13 148mm | T Piece (Branch)<br>90 deg = 1<br>Gate valve |
| 4E | Control valve | 300NB | | |
| 5A | Pipe | ID 100 x WT 25 | 2 920mm | 90 deg = 1 (long) |
| 5B | Control valve | 100NB | | |
| 5C | Pipe | ID 100 x WT 25 | 250mm | |
| 5E | Pipe | 100NB | 13 475mm | 90 deg = 4<br>45 deg = 2<br>Swing check NRV |
| 5F | Orifice | | | Hole dia 60mm |
| 5G | Pipe | 100NB | 79 037mm | 90 deg = 8<br>45 deg = 5 |

| Label | Instrument Tag | Description |
|---|---|---|
| L1 | RM24L097 | Storage tank liquid level |
| T1 | RL11T121 | Storage tank temperature |
| T2 | RL11T606 | Pump suction temperature |
| P1 | RM24P002 | Storage tank pressure |
| P2 | RL11P603 | Pump suction pressure |
| P3 | RL21P601 | Pump discharge pressure |
| F1 | RL21F001 | Feed water flow |
| F2 | RL21F611 | Leak off flow |

*Figure 5-7: Binary (Integrated) system type line diagram*

Figure 5-7 shows the system line diagram for the binary (Integrated) leak off type system. With the multi stage pressure reduction forming part of the valve itself, this type of systems consists of fewer high risk components than the binary (Separate) type of system.

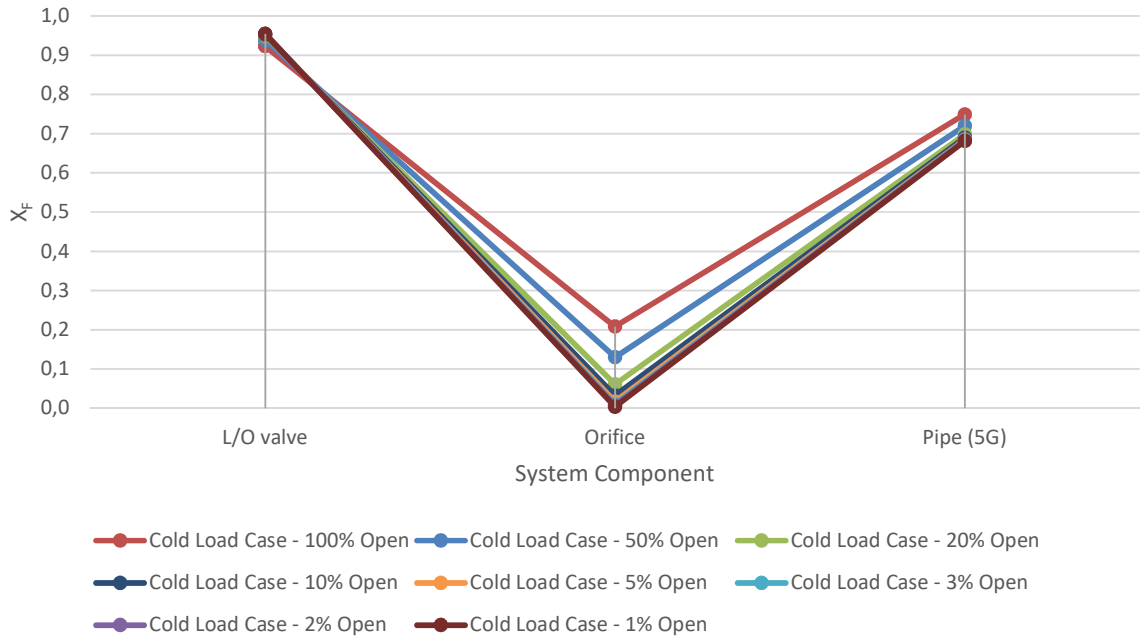


*Figure 5-8: Binary type (Integrated) – Cold case with various openings*

From Figure 5-8 is can be seen that the leak off valve on this system is by far the most critical component with $X_F$ values higher than 0.9 throughout the entire stroke of the valve. Special consideration must be given to the design of this type of leak off valve to ensure extremely high values of $X_{FZ}$ are achieved. For a possible option to reduce the $X_F$ value of the leak off valve see section 5.7.1.

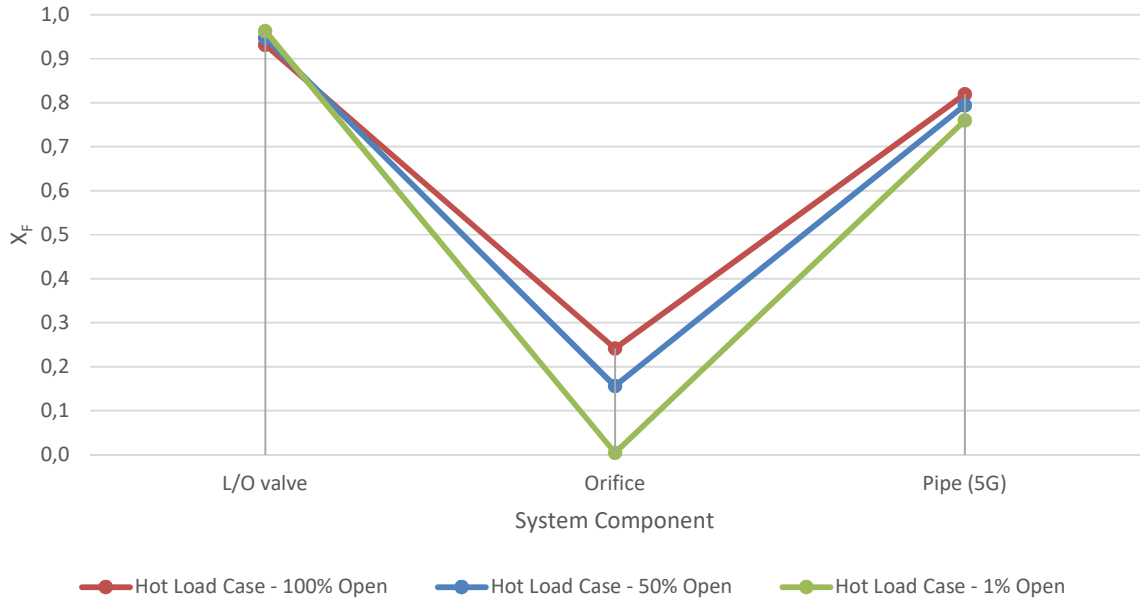


*Figure 5-9: Binary type (Integrated) – Hot case with various openings*

Figure 5-9 shows the hot case for three different openings (1 %, 50 % and 100 %). All $X_F$ values for the hot case are slightly higher than the values for the cold case, but there are no noteworthy differences.

The $X_F$ values of the piping section between the leak off valve and the orifice, not displayed on Figure 5-8 or Figure 5-9, fall below 0 when the valve is open at small percentages. This is due to the outlet pressure of the piping section being higher than the inlet pressure. The increase in pressure is due the outlet termination point being statically lower than the inlet. As the flow is increased, the friction losses over this section of pipe become larger than the static pressure gained due to the height difference and the $X_F$ value becomes positive. Pipe (5E) as well as pipe (5C) situated between the valve and the orifice were removed from Figure 5-8 as it is does not add any value to the plot with the $X_F$ values for both piping sections ranging between -0.042 and 0.015.

The flow measuring orifice for this system has a much lower $X_F$ value than the model with the separate leak off isolation valve and diffuser. The lower $X_F$ value is due to a new design orifice with an increased internal orifice diameter of 60mm.

The same comment applies to pipe (5G) as per the previous model and no other high risk components have been identified on this system.

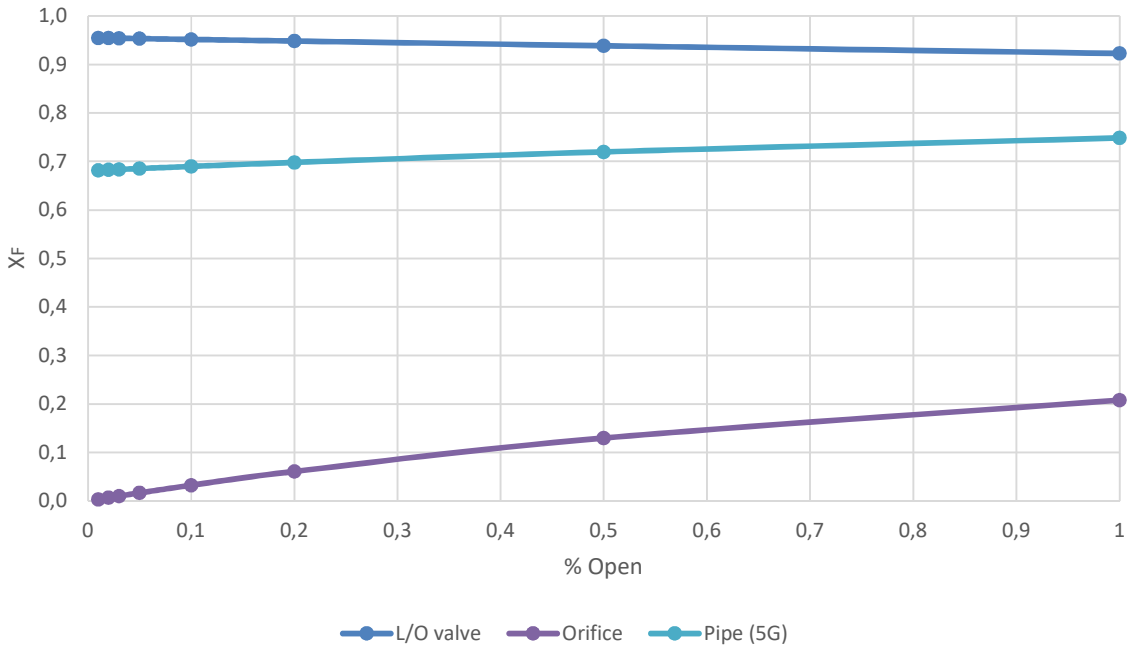


*Figure 5-10: Binary type (Integrated) – $X_F$ vs percentage open (Cold case)*

Figure 5-10 shows the change in $X_F$ value for each component with the change in flow rate as the valve is opened. It is clear that the leak off valve is the only critical component in this system throughout the entire flow range.

## 5.5 Modulating type leak off valve (Station K)

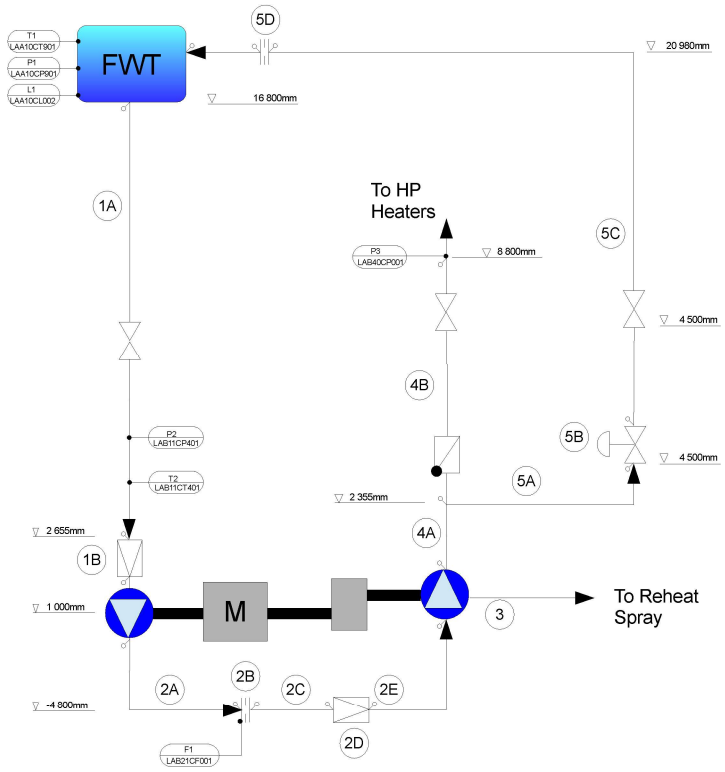


| Item | Description | Size | Length | Comment |
|---|---|---|---|---|
| 1A | Pipe | 400NB (Std Sch) | 27 811mm | 90 deg = 4<br>Gate valve |
| 1B | Strainer | | | |
| 2A | Pipe | 400NB (XS) | 12 279mm | 90 deg = 3 |
| 2B | Orifice | | | Hole dia 247.65mm |
| 2C | Pipe | 400NB (XS) | 7 135mm | 90 deg = 2 |
| 2D | Strainer | | | |
| 2E | Pipe | 400NB (XS) | 3 673mm | |
| 3 | Pipe | | | |
| 4A | Pipe | 330 ID x 35 WT | 370mm | |
| 4B | Pipe | 330 ID x 35 WT | 32 028mm | 90 deg = 6<br>Swing check NRV<br>Gate valve<br>Tees = 3 |
| 5A | Pipe | 200NB (XXS) | 10 621mm | 90 deg = 3 |
| 5B | Control valve | 200NB | | |
| 5C | Pipe | 200NB (Sch 30) | 44 247mm | 90 deg = 8<br>45 deg = 2<br>Gate valve |
| 5D | Sparge pipe | 200ND | | 3 holes (Dia 34,5mm)<br>3 holes (Dia 34,5mm)<br>1 hole (Dia64.6mm)<br>In series |

| Label | Instrument Tag | Description |
|---|---|---|
| L1 | LAA10CL002 | Storage tank liquid level |
| T1 | LAA10CT901 | Storage tank temperature |
| T2 | LAB11CT401 | Pump suction temperature |
| P1 | LAA10CP901 | Storage tank pressure |
| P2 | LAB111CP401 | Pump suction pressure |
| P3 | LAB40CP001 | Pump discharge pressure |
| F1 | LAB21CP001 | Feed pump flow |

*Figure 5-11: Modulating system type line diagram*

The line diagram for the modulating system is shown in Figure 5-11. The majority of the pressure break down takes place within the control valve itself (5B), through the disk stack as explained in section 2.4. Component 5D displayed as an orifice represents the 3 stage sparge pipe situated inside the FWT.

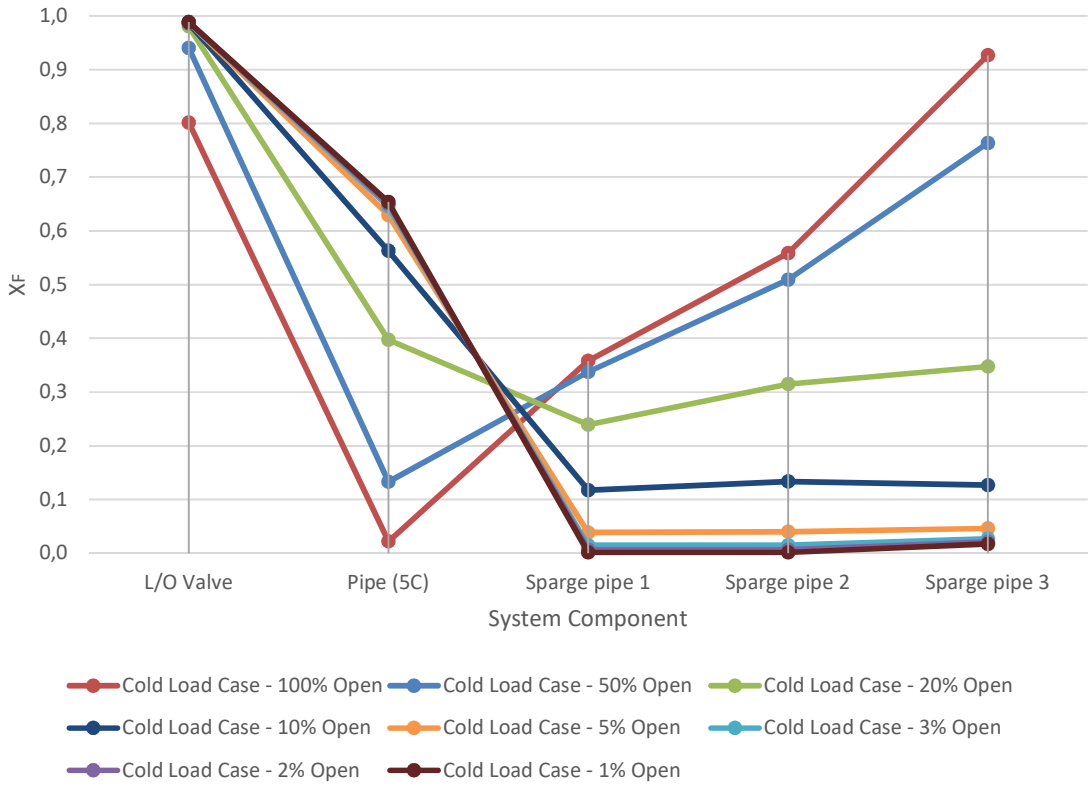


*Figure 5-12: Modulating type – Cold case with various openings*

The modulating valve has the highest $X_F$ value (0.988 during the hot condition) recorded in this study. Extremely high $X_F$ values are found at small openings, but drops to 0.8 when the valve is fully open. The decrease in $X_F$ value of the valve is mainly due to the high back pressure caused by the sparge pipe. The valve design is that of a no damage approach as explained in section 3.5.2 and vindicates the high $X_F$ value.

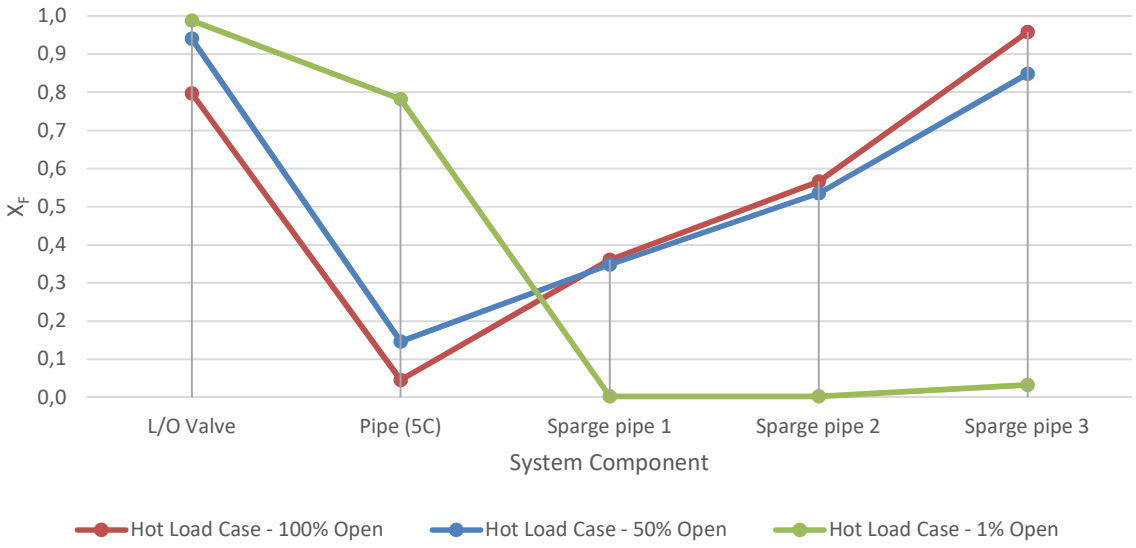


*Figure 5-13: Modulating type – Hot case with various openings*

The various orifice like stages of the sparge pipe acts as further pressure breakdown stages and create a large back pressure on the leak off system at high flow rates. By creating a back pressure on the upstream components, the sparge pipe ensures no flashing takes place within the leak off pipework, but rather flashes directly into the FWT away from the vessel wall where cavitation erosion or washing could take place. This can be seen in Figure 5-12 with extremely high $X_F$ values for the final stage of the sparge pipe at high flow rates.

The opposite occurs at lower flow rates. The $X_F$ values of the sparge pipe decreases significantly with increasing $X_F$ values for the valve as well as the pipework which is due to the large static height difference between the pipe in- and outlet.

The change in temperature has a very small effect on the modulating type system, as can be seen when comparing the plots of Figure 5-13 to the 1 %, 50 % and 100 % opening plots of Figure 5-12. The greatest change is found over the piping section (5C).

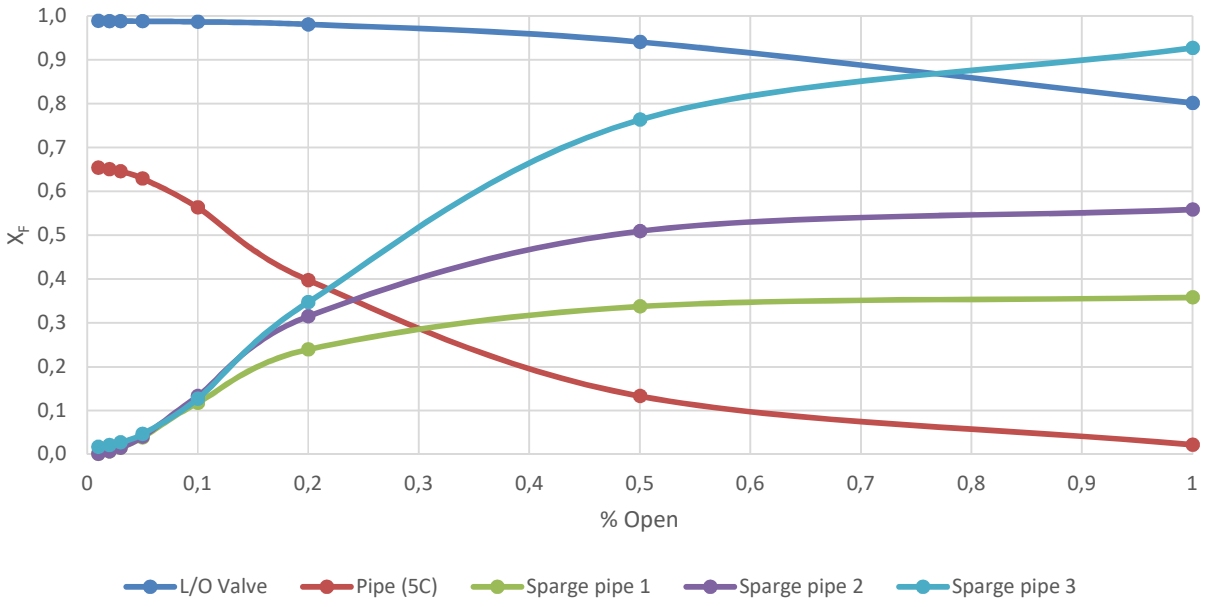


*Figure 5-14: Modulating type $X_F$ vs percentage open (Cold case)*

Figure 5-14 clearly shows how the $X_F$ value of the leak off valve decrease when the valve is opened. Due to the increase in flow rate the $X_F$ values of the sparge pipe stages increase significantly. The back pressure created by the sparge pipe also causes a reduction in the $X_F$ value for the upstream piping section.

## 5.6 ARC type leak off valve (Station O)

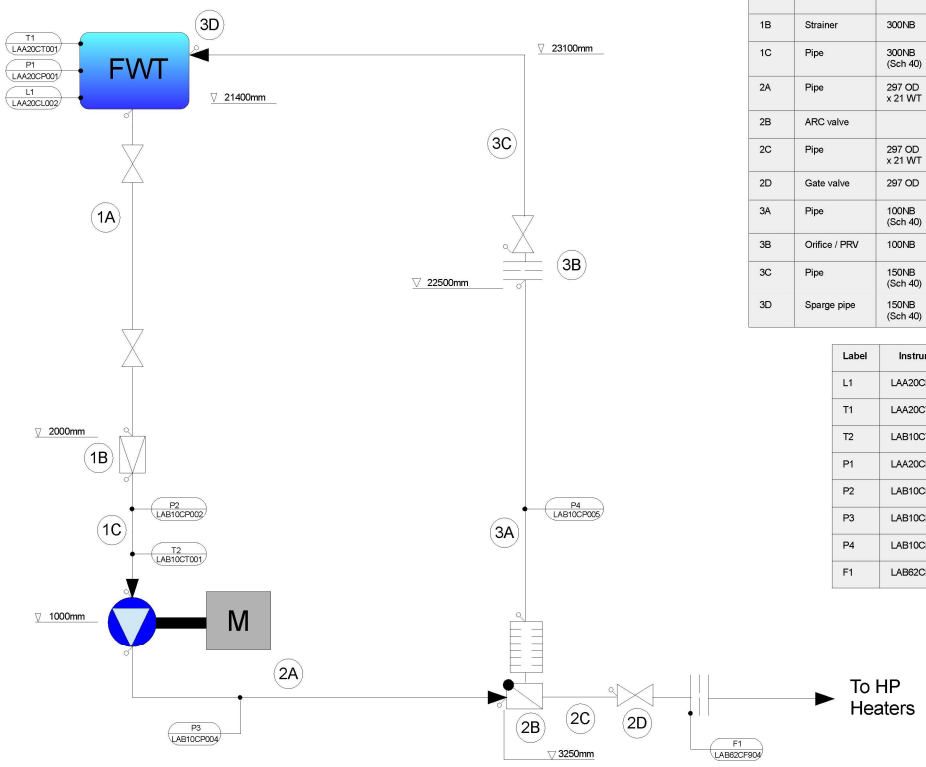


| Item | Description | Size | Length | Comment |
|---|---|---|---|---|
| 1A | Pipe | 300NB (Sch 40) | 38 665mm | 90 deg = 8<br>T branch = 1<br>Gate valves = 2 |
| 1B | Strainer | 300NB | 1 440mm | |
| 1C | Pipe | 300NB (Sch 40) | 4 100mm | 45 deg = 1 |
| 2A | Pipe | 297 OD x 21 WT | 4 100mm | 45 deg = 1 |
| 2B | ARC valve | | | |
| 2C | Pipe | 297 OD x 21 WT | 1 400mm | |
| 2D | Gate valve | 297 OD | | |
| 3A | Pipe | 100NB (Sch 40) | 47 755mm | 90 deg = 15<br>T straight = 1 |
| 3B | Orifice / PRV | 100NB | | Set at 12 bar / Dia 40mm |
| 3C | Pipe | 150NB (Sch 40) | 2 845mm | 90 deg = 2<br>Ball valve |
| 3D | Sparge pipe | 150NB (Sch 40) | 1 200mm | 3 holes (80 x 200 each) |

| Label | Instrument Tag | Description |
|---|---|---|
| L1 | LAA20CL002 | Storage tank liquid level |
| T1 | LAA20CT001 | Storage tank temperature |
| T2 | LAB10CT001 | Pump suction temperature |
| P1 | LAA20CP002 | Storage tank pressure |
| P2 | LAB10CP002 | Pump suction pressure |
| P3 | LAB10CP004 | Pump discharge pressure |
| P4 | LAB10CP005 | Leak off pressure |
| F1 | LAB62CF904 | Feed water flow |

*Figure 5-15: ARC system type line diagram*

The leak off bypass section of the ARC valve type is completely open during start up conditions due to the NRV disk being forced closed by a spring. Start-up conditions are therefore not an issue with the ARC design. The ARC type system line diagram is displayed in Figure 5-15. The diagram shows the back pressure orifice as component 3B, which is replaced with a PRV on some units at Station O. The effect of replacing the orifice with a PRV is assessed section 5.7.3.

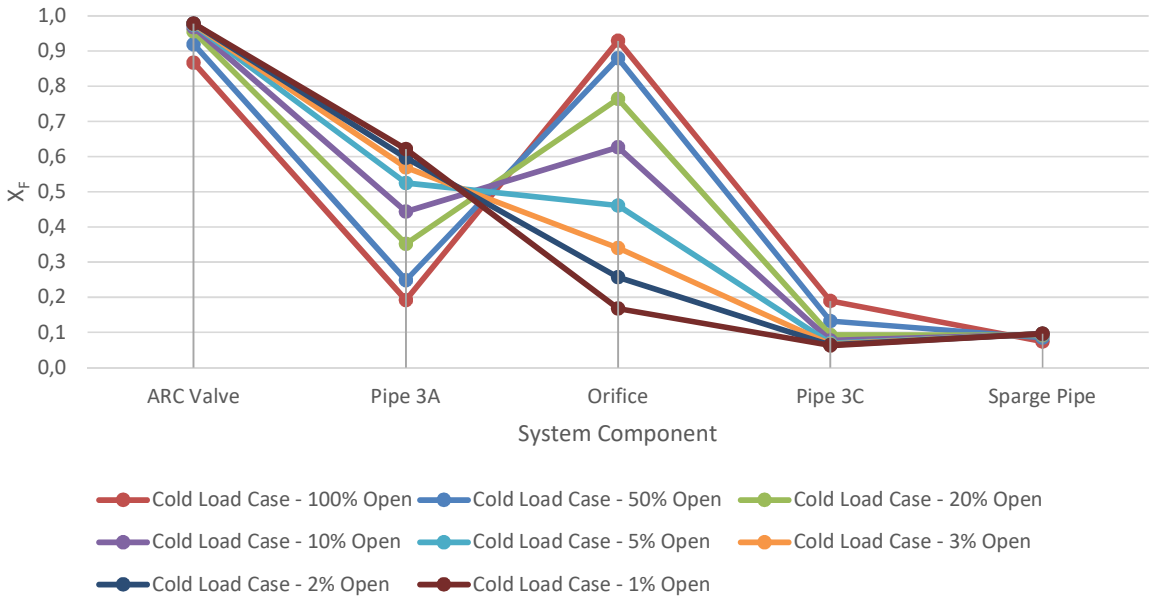


*Figure 5-16: ARC type – Cold case with various openings*

From Figure 5-16 it is clear that the back pressure orifices and the ARC valves are the largest risk in the system. The high $X_F$ values of the valve could be acceptable due to the multistage pressure reduction if the valve has a sufficiently high $X_{FZ}$ value. At a valve opening of 10 % the $X_F$ value of the orifice is already at 0.6 and increases to a value of 0.93 at 100 % open during the cold condition, which is extremely high for a single stage component. The high $X_F$ values are an indication that the outlet pressure is only slightly higher than that of the vapour pressure for various conditions.

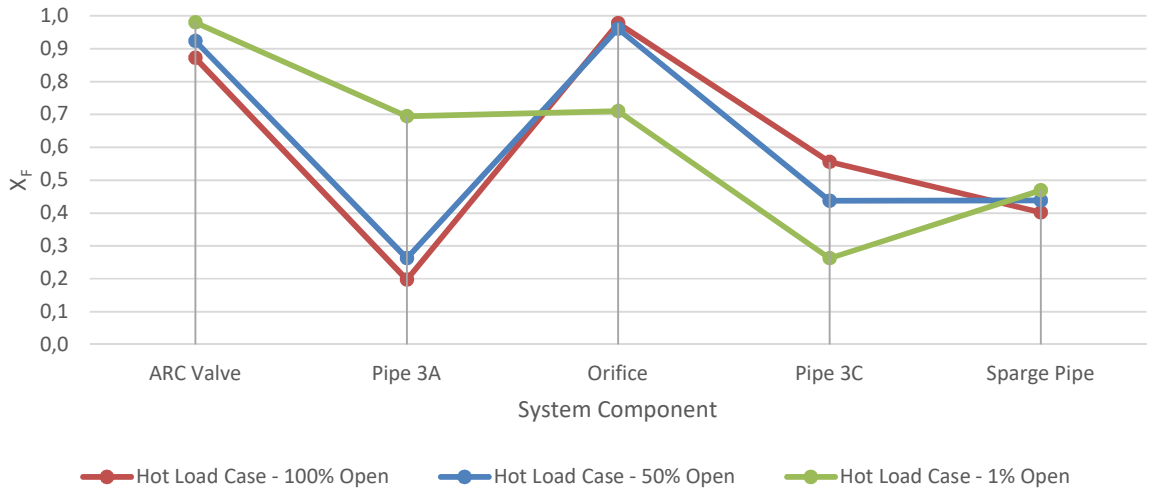


*Figure 5-17: ARC type – Hot case with various openings*

Figure 5-17 shows the hot condition at valve openings of 1 %, 50 % and 100 %. The ARC model shows the most significant change in $X_F$ values due to the change in fluid temperature. This is most evident

at the back pressure orifice which is installed just upstream of the FWT nozzle. The risk of flashing over the orifice is extremely high for most cases, except where the flow is low and the temperature of the water is cold.

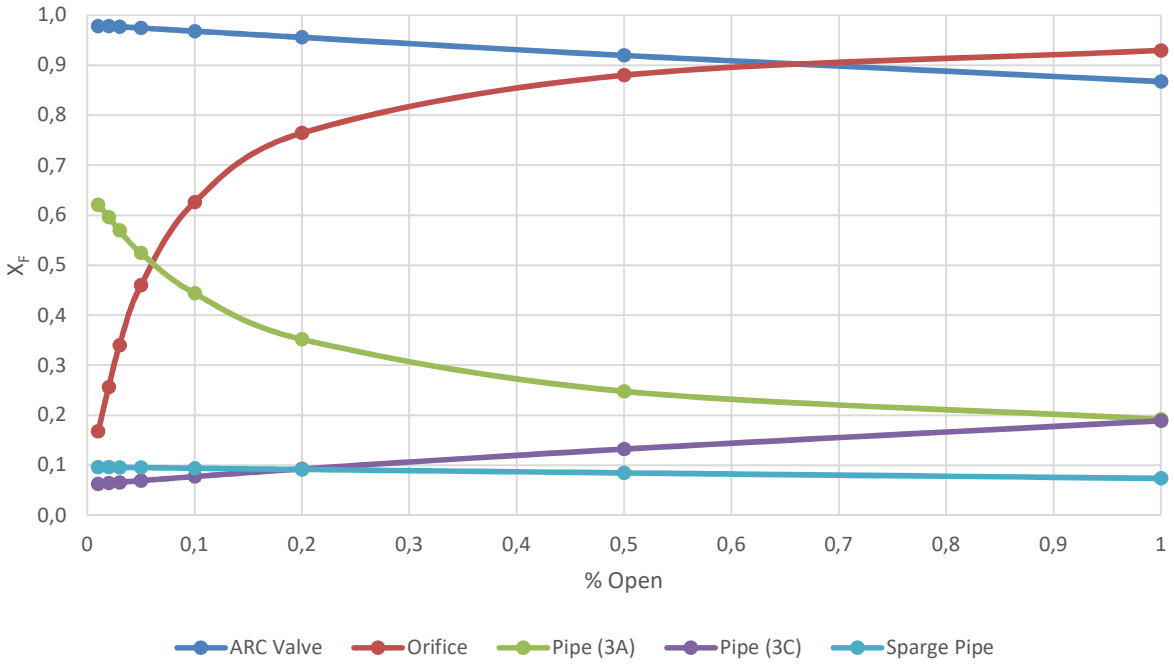


*Figure 5-18: ARC type $X_F$ vs percentage open (Cold case)*

Figure 5-18 shows how the $X_F$ values change as the valve is opened and the flow rate is increased through the leak off system for the cold case. The graph shows that the $X_F$ value of the valve drops below 0.9 at around the 65 % open position, which is also the same position where the $X_F$ value of the orifice reaches the 0.9 value.

Operating both 100 % EFPs at the same time to achieve full load puts the leak systems at risk of cavitation. At 100 % turbine MCR the required feed water flow is 125.2 kg/s according to the plant heat balance diagram. Assuming both pumps are identical in performance, each pump will deliver 62.6 kg/s of feed water. This will result in both EFPs operating with their respective ARC valves at 6 % open on the leak off bypass ($X_F$ value in excess of 0.97 for the hot and cold conditions).

## 5.7 Other studies

### 5.7.1 Flow orifice size on the binary type system

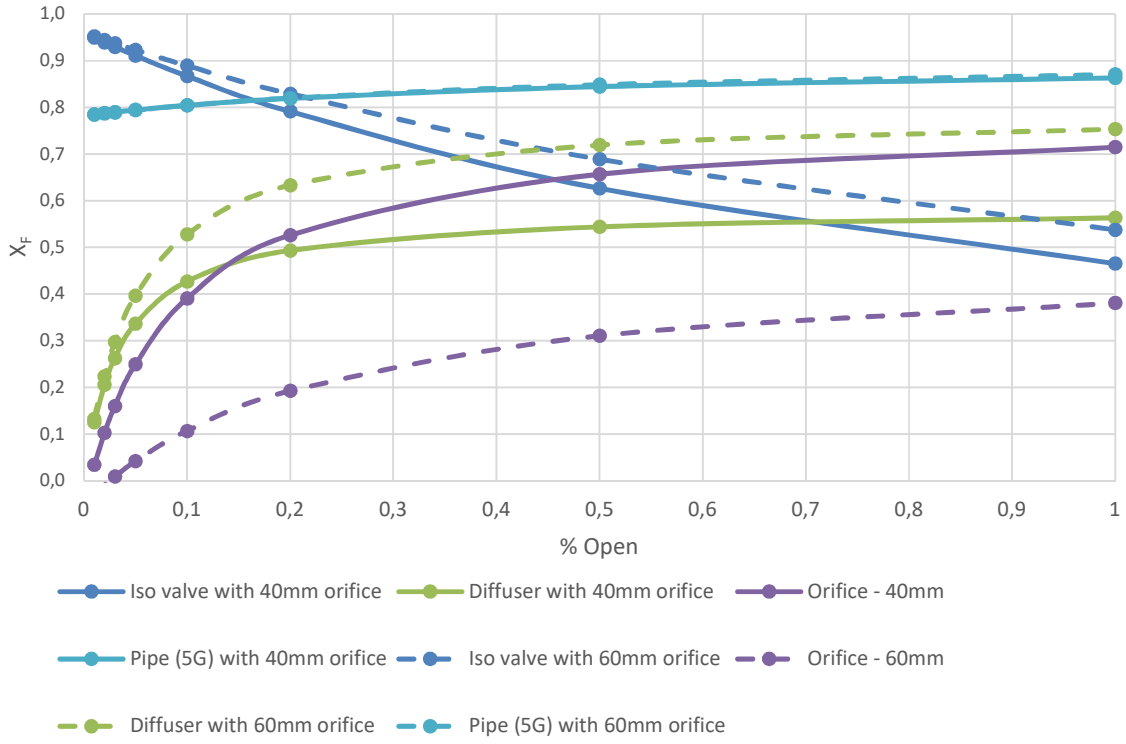


*Figure 5-19: Binary (Separate) type system orifice size comparison – Hot case*

By increasing the inside diameter of the flow measuring orifice on the binary (Separate) type leak off system from 40 mm to 60 mm, a significant decrease in the $X_F$ value over the orifice is noticed with a substantial increase in $X_F$ value over the diffuser. Refer to Figure 5-19.

For the hot case with the valve at 100 % open, the $X_F$ value of the orifice is reduced from 0.715 to 0.381 and the diffuser increases from 0.563 to 0.753. This is ideal considering that the diffuser is designed for the purpose of pressure reduction. A small increase in $X_F$ value of the isolation valve is also noted.

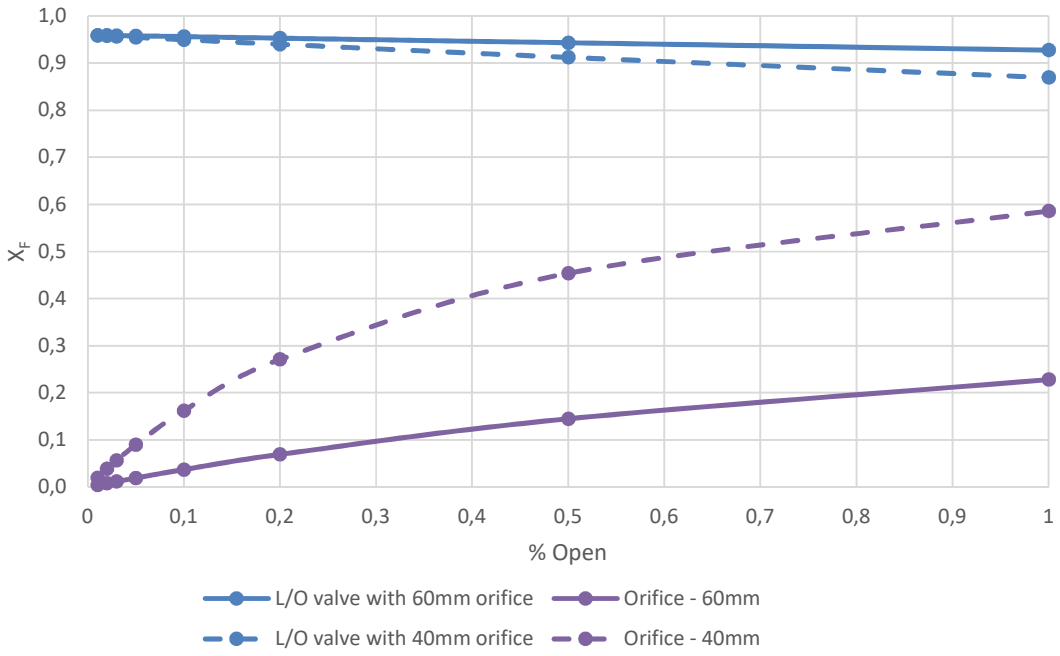


*Figure 5-20: Binary (Integrated) leak off system with a 40mm vs 60mm flow orifice*

The current design of the binary (Integrated) type leak off system at Station A recommends a flow measuring orifice size of 60mm downstream of the leak off valve. As seen in section 5.4 the $X_F$ values of the leak off valve itself are extremely high. By reducing the size of the flow measuring orifice back to the original 40mm the $X_F$ value of the valve can be decreased to values lower than 0.9 at larger leak off flow rates. This is due to the additional back pressure created by the downstream flow measuring orifice and is a function of the flow rate. The risk of cavitation over the orifice is however significantly increased and the risk of cavitation of the leak off valve at low flow rates remains unchanged.

## 5.7.2 Temperature effect on the different leak of types

Figure 5-21 to Figure 5-24 compare the change in $X_F$ values for each leak off system through the entire valve travel for the hot and cold conditions.

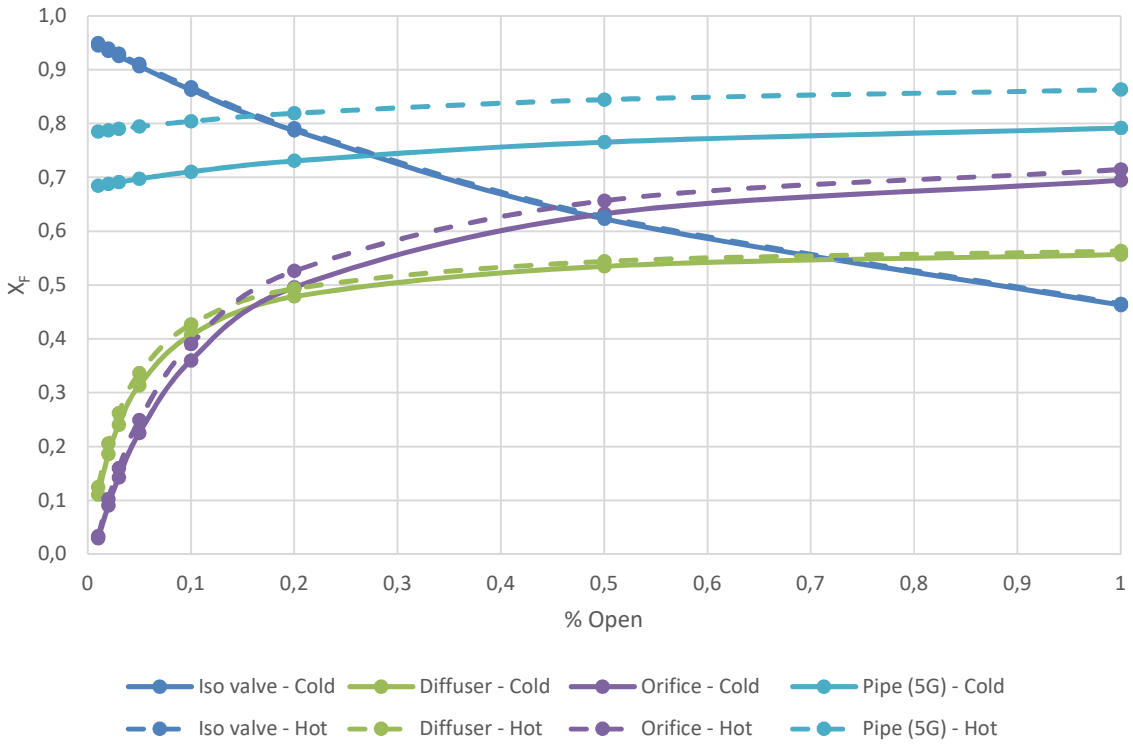


*Figure 5-21: Binary (Separate) system temperature comparison*

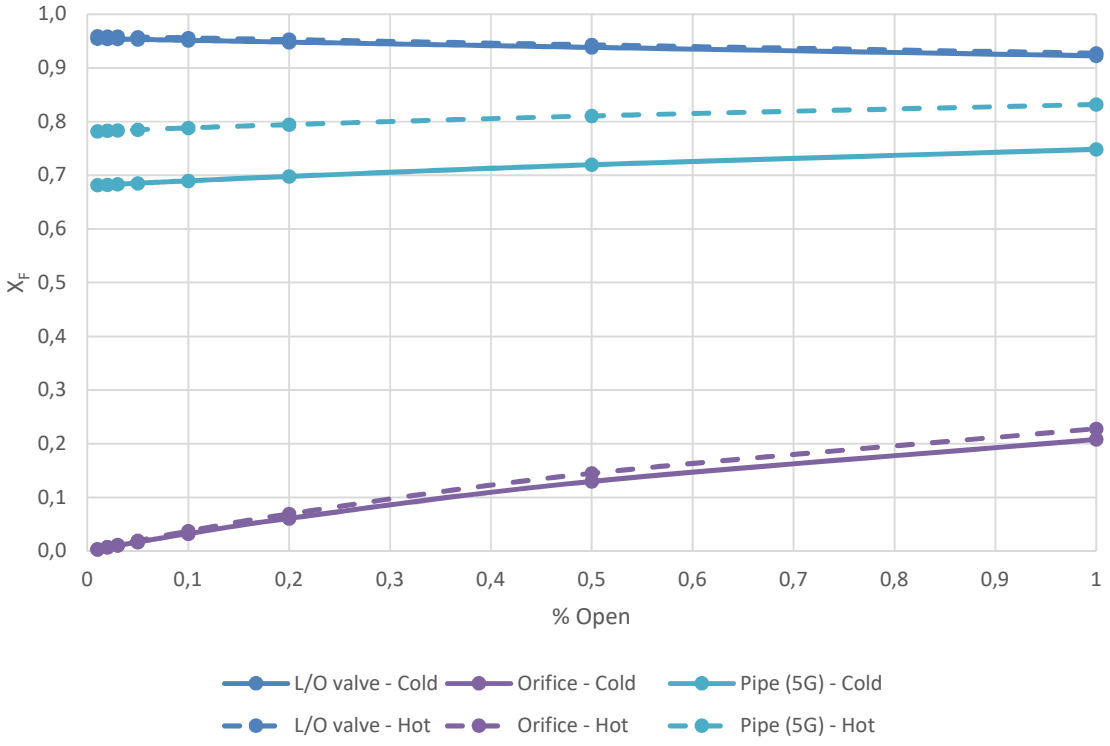


*Figure 5-22: Binary (Integrated) system temperature comparison*

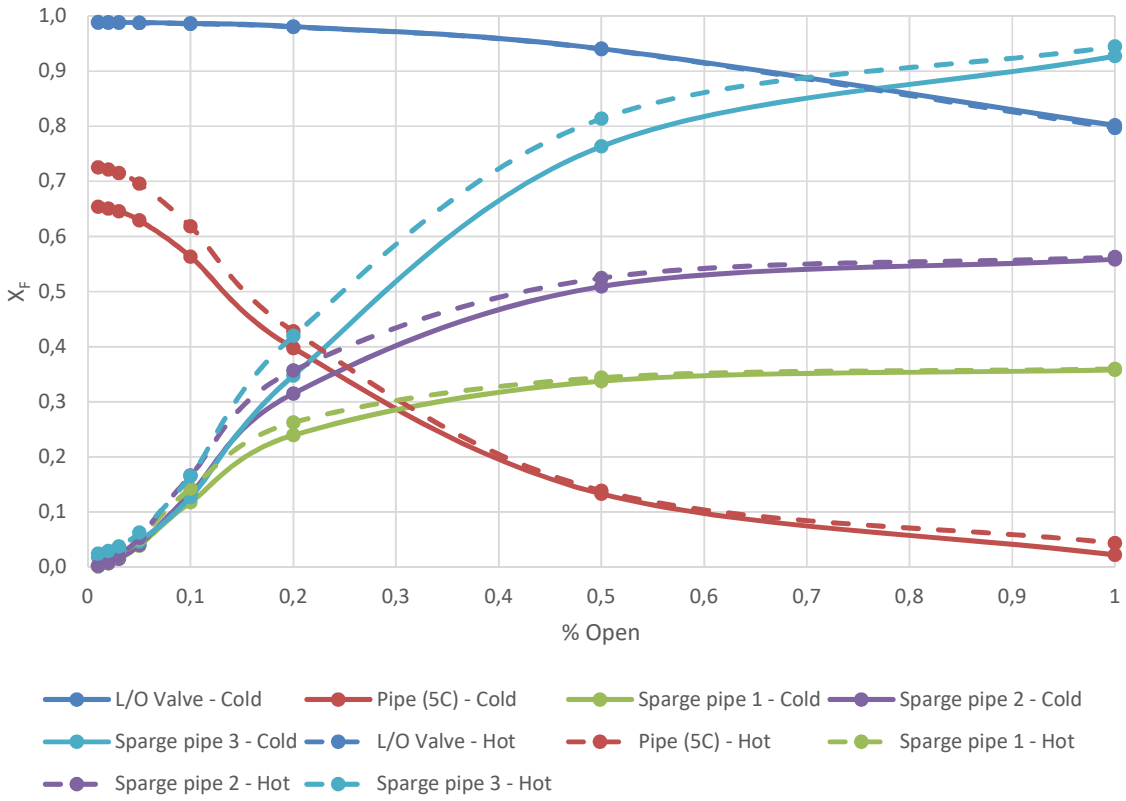


*Figure 5-23: Modulating system temperature comparison*

On both binary systems as well as the modulating leak off system type, a slight increase in $X_F$ values is noticed for all of the components. The increase in $X_F$ values is expected due to the higher vapour pressure as a result of the increase in fluid temperature. The increase is too small to have any significant impact on these systems.

The system with the greatest difference due to temperature is the ARC type system. All the components downstream off the orifice see a significant increase in $X_F$ values. The ARC valve itself has no significant change. It is important to note that the $X_F$ values of the orifice increase more rapidly during the hot condition as the valve is opened. With $X_F$ values larger than 0.9 with the valve opened larger than 15%, cavitation formation is expected across the orifice. With the static pressure at the orifice outlet already close to the vapour pressure, all the downstream components see an increase in risk of cavitation.

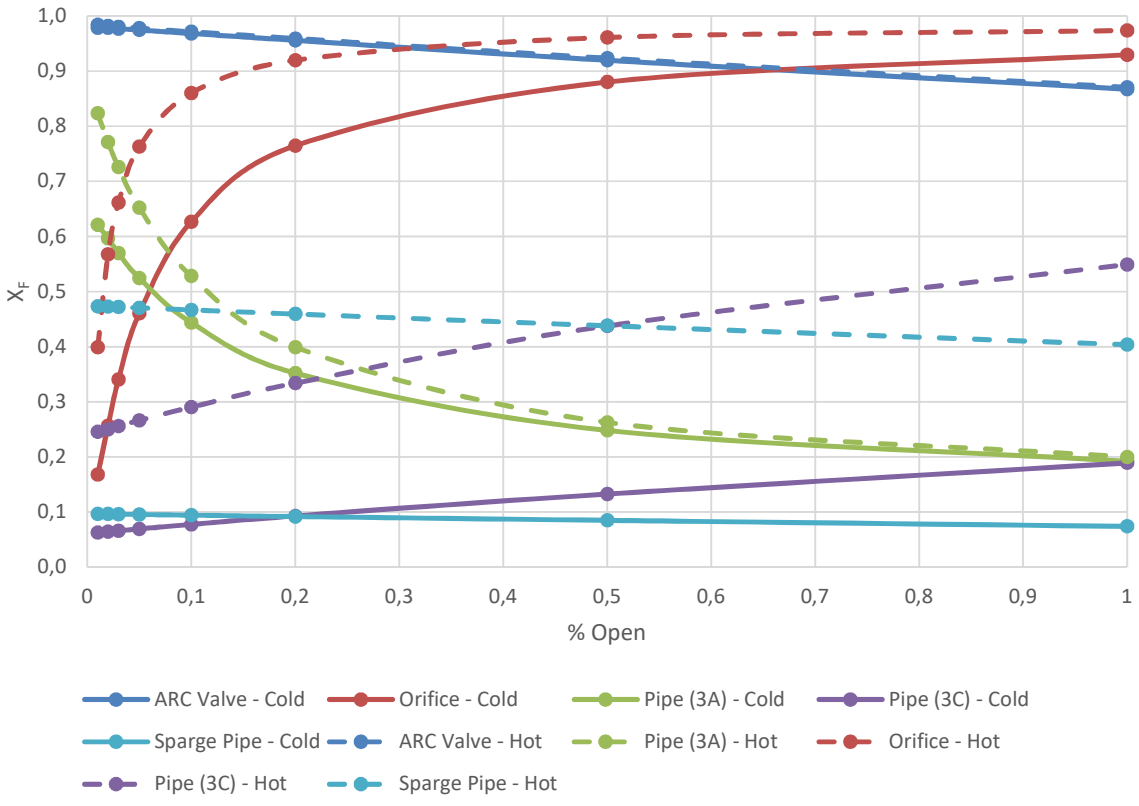


*Figure 5-24: ARC system temperature comparison*

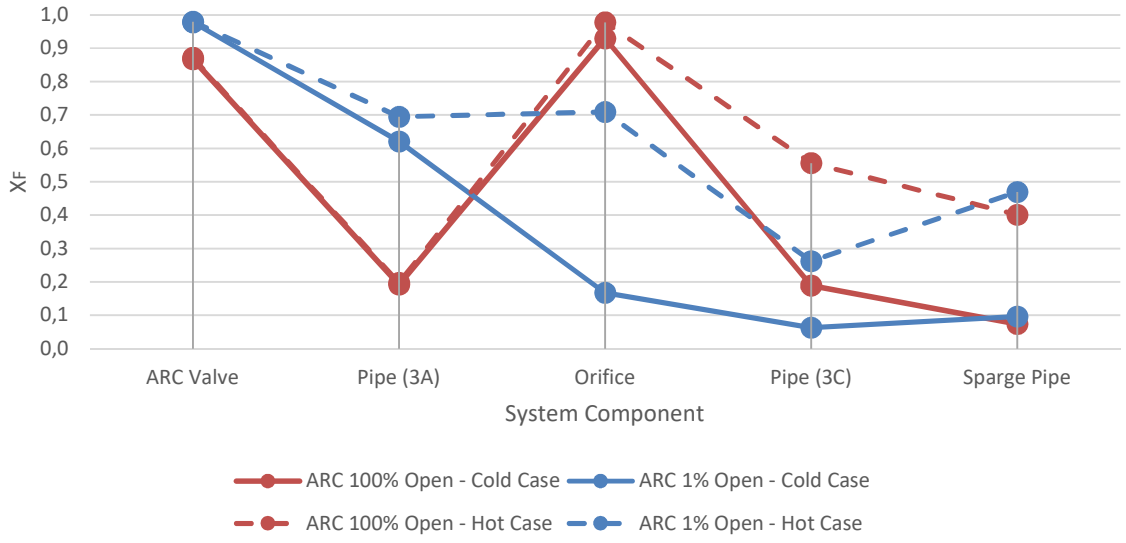


*Figure 5-25: ARC type - coefficient of cavitation comparison for cold and hot conditions*

The change in $X_F$ values due to fluid temperature for the ARC type leak off system is further highlighted in Figure 5-25, which compares the $X_F$ values of the different components at the valve switch point (1 % open) and when the valve is fully open (100 %). At small valve openings (near the

switch point) a large change in $X_F$ values for the orifice and the sparge pipe are noticed. This is due to the low outlet pressure of the ARC compared to the vapour pressure of the fluid in the hot condition. All the downstream components' in- and outlet sides static pressure are much closer to the fluid vapour pressure which results in the higher $X_F$ values. At larger valve openings the $X_F$ value of the orifice is not so much affected by the change in temperature due to the outlet pressure of the ARC valve still being much higher than the fluid vapour pressure. The $X_F$ values of the pipework downstream of the orifice and the sparge pipe are noticeably large due to the low static pressure at the outlet of the orifice compared to the vapour pressure. The high pressure drop over the orifice is a function of the high volume flow rates as per equation (31). The ARC type system FWT conditions that were used to model the hot condition (actual plant transmitter data) are much closer to the saturation conditions than that of the other systems, which also has an effect on the system.

Although the temperature does not have a considerable effect on the majority of the leak off system types in terms of $X_F$ values, the aggressiveness of cavitation defined as the cavitation intensity factor (I) is greatly affected. Although the cavitation intensity factor itself cannot be calculated due to the unavailability of the component reference data, from equation (16) it can be seen that the intensity factor is directly proportional to the fluid temperature factor ($F_T$) which can be calculated using equation (14).

The fluid temperature factor value ranges between a minimum value of 1 and reaches a maximum value of 3 when the fluid temperature is halfway between the freezing and boiling temperature which corresponds to the research by Dular and Heathcock discussed in Appendix 8.B.2.3.

*Table 7: Fluid temperature factor for the different leak off system types*

| | **Fluid Temperature Factor ($F_T$)** | |
|---|---|---|
| **Leak Off Type** | **Cold Case** | **Hot Case** |
| Binary (Separate) | 1,234 | 2,849 |
| Binary (Integrated) | 1,234 | 2,848 |
| Modulating | 1,167 | 2,540 |
| ARC | 1,172 | 2,501 |

The fluid temperature factors shown in Table 7 were calculated for the cold and hot cases using the fluid boiling temperatures (based on the specific pump discharge pressures), as well as the ambient and hot case fluid temperatures at the leak off valve inlet.

During the cold load case (unit start up) the fluid temperature factors are around 1.2 which is at the lower end of the scale. For the hot load case (100 % turbine MCR), the fluid temperature factor for all the stations are greater than 2.5. This means that if a component does suffer from cavitation

damage during the hot condition, it will have more than double the intensity than that of the cold condition and should be avoided as far as possible.

### 5.7.3 Replacing the orifice with a PRV on the ARC system

The proposal to replace the remaining orifices in the ARC systems also with pressure regulating valves were investigated. The results for the cold case are graphically displayed in Figure 5-26.

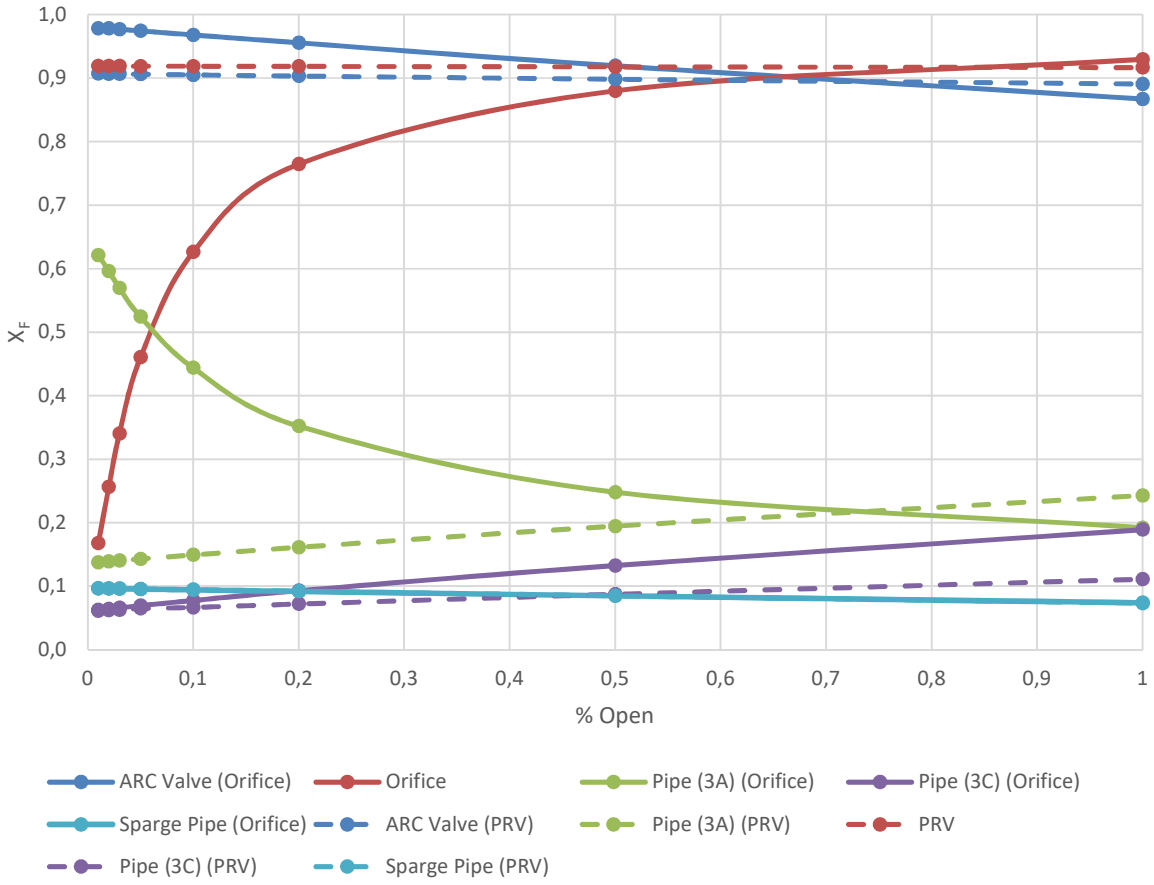


*Figure 5-26: ARC type with PRV $X_F$ vs percentage open (Cold case)*

By replacing the orifice with a PRV, the $X_F$ values of the ARC valve remain more constant over the complete travel range of the valve. At low flow rates the valve's $X_F$ values are reduced from 0.978 to 0.907 and at high flow rates the $X_F$ values slightly increase from 0.867 to 0.891.

The $X_F$ values of the PRV also remain constant across the entire flow range at 0.919. The $X_F$ values of pipe (3A) are significantly reduced at low flow rates and slightly higher at full valve opening. Small changes in $X_F$ values are noticed on piping section (3C) and the sparge pipe.

The main benefit gained by the PRV is seen at small openings of the ARC valve. If unnecessary operation around the switch point of the valve and prolonged periods of operation at low leak off

flow conditions can be avoided, there is no need to spend money on costly plant modifications to replace the orifices with the PRVs.

### 5.7.4 Moving the PRV closer to the ARC outlet

The effect of moving the PRV closer to the ARC valve outlet (statically lower in the system) was investigated to determine if it would reduce the $X_F$ values of the PRV. By reducing the static height of the component, the outlet pressure of the PRV increases due to the pressure head generated by the water in the downstream pipework.

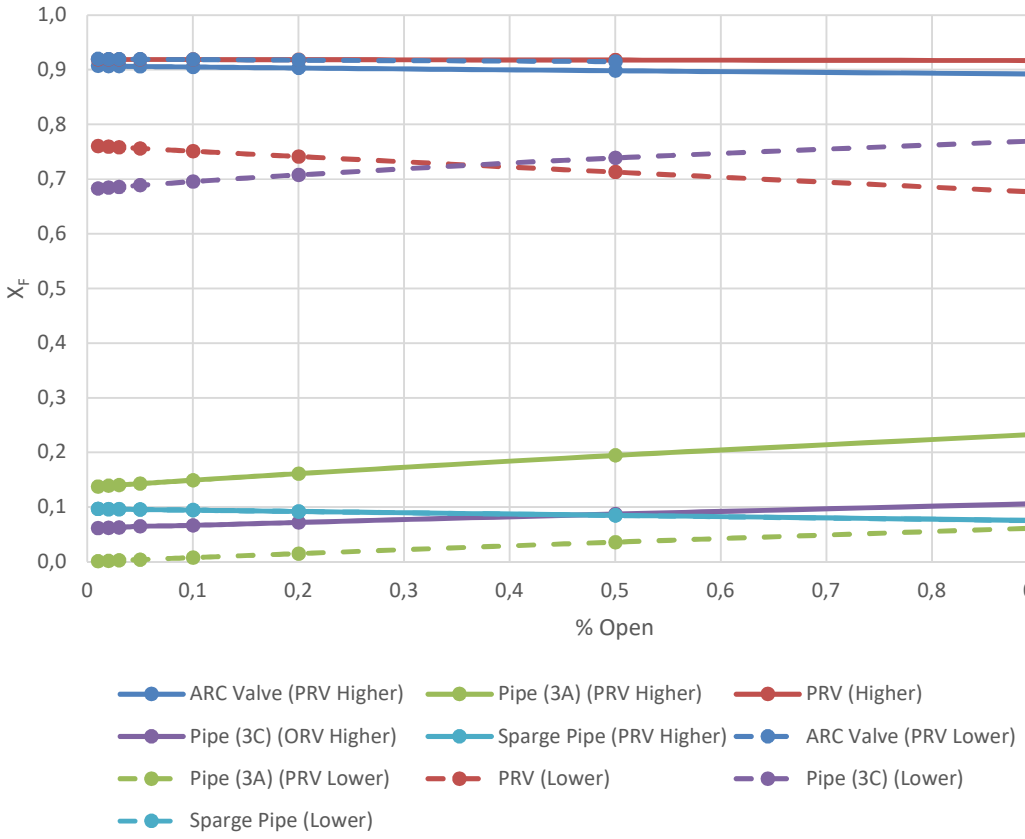


*Figure 5-27: ARC system with PRV location comparison*

It was found that by placing the PRV at 3.25 m level (at the ARC valve outlet), its $X_F$ value is only reduced to values just below 0.8 for the cold case. The outlet pressure of the ARC valve is slightly reduced resulting in a higher $X_F$ value. With the PRV at the 22.5 m level, the outlet pressure on the ARC valve is the sum of the PRV set point pressure, the static head between the ARC and the PRV and the system generated losses between the two valves. When the PRV is lowered to the same level as the ARC, the outlet pressure of the ARC valve is the sum of the set pressure of the PRV and the system generated losses on the short piece of pipe between the two valves. The pressure set

point of the PRV will have to be increased if it is installed closer to the ARC to offer more protection to the ARC. By increasing the PRV pressure set point higher $X_F$ values are expected for the PRV and downstream components.

The $X_F$ value of the pipe (3C) on the outlet side of the PRV increases significantly across the entire range of ARC valve travel. At 100 % open the $X_F$ value increases from 0.189 to 0.778 for the cold case and reaches values as high as 0.935 for the hot case.

No benefit is realised by moving the PRV or the orifice closer to the ARV valve. The $X_F$ value of the orifice and the PRV is only slightly reduced and cavitation inception is still expected at these components during hot conditions. Larger bore downstream piping will be required to stay within the allowable fluid velocity as a result of the increased fluid volume (lower fluid density) on the PRV outlet. More rigorous inspection will also be required to ensure safe operation of the leak off system due to cavitation erosion in the downstream pipework from the PRV.

### 5.7.5 Moving the FWT nozzle to the bottom of the tank

To ensure the leak off system is always charged with water when the plant is made standby, it is often proposed to move the nozzle to enter the tank below the water level. Yet, at all Eskom plants the leak off nozzles on the FWTs are found on the top half of the tank i.e. enters the tank above the water level. The effect of moving the leak off nozzle to enter the FWT at the bottom, below the water level, was investigated.

The investigation was also used to determine the effect on the $X_F$ values of the leak off components due to the leak off system termination point condition (water versus steam) as well as the change in height of the connection nozzle on the FWT.

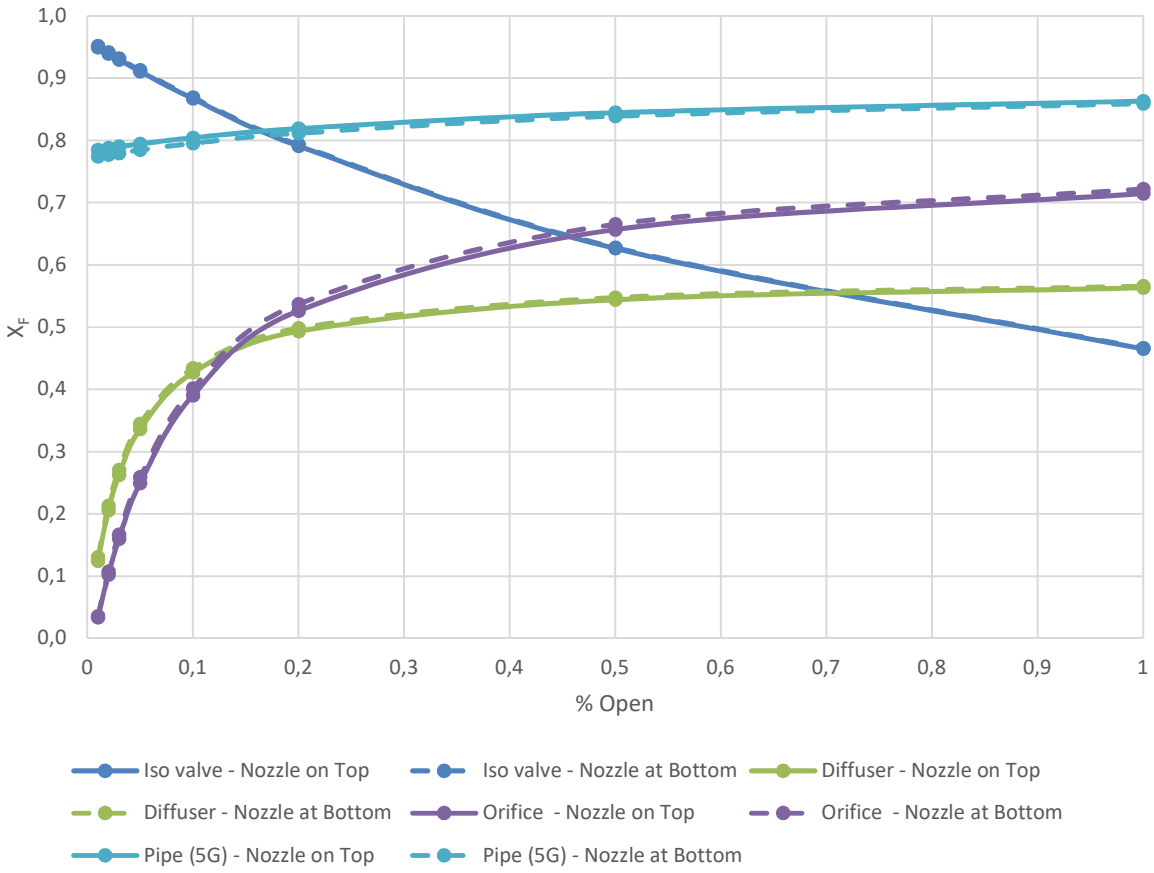


*Figure 5-28: Binary (Separate) system FWT nozzle position comparison*

Figure 5-28 compares the $X_F$ values for the different components of the binary (separate) type leak off system at the hot condition with the FWT nozzle located at the top and bottom of the tank. The change in $X_F$ values is practically negligible. The same was found for all leak off system types.

With the FWT nozzle located at the top of the tank, the leak off pipework reaches a point that is statically higher than the water level inside the tank. The additional static height creates a small amount of increased back pressure on the upstream system components. This decreases the $X_F$ values of the upstream components which makes the higher nozzle location ideal.

Very small changes are observed and therefore does not justify the move of the leak off nozzle to the bottom of the tank.

# 6. Summary of results

The four leak off systems are compared for each of three valve opening percentages (1 %, 50 % and 100 %) at the hot condition and displayed in Figure 6-1, Figure 6-2 and Figure 6-3 below. Table 8 serves as the legend for the component numbering in each figure. The graphs compare the $X_F$ value on the vertical axis with the components in sequential order starting with the leak off valves numbered as 1 and the sparge pipe or final connection to the FWT numbered as 5 on the horizontal axis.

*Table 8: Numbering legend for Figure 6-1, Figure 6-2 and Figure 6-3*

| Component | ARC Valve | Binary (Separate) | Binary (Integrated) | Modulating |
|---|---|---|---|---|
| 1 | ARC Valve | Iso valve | LO valve | LO Valve |
| 2 | Pipe 3A | Pipe (5C) | Pipe (5C) | Pipe (5C) |
| 3 | Orifice | Diffuser | Pipe (5E) | Sparge pipe 1 |
| 4 | Pipe 3C | Orifice | Orifice | Sparge pipe 2 |
| 5 | Sparge Pipe | Pipe (5G) | Pipe (5G) | Sparge pipe 3 |

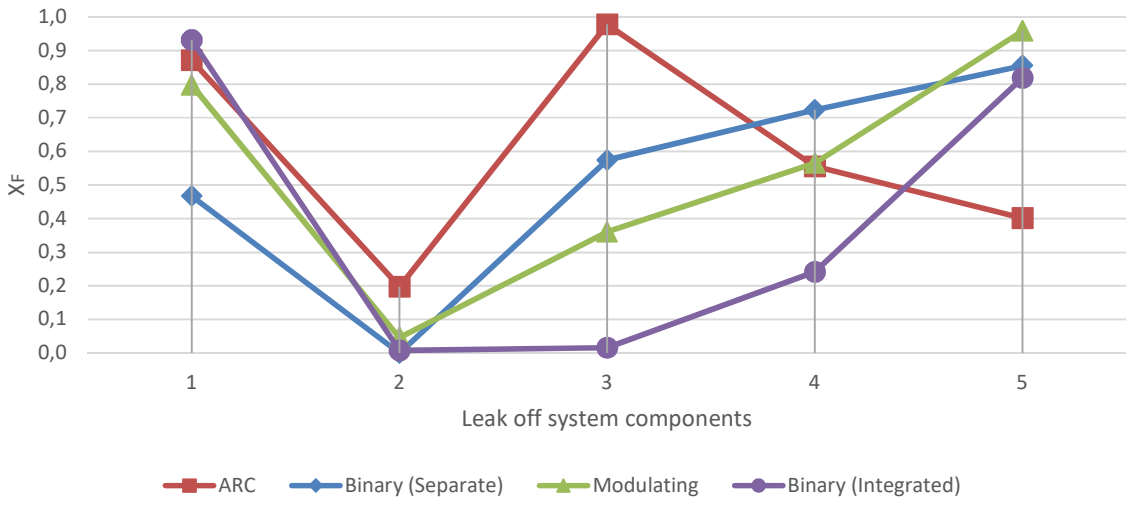


*Figure 6-1: Results of all leak off types – Hot case with valves at 100 %*

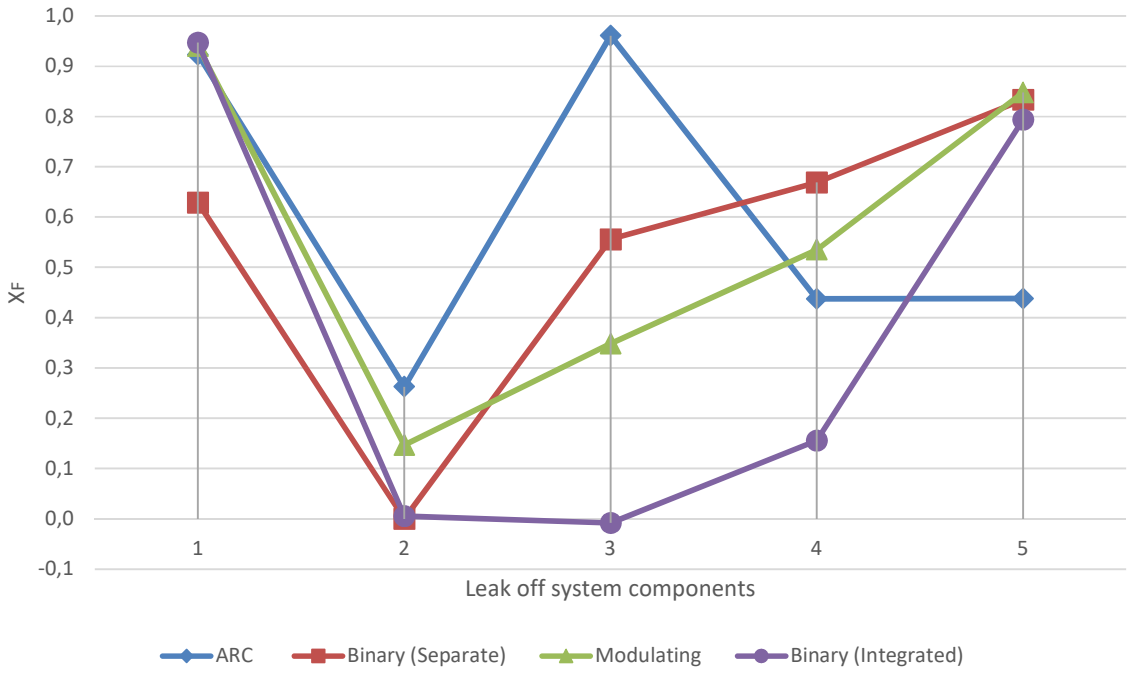


*Figure 6-2: Results of all leak off types – Hot case with valves at 50 %*

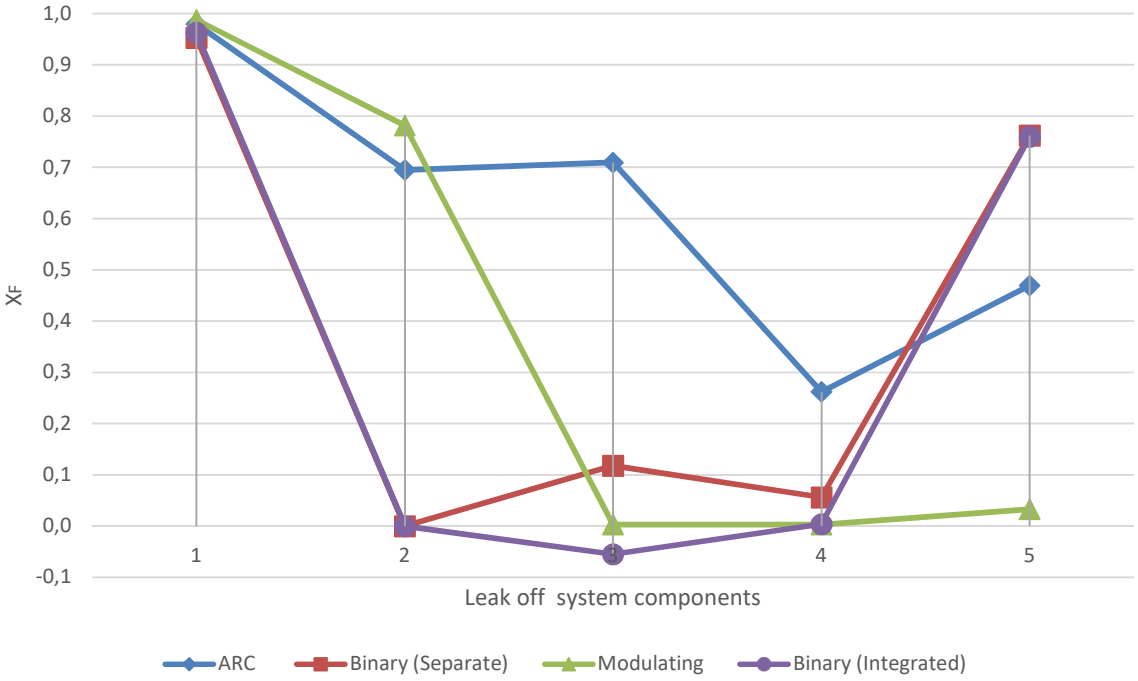


*Figure 6-3: Results of all leak off types – Hot case with valves at 1 %*

As expected, all the leak off valves have extremely high $X_F$ values across all leak off system types, especially at small valve openings (around the switch point of the valves) which is evident from component 1 in Figure 6-3. All the valves are consequently highlighted as high risk components.

Ultimately the design of each valve determines the $X_{FZ}$ value which governs the onset of cavitation. It is clear that the modulating type has the highest $X_F$ values at low flow rates and are justified through the valve design as explained in paragraph 5.5.

The ARC and both binary type systems follow the no damage approach as discussed in paragraph 3.5.2. Between these three types of systems, the binary (separate) type system has to be singled out the highest risk at low flow rates due to the extremely high $X_F$ values found over the isolation valve as a single stage parallel slide valve. The no damage approach is based on the multi stage design of the diffuser, which offer insufficient back pressure to the isolation valve at small flow rates.

Components situated downstream can decrease the $X_F$ values of the upstream components by creating a back pressure, but in doing so also increase the $X_F$ values and risk of the downstream component. Each system has at least one other component with a high $X_F$ value. These components require individual consideration to determine the risk of cavitation inception and damage.

The high $X_F$ value component is located close to the FWT for all the systems. For components with small openings, such as orifices, the risk increases significantly at higher flow rates. These secondary risk components for each system are:

1. back pressure orifice for the ARC type;
2. sparge pipe for the modulating type;
3. final section of pipe connecting to the FWT nozzle for both the binary types;
4. diffuser and flow measuring orifice for the binary (separate) type system.

The back pressure orifice of Station O (point 1) carries a very high risk as well as the flow orifice (point 4) of the binary (separate) system type of Station A. It was expected that the diffuser will have a significantly higher $X_F$ value than what is found in the model. This is mostly due to the high back pressure created by the flow measuring orifice situated downstream of the diffuser, which could also be seen as an oversized diffuser for the system. The low $X_F$ value result of the diffuser agrees with to the outage inspection reports noting the exceptionally good condition of the internal stages of the component across all units after many years of service.

As discussed in paragraph 5.3, the piping sections mentioned in point 3 above are not of great concern and connect directly to the FWT above the water level. The modulating system's sparge pipe (point 2 above) is discussed in paragraph 5.5 and also not of a great concern.

The modulating and binary (integrated) type leak off systems have the lowest amount of high risk components compared to the other types. The modulating type system is mostly protected by the multi stage sparge pipe. Cavitation formation is expected inside the valve. The location of the bubble collapse needs to be closely monitored. The only factor separating the two designs are the unknown

$X_{FZ}$ value of the multi stage binary (integrated) valve. If the valve has a sufficiently high $X_{FZ}$ value, this system type shows to have the least amount of components that are at risk of cavitation.

The conditions in the FWT influences the leak off system components close to the tank. Changes in $X_F$ values of the leak off system components close to the FWT are noticed when the selected conditions in the FWT are close to saturation conditions. The effect was noticed when modelling the ARC system. As the conditions in the FWT nears saturation conditions, the risk of cavitation formation at the final component increases due to the outlet pressure of the component approaching vapour pressure.

# 7. Conclusion and Recommendations

## 7.1 Summary

As part of this study the leak off system methodologies and available component data for all the coal fired power stations within the Eskom fleet were collected and categorised into 4 different types namely Binary (Separate), Binary (Integrated), Modulating and ARC type.

An extensive literature study was completed to understand the different aspects of cavitation with specific focus placed on the inception of cavitation, different types and methods of reducing the effects of cavitation. Methods of numerically predicting incipient cavitation in valves where also investigated, but could not be applied due to the constraint of valve specific design and manufacturing data which is the intellectual property of the valve manufacturers. Instead the different leak off system components were categorised based on their risk of cavitation. Using Computation Fluid Dynamic (CFD) modelling on the high-risk components is recommended for future work.

A representative plant from each type were modelled using Flownex Simulation Environment software and verified using actual plant data. Hot and cold conditions at various valve opening / leak off flow rates were assessed to determine conditions that increase the risk of cavitation and which components are mostly affected. Methods of reducing the effects of cavitation from literature as well as proposed design changes were investigated through the use of the models and the results were discussed. Conclusions were drawn based on the results and recommendations were made whether the investigated proposals would be feasible and new proposals were identified and documented.

## 7.2 General observations and recommendations

The leak off valves across all systems are considered critical and require detailed and accurate specification when being replaced. The binary (Integrated) type leak off system has the lowest amount of components which are at risk of cavitation. The valves themselves will have to be assessed based on the $X_{FZ}$ values which are tested and provided by the manufacturer. Based on the specification in Table 3 the multistage linear control valves could have $X_{FZ}$ values as high as 1, making the 6 stage linear valves used throughout Eskom acceptable. The modulating system is also an improvement on the binary (separate) and ARC leak off system types in terms of the location of the back pressure device (sparge pipe). The design of the valve itself allows for operation under cavitation conditions.

Also based on the information provided by Table 3 the critical pressure drop per stage increases as the amount of stages increase. If the values provided are extrapolated, it is estimated that the critical pressure drop per stage of a 6 stage linear valve should be limited to 43 bar. With the majority of the Eskom BFP leak off valves having 6 stages, it is recommended that the 50 bar rule of thumb be reduced to 43 bar per stage. It is also important that the correct pressure at the valve outlet is specified, taking into account the static head pressure in the leak off pipework and the FWT conditions at all load cases.

Consideration was given to the placement of the leak off nozzles on the FWT. It is not recommended to move the position of the nozzles to a statically lower position on the tank.

Sparge pipes that provide sufficient back pressure are recommended on systems where upstream components suffer from cavitation damage at higher flow rates. This correlates well with the recommendations found in literature discussed in section 3.5.3 and 3.5.6. It is further recommended that the system should be modelled first to ensure that the minimum flow requirement of the pump is still met.

Leak off system operation with leak off valves at small open percentages should be avoided as far as possible. This includes the valve switch points as well as passing leak off valves especially at hot conditions when the cavitation intensity is at its highest.

The hot load cases showed the greatest risk of cavitation with a significantly higher cavitation intensity.

## 7.3 System specific recommendations

### 7.3.1 Binary type (Separate)

The switch points at which the valve opens and closes (40 l/s and 45 l/s feed water flow) should be avoided as far as possible. With each opening or closing, the valve is at severe risk of cavitation. To reduce the amount of these occurrences, it is recommended that the pumps are started with the valves at 100% open.

The proposal to increase the orifice size from 40 mm to 60 mm is supported. The increase in $X_F$ value of the diffuser is substantial and will prevent damage to the flow measuring orifice and downstream pipework. The increase in $X_F$ value of the isolation valve is relatively small compared to the current $X_F$ value and no further risk to the component is expected. When the $X_F$ value of a downstream component is decreased, the $X_F$ values of the upstream components increase because the overall pressure reduction of the entire system remains the same.

It is recommended to investigate the option of adding a time dependant trip to prevent the valve from operating at partially open positions for extended periods of time. This could be due to sticky valve seats, too tightly packed glands or manual valve operation. Currently Station B has a similar type leak off bypass system that does not suffer from cavitation damage on the isolation valve. This could be attributed to the time dependant trip protection that monitors the valve open and closing time to ensure the valve does not fail or stop at a partially open position with the feed pump in service.

Care should be taken to ensure the isolation valves seal tightly in the closed position after refurbishment. A passing isolation valve is undesired and will have a similar effect to that of a valve at a very small opening. An alternative is to investigate the possibility of coating the valve downstream seats with Stellite grade 6 as discussed in section 3.5.1.

### 7.3.2 Binary type (Integrated)

The leak off valve shows a high risk of cavitation. Unfortunately the exact $X_{FZ}$ value of the valve is unknown, and therefore no recommendation can be made on the valve itself other than recommendations based on literature. An $X_F$ value of close to 1 is acceptable for multistage linear valve as per Table 3. The binary (Integrated) type leak off valve is a 6 stage linear valve and should therefore be acceptable. In the event that valves do show signs of cavitation after some time in operation, it is recommended that a back pressure device such as a sparge pipe with small openings be installed at the entrance to the FWT.

It is also recommended that the switch point (40 l/s and 45 l/s feed water flow) of the valve be avoided as far as possible to reduce the amount of operation at small opening and closing values under which the valve shows the highest $X_F$ values.

No other component in the system shows any risk of cavitation damage.

### 7.3.3 Modulating type

Extremely high $X_F$ values are not a concern with the modulating type system's leak off valve due to the design methodology. It is recommended that valve outlet nozzles and connected downstream piping sections be inspected regularly to confirm that the bubble collapse does not take place in the outlet nozzle area or pipework.

Another area which requires regular inspection is the final stage of the sparge pipe. Although it carries no safety risk due to the sparge pipe positioned inside the FWT, enlargement of the flow area on the final stage as a result of cavitation could result in lower back pressures on the upstream stages. This will further increase the risk of cavitation on the upstream components which would

result in a higher leak off flow rate as well as the possibility of two phase flow in the leak off pipework if insufficient pressure recovery takes place at the valve outlet.

### 7.3.4 ARC type

The leak off bypass section of the ARC valve type is completely open during start up conditions due to the NRV disk being forced closed by a spring. Start-up conditions are therefore not an issue with the ARC design.

It is recommended to avoid the switch point of the valve which is at 70 kg/s feed water flow. This will reduce the risk of operating the valve at $X_F$ values in greater than 0.9. Running of both EFPs to achieve 100 % turbine MCR is not recommended as the ARC of both EFPs will be operating around the switch point of the valves.

If the switch point and prolonged periods of operation at low leak off flow conditions can be avoided, it is not necessary to replace the existing orifices with PRVs. The only benefit gained by the PRV is seen at small openings of the ARC valve. Due to the scale of plant modification required to fit the PRVs, it is not recommended when compared to the marginal added benefit.

Lastly it is not recommended to reposition the PRV or the back pressure orifice to a statically lower position which is closer to the ARC valve. The $X_F$ value of the orifice and the PRV is only slightly reduced and cavitation inception is still expected at these components during hot conditions. Larger bore downstream piping sections will be required to allow for the increase in fluid volume if the fluid remains two phase flow or more rigorous inspection to ensure safe operation due to cavitation erosion.

## 7.4 Closing remarks

Models such as the ones developed for this study can be used to identify plant components that are at risk based on their service conditions. The risk includes any process related risks such cavitation damage, flashing, choking, high fluid velocities etc. These components could be highlighted for inspection during outages and premature component failures could also be explained.

The models can also be used to predict the effect on the process conditions of the plant due to mechanical changes or changes to the operating conditions such as replacing the back pressure orifices on the ARC type leak off systems with PRVs, relocating the leak off nozzles on the FWT or increasing the leak off flow measuring orifice size.

It must be noted that the models created for this study are specific to the plants they are based on, but are representative of all the different types of leak off systems found within Eskom. The models

made it easy to compare the different types of systems and recommendations could be made based on the results.

Cavitation is a complex phenomenon and a detailed literature study was necessary to understand the concept of cavitation as well as the influencers, development, effects, intensity and how to reduce the effects caused by cavitation. The majority of the laboratory studies found in literature was used to gain insight into the standards and general practise used in industry. The majority of numerical studies on cavitation go hand in hand with actual test data and detailed component information is required to carry out cavitation inception prediction on a component level. Due to the unavailability of this information and testing facilities, the study could not be performed at a component level and cavitation prediction was not possible.

In conclusion, the Flownex software has proven to be a great one-dimensional process modelling tool to investigate, analyse and compare complete process systems such as the different types of BFP leak off systems. The software proved to be great at modelling the overall system process and highlighting problematic areas in the plant. Unfortunately, detailed component modelling cannot be carried out with one-dimensional software packages and CFD models are required to analyse the flow characteristics inside complex components such as leak off valves and diffusers.

# 8. List of References


[1] Schroeder, *SHP10-Presentation Agentsmeeting,* 2015.

[2] EPRI, “Severe Duty Valve Maintenance Guide,” Palo Alto, 2005.

[3] Sulzer, Centrifugal Pump Handbook, Amsterdam: Elsevier, 1998.

[4] SPX Valves & Controls, “Boiler Feedpump Recirculation - UEC Control,” 2012. [Online]. Available: http://www.ueccontrol.com. [Accessed 17 January 2018].

[5] J. Gülich, Centrifugal Pumps, Villeneuve: Springer, 2010.

[6] S. Gopalakrishnan, “A new method for Computing Minimum Flow,” in *Texas A&M 5th International Pump User Symposium*, Houston, 1988.

[7] M. Thompson, “Pump Minimum Flow Protection Using Automatic Recirculation Valves,” in *Pumps and Compressors Conference*, Perth, 2013.

[8] Schroedahl, *Pump Protection Valves from the Specialist,* 2010.

[9] J. P. Franc and J. M. Michel, Fundamentals of Cavitation, Dordrecht: Kluwer Academic Publishers, 2004.

[10] G. Libera, “State of the Art and Perspectives on the Study of Valve Cavitation,” 2015.

[11] J. N. Tilton, “Fluid and Particle Dynamics,” in *Perry's Chemical Engineering Handbook*, McGraw-Hill, 2008.

[12] R. Garcia and F. G. Hammitt, “Cavitation Damage and Correlations with Material and Fluid Properties,” *Journal of Basic Engineering,* pp. 753-763, 1967.

[13] Native Dynamics, “Neutrium,” 11 February 2015. [Online]. Available: https://neutrium.net. [Accessed 27 December 2018].

[14] P. Eisenberg, “A Brief Survey of Progress on the Mechanics of Cavitation,” Washington D.C., 1953.

[15] C. E. Brennen, Cavitation and Bubble Dynamics, New York: Cambridge University Press, 2014.

[16] R. T. Knapp, “Cavitation Mechanics and its Relation to the Design of Hydraulic Equipment,” *Proceedings of the Institution of Mechanical Engineers,* vol. 166, no. 1, pp. 150-163, 1952.

[17] CISM Courses and Lectures, “The Rayleigh-Plesset equation: a simple and powerful tool,” in *Fluid Dynamics of Cavitation and Cavitating Turbopumps*, Udine, Springer, 2007, pp. 1-28.

[18] M. S. Plesset, “The Dynamics of Cavitation Bubbles,” *Journal of Applied Mechanics,* vol. 16, pp. 277-282, 1949.

[19] The Instrument Society of America, *ISA-RP75.23-1995 Considerations for Evaluating Control Valve Cavitation,* North Carolina, 1995.

[20] The Instrument Society of America, *ISA-75.01.01-2007 Flow Equations for Sizing Control Valves,* North Carolina, 2007.

[21] Parcol S.p.A., Handbook for Control Valve Sizing, Canegrate, 2016.

[22] J. P. Tullis, “Cavitation Guide for Control Valves,” Logan, 1993.

[23] R. W. Kermeen, “Some Observations of Cavitation on Hemispherical Head Models,” California Institute of Technology Report E-35, 1952.

[24] A. F. Lehman and J. O. Young, "Experimental Investigations of Incipient and Desinent Cavitation," *Journal of Basic Engineering,* pp. 275-281, 1964.

[25] Samson, "Cavitation in Control Valves - Samson AG," 2003. [Online]. Available: http://www.samson.de. [Accessed 22 04 2018].

[26] R. Becker and W. Döring, "Kinetische Behandlung in übersättigten Dämpfen," in *Kinetik der Phasenbildung*, Leipzig, Verlag Steinkopf, 1939, p. 156–165.

[27] L. J. Briggs, "Limiting Negative Pressure of Water," *Journal of Applied Physics,* vol. 21, pp. 721-722, 1950.

[28] A. P. Keller, "Beginnende Kavitation, Zugspannungen in Flüssigkeiten," Laboratory for Hydraulic Engineering and Water Resources Management, Technical University Munchen/Obernach, Germany, 1980.

[29] K. A. Mørch, "Cavitation inception from bubble nuclei," 2015. [Online]. Available: http://dx.doi.org/10.1098/rsfs.2015.0006. [Accessed 26 June 2018].

[30] M. Dular, "Hydrodynamic cavitation damage in water at elevated temperatures," in *International Symposium on Transport Phenomena and Dynamics of Rotating Machinery*, Honolulu, 2016.

[31] C. J. Heathcock, "Cavitation Erosion of Materials," University of Cape Town, Cape Town, 1980.

[32] R. T. Knapp, "Recent Investigations of the Mechanics of Cavitation and Cavitation Damage," California Intitute of Technology, Pasadena, 1955.

[33] J. Foldyna, J. Klich, P. Hlaváček, M. Zeleňák and J. Ščučka, "Erosion of Metals by Pulsating Water Jet," *Tehnički vjesnik,* vol. 19, no. 2, pp. 381-386, 2012.

[34] A. Danlos, F. Ravelet, O. Countier-Delgosha and F. Bakir, "Cavitation regime detection through Proper Orthogonal Decomposition: Dynamics analysis of the sheet cavity on a grooved convergent-divergent nozzle," *International Journal of Heat and Fluid Flow,* no. 47, pp. 9-20, 2014.

[35] P. Tomov, S. Khelladi, F. Ravelet, C. Sarraf, F. Bakir and P. Vertenoeuil, "Experimental study of aerated cavitation in a horizontal venturi nozzle," *Experimental Thermal and Fluid Science,* no. 70, pp. 85-95, 2015.

[36] IEC Publication 534-8-2, "Laboratory Measurement of Noise Generated by Liquid Flow Through Control Valves," Geneva, 1991.

[37] J. P. Tullis, "Cavitation Scale Effects for Valves," *Journal of the Hydraulics Division,* vol. 99, no. HY7, p. 1109, 1973.

[38] "Flownex," M-Tech Industrial, [Online]. Available: https://www.flownex.com/. [Accessed 11 12 2019].

[39] Flownex, *Flownex Library Manual,* 2017.

[40] A. L. Buck, "New Equations for Computing Vapor Pressure and Enhancement Factor," *Journal of Applied Meteorology,* vol. 20, pp. 1527-1532, 1981.

[41] L. Malan, "Direct Numerical Simulation of Free-Surface and Interfacial Flow Using the VOF Method: Cavitating BubbleClouds and Phase Change," University of Cape Town, Cape Town, 2017.

[42] O. M. Rayleigh, “The pressure developed in a liquid during the collapse of a spherical cavity,” *Philosophical Magazine,* vol. 6, no. 34:200, pp. 94-98, 1917.

[43] T. G. Leighton, “Derivation of the Rayleigh-Plesset Equation in Terms of Volume,” ISVR University of Southampton, Southampton, 2007.

# Appendix A. Eskom leak off system type list

| Station | Pump set | Leak off device OEM | Number of stages | Valves per pump | Leak off flow as % of BEP |
|---|---|---|---|---|---|
| **Binary type – Separate** | | | | | |
| Station A | EFP | Hopkinsons Parallel slide with Zikesch diffuser | 6 | 1 x 100 % | 15 % |
| Station B | EFP | Hopkinsons Parallel slide with Hopkinsons diffuser | 6 | 1 x 100 % | 15 % |
| | SFP | Hopkinsons Parallel slide with Hopkinsons diffuser | 6 | 2 x 50 % Valves<br>1 x 100 % Diffuser | 15 % |
| **Binary type – Integrated valve** | | | | | |
| Station A | SFP | Welland & Tuxhorn | 6 | 1 x 100 % | 15 % |
| | EFP (Unit 6) | Welland & Tuxhorn | 6 | 1 x 100 % | 15 % |
| Station C | EFP | Flowserve Kammer Multi-Z | 6 | 1 x 100 % | 15 % |
| | SFP | CCI Valves | - | 1 x 100 % | 15 % |
| Station D | EFP | Welland & Tuxhorn | 6 | 1 x 100 % | 15 % |
| | SFP | Welland & Tuxhorn | 6 | 1 x 100 % | 20 % |
| Station E | EFP | Welland & Tuxhorn | 6 | 1 x 100 % | 28 % |
| Station F | EFP | Welland & Tuxhorn | Unit 1-3: 4<br>Unit 4-6: 6 | 1 x 100 % | 15 % |
| | SFP | Welland & Tuxhorn | Unit 1-3: 4<br>Unit 4-6: 6 | 2 x 50 % | 17 % |
| Station G | EFP | Yarway | 6 | 2 x 50 % | 34 % |
| Station H | EFP (Unit 1-3) | Welland & Tuxhorn | 6 | 1 x 100 % | 20 % |
| | EFP (Unit 4-6) | Yarway | 6 | 1 x 100 % | 26 % |
| Station I | EFP | Welland & Tuxhorn | 6 | 1 x 100 % | 28 % |
| | SFP | Welland & Tuxhorn | 6 | 2 x 50 % | 16 % |
| **Modulating type** | | | | | |
| Station J | EFP | CCI Valves | N/A | 1 x 100 % | 28 % |
| Station K | EFP | CCI Valves | N/A | 1 x 100 % | 28 % |

| **ARC type - Schroedahl** | | | | | |
|---|---|---|---|---|---|
| Station L | EFP | TDM 138 | 5 | 1 x 100 % | 25 % |
| | SFP | TDM 168 | 5 | 1 x 100 % | 25 % |
| Station M | EFP | TDM 138 | 5 | 1 x 100 % | 25 % |
| | SFP | TDM 168 | 5 | 1 x 100 % | 25 % |
| Station N | EFP | TDM 138 | 5 | 1 x 100 % | 25 % |
| | SFP | TDM 168 | 5 | 1 x 100 % | 25 % |
| Station O | EFP | Unit 1-5: TDM 138<br>Unit 6-9: TDM 158 | 5 | 1 x 100 % | 25 % |

# Appendix B. Cavitation bubble evolution and collapse

## B.1 Evolution of the bubble

### B.1.1 Nucleus evolution in a low pressure region

Franc and Michel [9] describes the evolution of a nucleus through a low pressure region of limited extent using Blake's model, where it is assumed that the nucleus undergoes an isotherm transformation with a constant mass of gas.

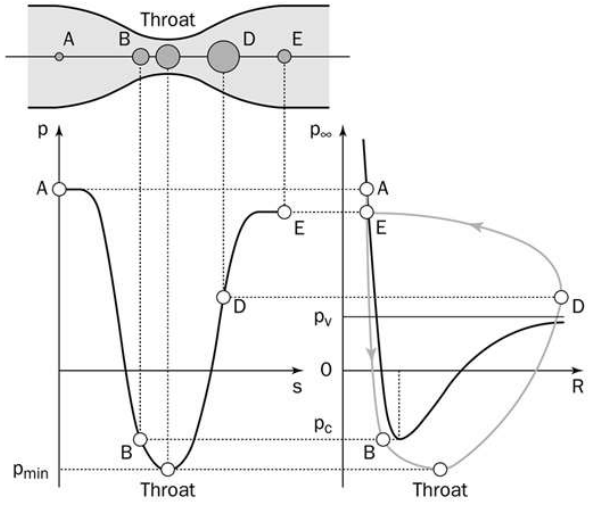


*Figure B-1: Nucleus evolution in a venturi* [9]

If a nucleus is observed as it travels through a venturi (Figure B-1), the local pressure (p) is measured at a distance (s) in the one-dimensional system. As the nucleus approaches the throat area, from A to B, the local pressure reduces. A minimum local pressure ($p_{min}$) is found in the throat area before the pressure recovery (Throat to E).

In terms of the growth of the nucleus, two cases are considered in terms of the minimum pressure ($p_{min}$) and this critical pressure ($p_c$):

1. The minimum pressure is higher than the critical pressure of the nucleus ($p_{min} > p_c$), the nucleus starts to grow and returns to its initial state as it passes through the throat.
2. The minimum pressure is lower than the critical pressure of the nucleus ($p_{min} < p_c$), the nucleus with radius (R) becomes unstable and grows to a maximum size at point D, which is downstream of the throat area before it violently collapses to its original size due to the increase in external pressure (point D to E).

## B.1.2 Releigh-Plesset equation

The Releigh-Plesset equation can be used to determine the time evolution of the bubble radius R(t) through the second order differential equation below.

$$\rho\left[R\ddot{R}+\frac{3}{2}\dot{R}^2\right]=\left[p_v-p_\infty(t)\right]+p_{g0}\left(\frac{R_0}{R}\right)^{3k}-\frac{2S}{R}-4\mu\frac{\dot{R}}{R} \tag{39}$$

Where $\dot{R}\ and\ \ddot{R}$ are first and second order derivatives of the bubble radius with respect to time and $R_0$ is the original radius of the bubble. An explanation of the equation is given by Franc [17] and is summarised in the following paragraphs.

The first term on the right hand side of the equation $\left[p_v-p_\infty(t)\right]$ measures the closeness of the applied pressure to the vapour pressure. It is the driving factor for evolution of the bubble, be it growth, collapse or oscillation.

The second term $p_{g0}\left(\frac{R_0}{R}\right)^{3k}$ is the contribution by the non-condensable gasses in the bubble. To derive this term, some assumptions are made. Please refer to the section on assumptions below.

The third term $\frac{2S}{R}$ is the contribution made by the surface tension (S) of the liquid and is more relevant for bubbles with a small radius.

The fourth and final term $4\mu\frac{\dot{R}}{R}$ is the effect of dynamic viscosity (μ) of the liquid. Similar to the effect of the surface tension, the effect of the dynamic viscosity is more relevant for small radii.

The equilibrium equation, equation (6), can easily be deduced form the Releigh-Plesset equation by setting all time derivatives to zero, assuming a constant external pressure and assuming the gas transformation as isothermal (k=1) as the temperature can be considered as continuously fixed. Equation (6) can be rearranged as follows:

$$p_\infty=p_{g0}\left[\frac{R_0}{R}\right]^3+p_v-\frac{2S}{R} \tag{40}$$

Again, the equilibrium equation shows that the difference between the pressure inside and outside of the bubble is due to the surface tension of the liquid. By solving the equation, with respect to R, the bubble radius at equilibrium can be obtained for any given external pressure ($p_\infty$).

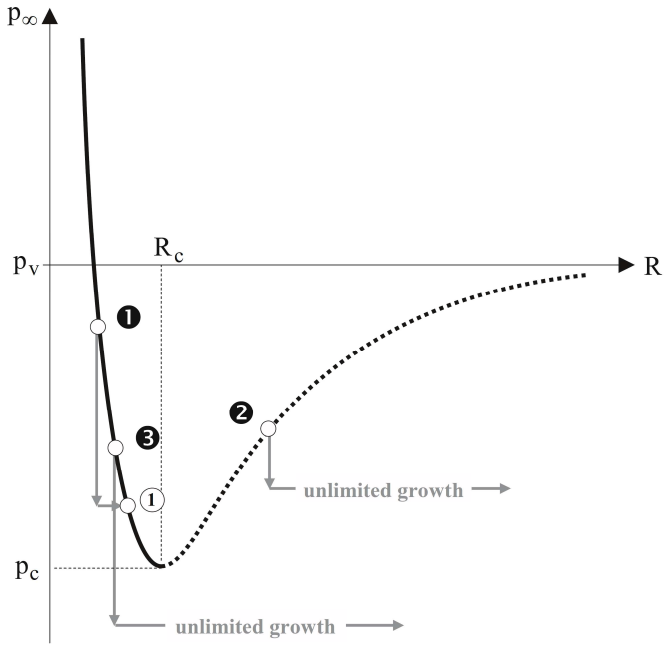


*Figure B-2: Equilibrium bubble radius vs external pressure curve* [17]

The relationship that exists between the bubble radius (R) and the external pressure ($p_\infty$) is best explained by Figure B-2. The critical pressure ($p_c$) and radius ($R_c$) as calculated by equations (8) and (9) determines if the nuclei crosses the equilibrium line (solid line in Figure B-2) and is stable.

Consider a nucleus at point 1 (Figure B-2). If the external pressure ($p_\infty$) is slightly reduced the equilibrium equation, equation (6), is no longer satisfied. The bubble growth will be stable as long as the lower pressure is still above the critical pressure ($p_c$). The right hand side of the Releigh-Plesset equation becomes positive and the bubble will grow to a new size. This will satisfy the equation and is also logically expected. A new equilibrium will be achieved at the lower pressure and larger bubble size.

Consider a nucleus at point 2. The bubble will grow indefinitely without crossing the equilibrium curve and is therefore unstable. The nucleus at point 3 is in equilibrium. If the external pressure is reduced below the critical pressure, which corresponds to the equilibrium curve, the nucleus will grow indefinitely without reaching a new equilibrium. The critical pressure is therefore the threshold for a microbubble to explode and become a macroscopic cavitation bubble [17].

From equation (9) it is clear than the critical pressure is numerically smaller than the vapour pressure, the difference is due to the surface tension of the liquid. As previously mentioned, the surface tension plays a larger role when the nuclei are smaller and becomes negligible for larger nuclei. This further justifies the claim that for most engineering applications it is sufficient to assume that cavitation will occur at the vapour pressure corresponding to the temperature of the liquid.

Releigh-Plesset equation assumptions [15] [17]

The following assumptions were made to derive the Releigh-Plesset equation:

1) The bubble was assumed to be spherical with a radius R(t), where t is time, in an infinite liquid domain.
2) The temperature and the pressure of the liquid are far away from the bubble are designated $p_\infty(t)$ and $T_\infty$ respectively. The temperature is assumed to be constant. The pressure assumed to be known or controlled and regulates the bubble growth or collapse.
3) The liquid density, ρ, is assumed to constant.
4) The dynamic viscosity of the liquid, μ, is assumed to be constant and uniform.
5) It is assumed that the contents of the bubble is homogeneous and the temperature, $T_B(t)$, and pressure, $p_B(t)$, within the bubble are always uniform.
6) The mass of the non-condensable gas inside the bubble remains constant during the evolution of the bubble.
7) The constant mass of the gas is assumed to follow a polytropic thermodynamic behaviour characterized by a given polytropic coefficient k. If it is isothermal then k=1. If it is adiabatic, k is the ratio ϒ of the heat capacities of the enclosed gas. The gas transformation is often assumed to be isothermal. The characteristic time for the evolution of a nucleus in real cavitating flows is usually much longer than what is required for heat transfer so that temperature equilibrium is continuously achieved. For big bubbles that result in the explosion of the nucleus, the behaviour is adiabatic [9]. The polytropic behaviour is defined by the relationship between partial pressure of the gas inside the bubble and the radius R: $p_g R^{3k} = p_{g0} R_0^{3k}$ where the subscript 0 denotes the initial conditions.

Other methods

Malan (2017) [41] used the volume of fluid (VOF) method to investigate the hydrodynamics of isothermal cavitation in large bubble clouds through the use of a modified PARIS code. He found that the effect of a boundary condition that is not spherically symmetric contributed significantly to his error. Otherwise, he found a reasonable agreement to the Releigh-Plesset method.

## B.1.3 Temperature drop in the vicinity of the growing bubble

It has been shown experimentally that the temperature drop in the vicinity of the growing bubble, due to thermal effects, is insignificant for water at room temperature, but becomes more significant as the water temperature increases. *Figure B-3* shows the increase in the ΔT value as the average temperature of the water increases.

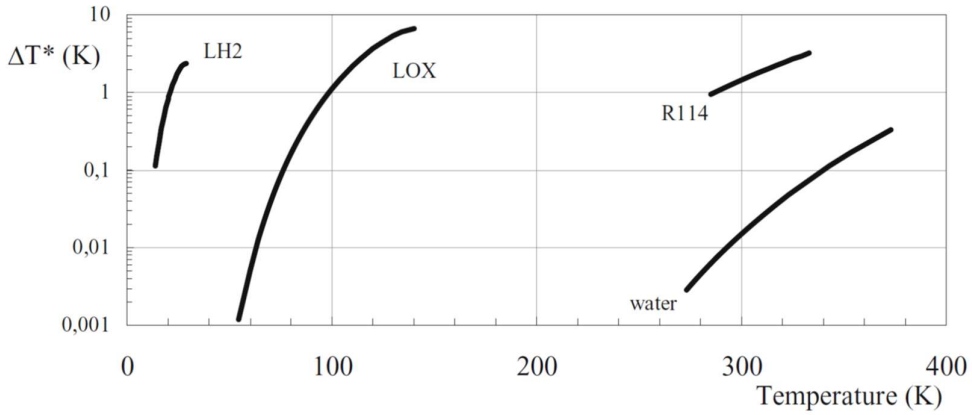


*Figure B-3: Temperature drop in the vicinity of the collapsed bubble* [17]

## B.2 Collapse of the bubble

The final phase of cavitation is the collapse of the bubble. This occurs when the local pressure surrounding the bubble is higher than the pressure within the bubble. The bubble becomes unstable and collapse violently. The increase in pressure can be due to pressure recovery where an increase in flow area exists, such as a diffuser, or as a result of local pressure recovery as the bubble trapped inside the tiny vortices in the boundary layer are dissipated and lose their rotational speed [22].

In case of an orifice, the primary cause for pressure recovery is a result of the dissipation of eddies due to a reduction in their rotational speed. The bubble is then subjected to a local pressure much higher than vapour pressure [22].

### B.2.1 Orders of magnitude

The variation in bubble size and the velocity over short periods makes the scaling as well as numerical and experimental analysis difficult when it comes to collapse. Some orders of magnitude given by Franc and Michel [9] are given for perspective:

A spherical vapour bubble of 1cm radius travelling in water under an external pressure of 1 bar will collapse in approximately 1millisecond.

The duration of the final stage of bubble or cavitating vortex collapse is of the order of one microsecond. This is an important part of the erosion process.

Rayleigh derived an equation to determine the pressure that develops in the liquid adjacent to the bubble during collapse. The ideal case was assumed with the bubble is perfectly spherical and does not contain any gaseous content in a static, non-viscous and incompressible fluid.

$$p_{\max} = \frac{p_L}{6.35}\left(\frac{R_m}{R}\right)^3 \tag{41}$$

Where $R_m$ is the maximum bubble radius. The bubble is assumed to be empty which results in an infinite value for $p_{max}$. In reality, the bubble contains non-condensable gas which limits the collapse pressure [31]. Rayleigh [42] published a numerical estimation done by Cook that the pressure generated during the collapse of a bubble (when the bubble reaches 1/20$^{th}$ of its original size) under 1 atmosphere fluid pressure results in a collapse pressure of 103000 atmospheres (1043.65 MPa).

## B.2.2 Bubble collapse velocity and time

Franc [17] gives the interface velocity of a bubble during collapse as:

$$\dot{R} \cong -\sqrt{\frac{2}{3}\frac{p_\infty - p_v}{\rho}\left[\left(\frac{R_0}{R}\right)^3 - 1\right]} \tag{42}$$

It does however disregard the effects of viscosity, non-condensable gas inside the bubble as well as surface tension.

The Rayleigh time is the bubble collapse time and is a function of the pressure difference (inside and outside of the bubble). For the ideal case it can be calculated as:

$$t_p \cong 0.915 R_0 \sqrt{\frac{\rho}{p_\infty - p_v}} \tag{43}$$

## B.2.3 Effect of fluid parameters on collapse of the bubble [31]

The cavitation processes is influenced by a number of fluid parameters which are discussed below.

Compressibility of the fluid

The effect of liquid compressibility is ignored by Rayleigh's analysis of the collapse of a bubble due to the mathematical complexity. A greater liquid compressibility results in a lower erosion rate as the collapse energy is stored in the bulk of the liquid.

Liquid vapour pressure

A higher liquid vapour pressure results in an increase in cavitation. When the vapour pressure inside the bubble is increased, a lower liquid pressure is required to initiate growth of the nucleus. During collapse of the bubble the vapour pressure has very little effect compared to that of the non-condensable gas. This is due to the slow process of vapour formation compared to cavity growth.

Viscosity

Compared to the effect of the non-condensable gas and compressibility, the effect of viscosity is small and only large variations will have a significant effect. The effect of viscosity is greater during the early stages of bubble growth and the final stages of collapse (small bubble radii).

Surface tension

The effect of surface tension is greater for smaller bubbles and always tends to act in a manner that will reduce the bubble size. During growth the wall velocity will be reduced by the surface tension and will increase during bubble collapse.

Temperature of cavitatinq fluid

The effect of liquid temperature on the erosion rate is well known and has been studied by various researchers, although it is not very well understood. A maximum erosion rate occurs at temperatures between 40 °C and 50 °C for constant atmospheric pressure. The reduction of cavitation erosion at temperatures higher than 50 °C is generally explained as a result of the increased vapour pressure. The low cavitation rate at low temperatures is due to an increase in dissolved gas content.

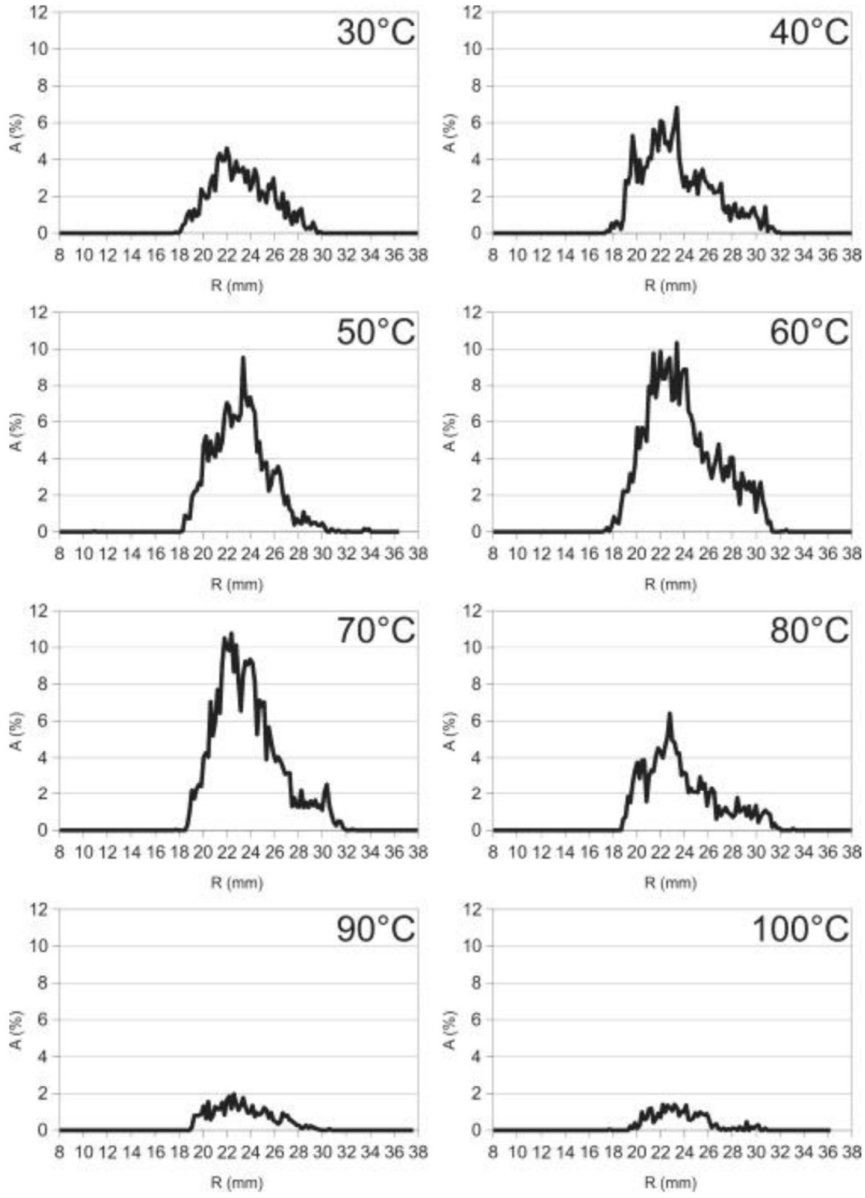


*Figure B-4: Effect of fluid temperature on cavitation aggression* [30]

Dular [30] found that the cavitation aggressiveness reaches a maximum at temperatures between 50 °C and 70 °C which is slightly higher than reported by Heathcock and shown in Figure B-4. The conclusion is consequently drawn that cavitation aggressiveness reaches a maximum at a temperature halfway between the freezing and boiling temperature of the fluid at the reference pressure.

Free and dissolved gas content

The gas content of a liquid can have a negative or positive effect on cavitation. Higher concentrations of gas increase the amount of free bubble nuclei which promotes gaseous cavitation

or rectified diffusion which results in the growth of subcritical nuclei to the critical size necessary for unstable, vaporous cavity growth. During bubble collapse the compression of non-condensable gas within the cavity causes a dampening of the collapse pressure. The collapse energy is partially used to compress the gas content inside the bubble and also in raising the temperature. The energy available for cavitation erosion is thus reduced and the damage is less severe.

Experiments done by Harrison (1952) shows that cavities formed in water with low air content do not rebound. Rebound is the regrowth of the bubble during collapse and is caused by a pressure increase inside the bubble due to the decrease in cavity volume. A conclusion was also made that only cavities containing a large amount of gas will oscillate [14].

# Appendix C. Flownex model screenshots

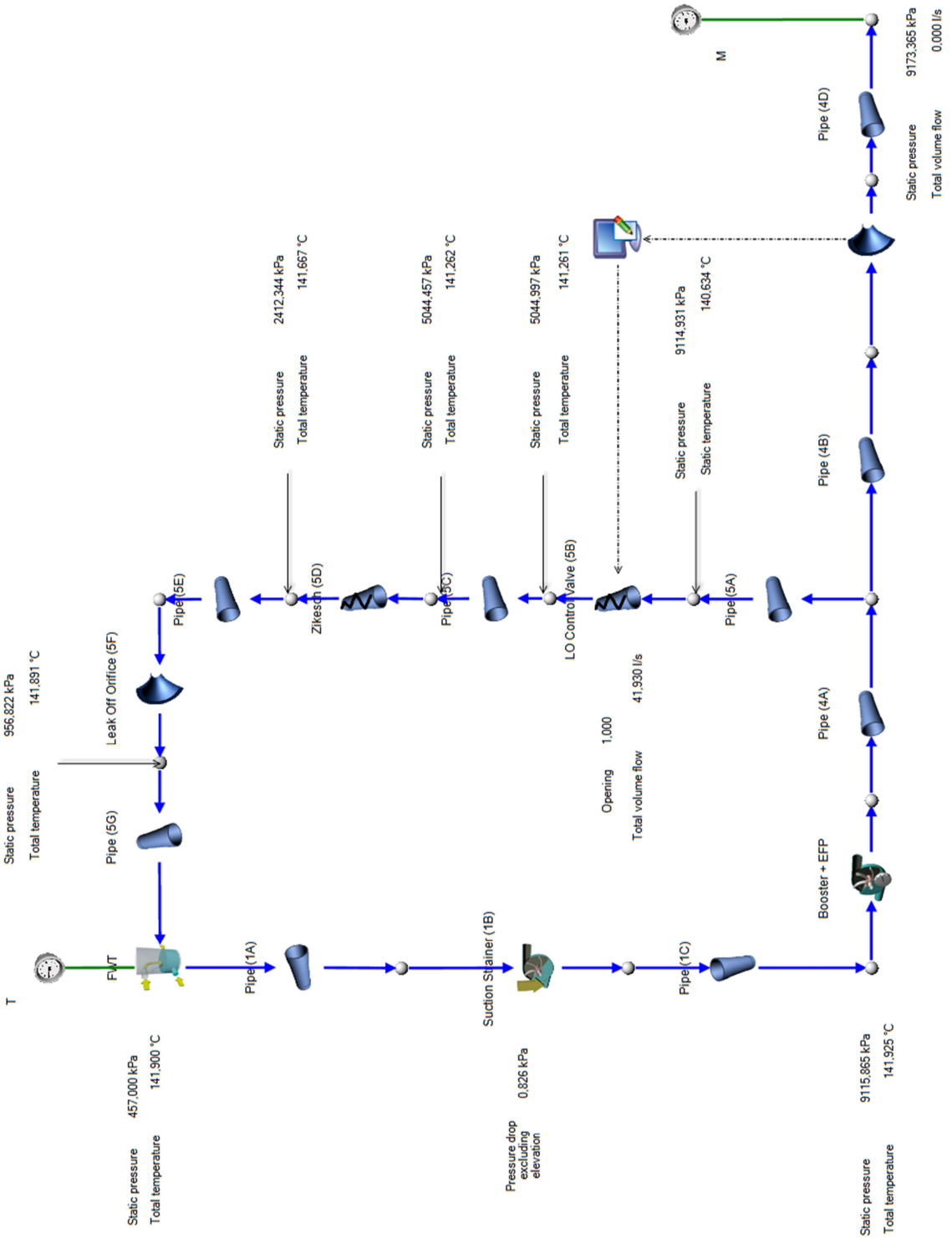

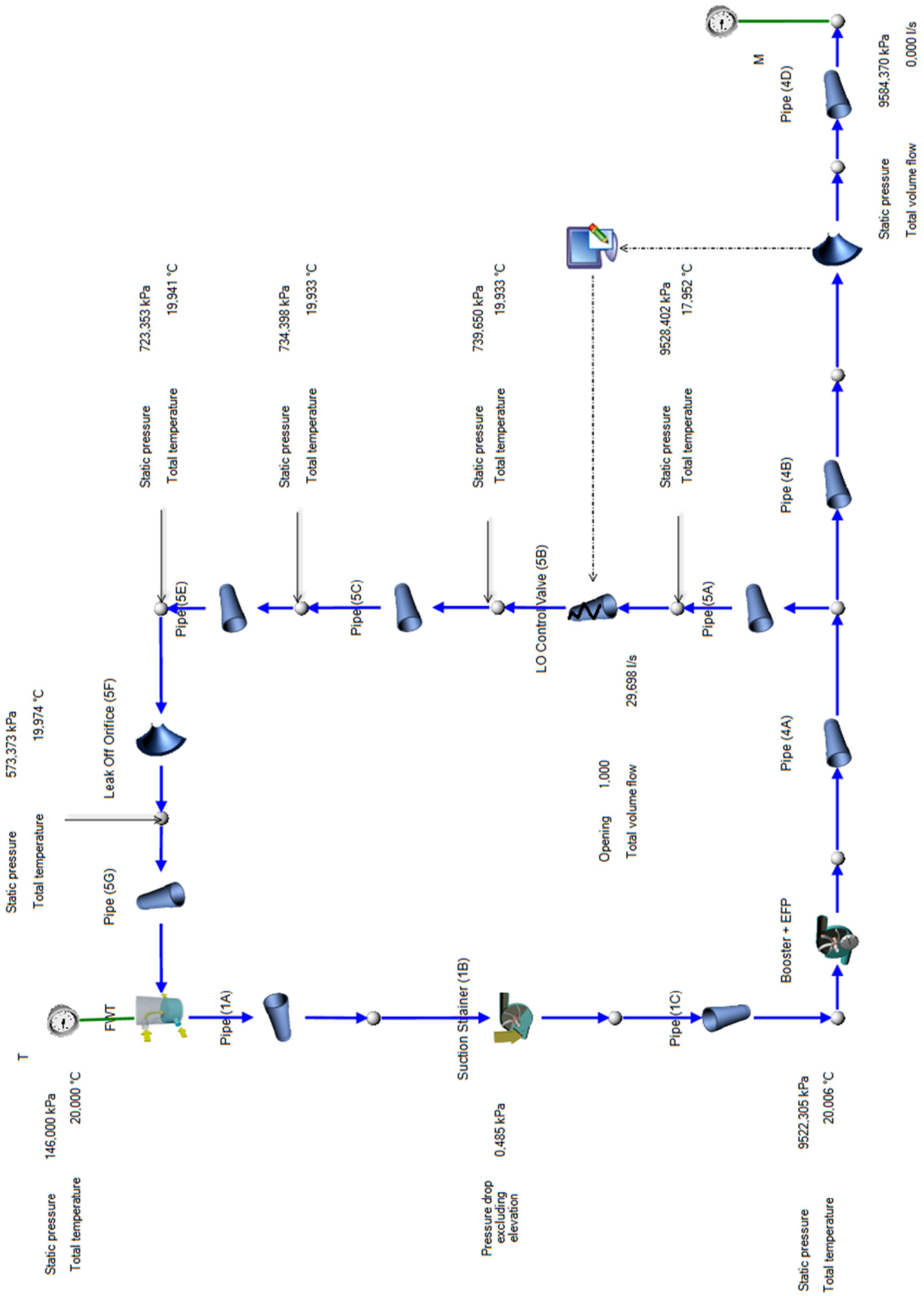
T
Static pressure 146.000 kPa
Total temperature 20.000 °C
FWT
Static pressure 573.373 kPa
Total temperature 19.974 °C
Leak Off Orifice (5F)
Pipe (5G)
Pipe (1A)
Suction Strainer (1B)
Pressure drop excluding elevation 0.485 kPa
Pipe (1C)
Booster + EFP
Static pressure 9522.305 kPa
Total temperature 20.006 °C
Pipe (4A)
Pipe (4B)
Static pressure 9528.402 kPa
Total temperature 17.952 °C
Pipe (5A)
LO Control Valve (5B)
Opening 1.000
Total volume flow 29.698 l/s
Static pressure 739.650 kPa
Total temperature 19.933 °C
Pipe (5C)
Static pressure 734.398 kPa
Total temperature 19.933 °C
Pipe (5E)
Static pressure 723.353 kPa
Total temperature 19.941 °C
M
Pipe (4D)
Static pressure 9584.370 kPa
Total volume flow 0.000 l/s

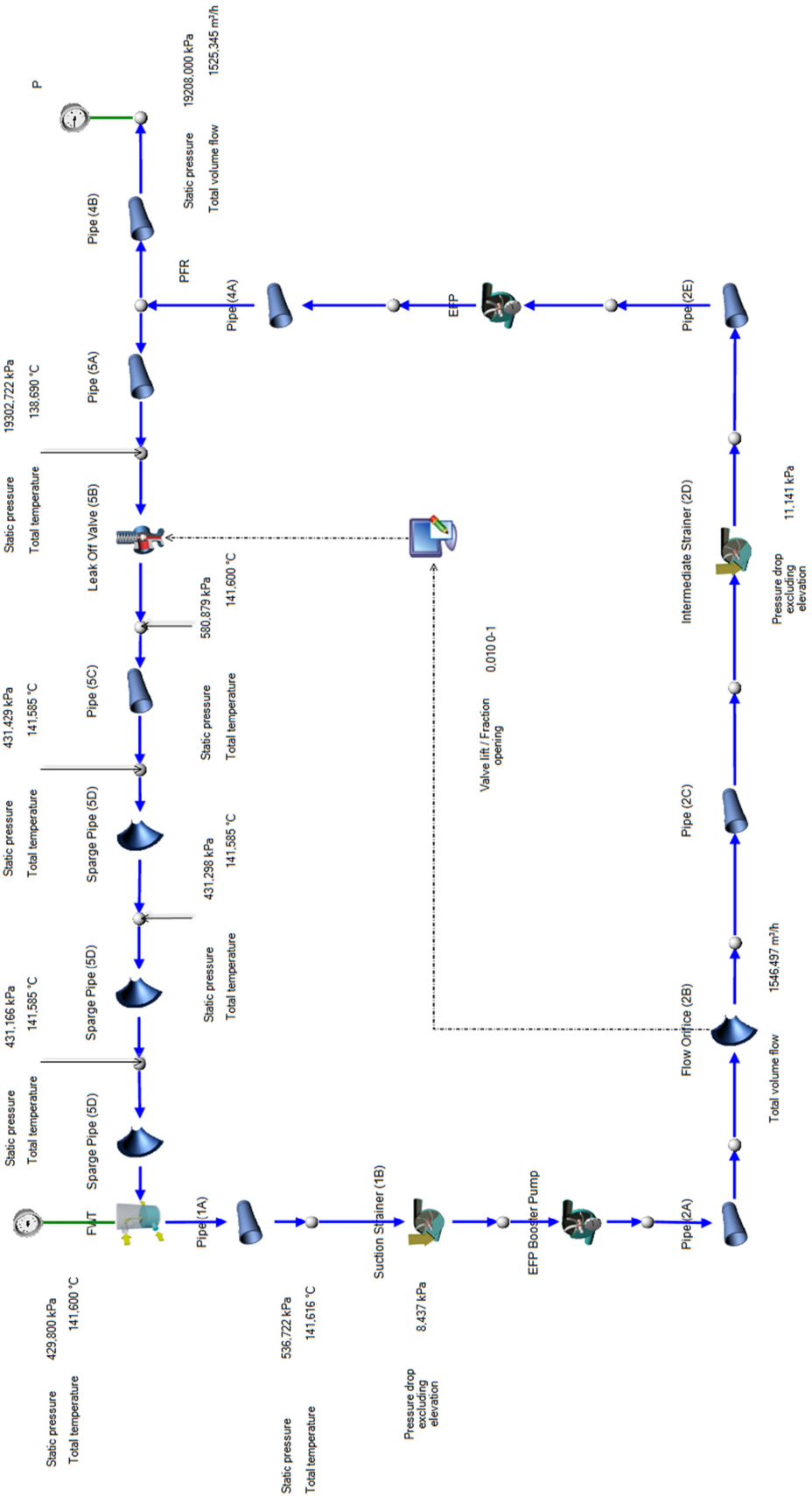
P
Static pressure 19208.000 kPa
Total volume flow 1525.345 m³/h
Pipe (4B)
PFR
Pipe (4A)
EFP
Pipe (2E)
Pipe (5A)
Static pressure 19302.722 kPa
Total temperature 138.690 °C
Leak Off Valve (5B)
Intermediate Strainer (2D)
Pressure drop excluding elevation 11.141 kPa
Pipe (5C)
Static pressure 580.879 kPa
Total temperature 141.600 °C
Valve lift / Fraction opening 0.010 0-1
Pipe (2C)
Sparge Pipe (5D)
Static pressure 431.429 kPa
Total temperature 141.585 °C
Sparge Pipe (5D)
Static pressure 431.298 kPa
Total temperature 141.585 °C
Flow Orifice (2B)
Total volume flow 1546.497 m³/h
Sparge Pipe (5D)
Static pressure 431.166 kPa
Total temperature 141.585 °C
FWT
Static pressure 429.800 kPa
Total temperature 141.600 °C
Pipe (1A)
Static pressure 536.722 kPa
Total temperature 141.616 °C
Suction Strainer (1B)
Pressure drop excluding elevation 8.437 kPa
EFP Booster Pump
Pipe (2A)

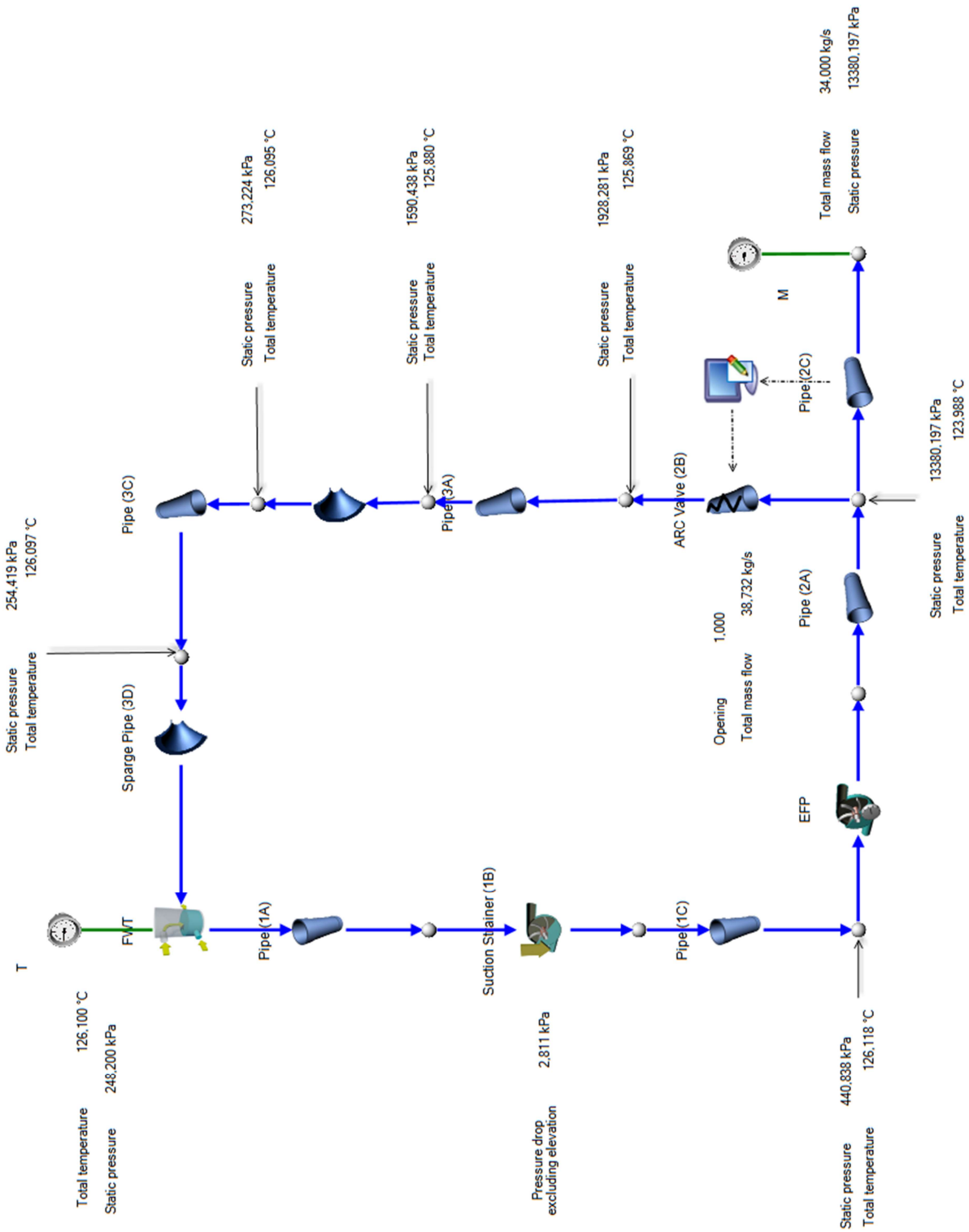
T
Total temperature 126.100 °C
Static pressure 248.200 kPa
FWT
Sparge Pipe (3D)
Static pressure 254.419 kPa
Total temperature 126.097 °C
Pipe (1A)
Suction Stainer (1B)
Pressure drop excluding elevation 2.811 kPa
Pipe (1C)
EFP
Static pressure 440.838 kPa
Total temperature 126.118 °C
Pipe (2A)
Opening 1.000
Total mass flow 38.732 kg/s
ARC Valve (2B)
Static pressure 1928.281 kPa
Total temperature 125.869 °C
Pipe (3A)
Static pressure 1590.438 kPa
Total temperature 125.880 °C
Pipe (3C)
Static pressure 273.224 kPa
Total temperature 126.095 °C
Pipe (2C)
M
Total mass flow 34.000 kg/s
Static pressure 13380.197 kPa
Static pressure 13380.197 kPa
Total temperature 123.988 °C